European Commission Grant Agreement Number: 869300

Call identifier: H2020-LC-CLA-2018-2019-2020 Topic: LC-CLA-06-2019

Type of action: RIA, Research and Innovation action

Starting date: 01.09.2020 Duration: 48 months

Project website: futuremares.eu

Project Deliverable Report
Seagrass and seaweed future projections

Dissemination level: **Public, after approval**

Type of deliverable: Report/Data

Due date: Project month 30[28/2/2023]

Project Milestone(s) achieved:

FutureMARES Project

FutureMARES - Climate Change and Future Marine Ecosystem Services and Biodiversity is an EU-funded research project examining the relations between climate change, marine biodiversity and ecosystem services. Our activities are designed around two Nature-based Solutions (NBS) and Nature-inclusive (sustainable) Harvesting (NIH):

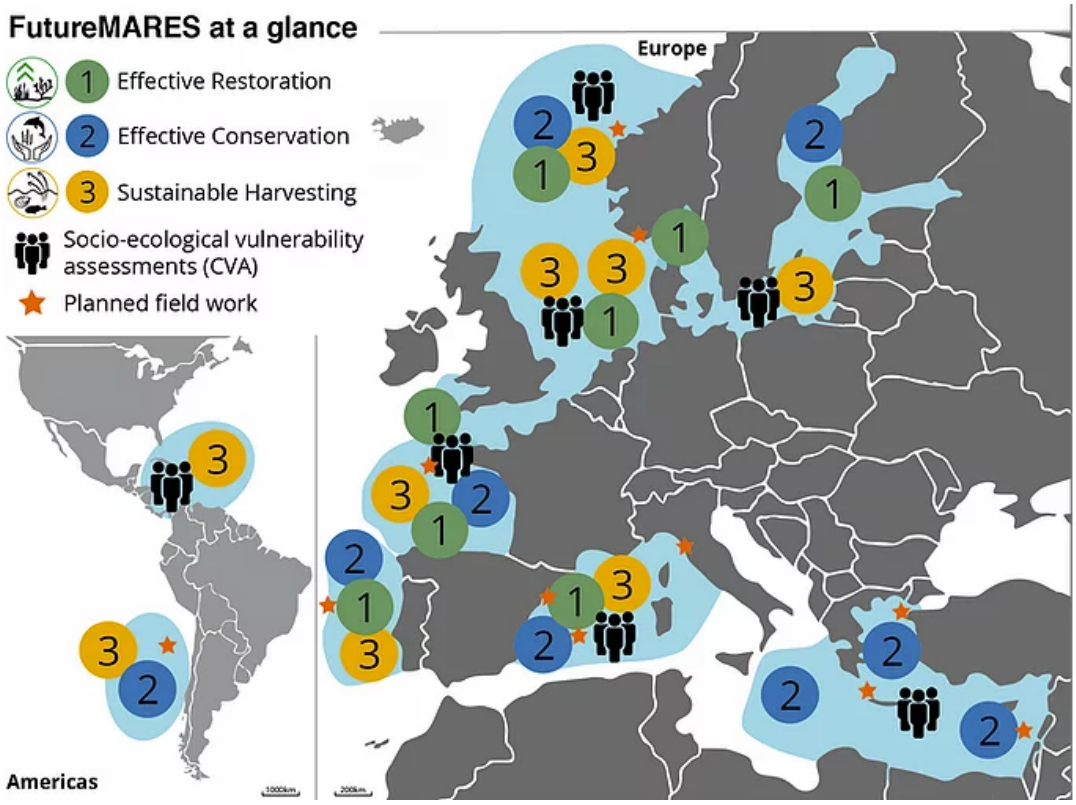

We are conducting our research and cooperating with marine organisations and the public in Case Study Regions across Europe and Central and South America. Our goal is to provide science-based policy advice on how best to use NBS to protect future biodiversity and ecosystem services in a future climate.

FutureMARES provides socially and economically viable actions and strategies in support of nature-based solutions for climate change adaptation and mitigation. We develop these solutions to safeguard future biodiversity and ecosystem functions to maximise natural capital and its delivery of services from marine and transitional ecosystems.

To achieve this, the objectives of FutureMARES defined following goals:

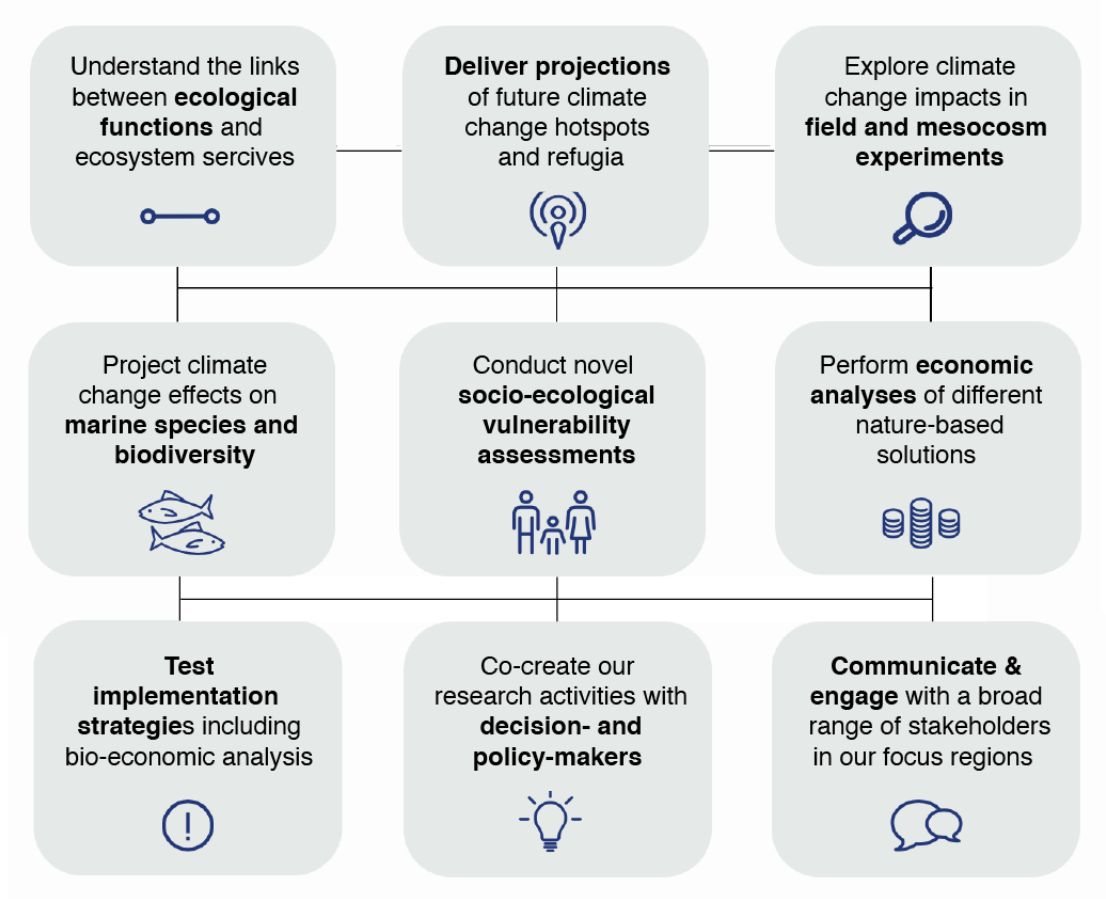
Understand the links between **ecological functions** and ecosystem sercives
Deliver projections of future climate change hotspots and refugia
Explore climate change impacts in **field and mesocosm experiments**
Project climate change effects on **marine species and biodiversity**
Conduct novel **socio-ecological vulnerability assessments**
Perform **economic analyses** of different nature-based solutions
Test implementation strategies including bio-economic analysis
Co-create our research activities with **decision- and policy-makers**
Communicate & engage with a broad range of stakeholders in our focus regions

Deliverable data	
Work Package(s) / Task(s):	WP4 - Mechanistic projections for species, food webs and habitats Task 4.1 – Projections of the impacts of climate change on seagrasses and seaweeds, and network analysis of eelgrass connectivity
Lead beneficiary:	Plymouth Marine Laboratory
Responsible author:	Robert Wilson, et al.
Contact:	rwi@pml.ac.uk
Co-authors:	Marie Maar, Dorte Krause-Jensen, Ana Queirós
Date of delivery:	10/03/2023
Deliverable type:	Report/ data sets
Date of internal approval (for the submission to EC)	13/03/2023

Involved partners

FutureMARES Project Partners: PML, AU.

Document history

Version	Date	Description
01	15/2/2023	V1.0 – Initial version, by R. Wilson, M. Maar, D. Krause-Jensen, A. Queirós
02	28/2/2023	v2.0 - Final version, by R. Wilson, M. Maar, D. Krause-Jensen, A. Queirós
03	06/03//202	V3.0 - final check by project scientific coordinator (Myron Peck)
04	10/03/2023	V4.0 – Final version by R. Wilson, M. Maar, D. Krause-Jensen, A. Queirós, implementing comments of scientific coordinator

Suggested citation for this report: Wilson, Robert, Maar, Marie, Krause-Jensen, Dorte, Queirós, Ana. (2023) Seagrass and Seaweed Future Projections. *FutureMARES Project Deliverable report 4.1*

FutureMARES receives funding from the European Union's Horizon 2020 research and innovation programme under grant agreement No 869300 "Climate Change and Future Marine Ecosystem Services and Biodiversity"

Table of content

List of symbols, abbreviations and a glossary

CC	Climate change
CMEMS	Copernicus Marine Service
CMIP6	Coupled Model Intercomparison Project (Phase 6)
DEB	Dynamic Energy Budget
DoA	Description of Action, a part of the project Grant Agreement describing the project work plan
EC	European Commission
ECS	Equilibrium Climate Sensitivity
EC GA	European Commission Grant Agreement – a contract between the European Commission and FutureMARES consortium
EEZ	Exclusive Economic Zone
EMODnet	European Marine Observation and Data Network
GA	Grant Agreement
IPCC	International Panel on Climate Change
ML	Machine Learning
NBS	Nature-based Solutions
PAR	Photosynthetically Active Radiation
SSP	Shared Socioeconomic Pathway
SST	Sea Surface Temperature
Tn.x	Task – a sub-component of a work package where “n” is a number of the work package and “x” is a number of the task within this work package
WP	Work Package

Executive summary

This report summarizes the modelling work carried out to fulfil Task 4.1 of the EU funded FutureMARES project. The overriding goals are to provide projections of the impact of climate change on seagrasses and seaweeds in European waters. Central to this was the recognition of uncertainty in future greenhouse gas levels and the response of the climate system. Climate change (CC) impacts were projected using three greenhouse gas emissions scenarios, and ecological changes were projected using outputs from multiple climate models.

Seagrasses and seaweeds are important habitats supporting marine biodiversity and are increasingly recognized as contributors to the storage of seabed organic carbon. However, these habitats experienced major losses in the 20th Century. About ⅓ of European seagrass areas have been lost due to disease, deteriorated water quality, and coastal development (de los Santos et al., 2019). All European seagrass species have been subject to losses, including *Zostera marina* (eelgrass), the dominant seagrass in the Northeast Atlantic Region, and *Posidonia oceanica*, the dominant seagrass in the Mediterranean Sea. Regarding seaweeds, a recent review of kelps identified net habitat losses in temperate regions over the past 50 years although trends vary markedly between areas (Wernberg et al., 2019).

Climate change is a threat to seagrasses and seaweeds. Rising temperatures are, for example, threatening the lower latitudinal edges of both seagrass and seaweed populations, and the iconic seagrass *Posidonia oceanica* is widely expected to decline during this century. Climate change is also affecting seaweeds in European waters, especially at the trailing edge of the distribution of species (Hawkins et al., 2008) while the leading edge of some boreal species is expanding in the Arctic (Krause-Jensen et al., 2020; Assis et al., 2022). In addition, extreme events such as heatwaves, are leading to the collapse of some North Atlantic kelp habitats (Filbee-Dexter et al., 2020). These challenges call for extra protection for these habitats by reducing stressors such as eutrophication and physical damage, as well as creating networks of marine protected areas (MPAs) which also consider future changes in habitat features projected in climate scenarios.

Alongside conservation efforts, there is a push for the expansion of seaweed farming as an industry with the potential to support several global Sustainable Development Goals if carefully carried out (Campbell et al., 2019; Duarte et al., 2022a). Seaweed farming may also revive economic growth to vulnerable coastal communities in European waters (Hasselstrom et al., 2020; Araújo et al., 2021) traditionally supported by a now dwindling fishing sector, and potentially bring carbon removal benefits (Spillias et al., 2023) although quantification of the sequestration is challenging and offsetting initiatives need to be carefully considered (Ricart et al., 2022).

If we want to increase the success of restoration (NBS1) and protection (NBS2) of seagrass and seaweed habitats, there is thus a need to identify climate-resilience to the spatial management of these activities. Specifically, it is critical that sites identified for habitat restoration and protection, and seaweed growth, are optimal and robust not only now but also in a future climate.

To enhance our understanding of these challenges and opportunities, T4.1 here provides projections of the impact of climate change on dominant habitat-forming European seaweed (the kelps *Saccharina latissima*, *Laminaria hyperborea*, and *Laminaria digitata*) and seagrass

species (*Posidonia oceanica* and *Zostera marina*) using newly developed, mechanistic ecological models across the European distributions of these species. We use 3 climate change scenarios and multiple climate models to capture the uncertainty in future climate change.

The first output of the task is a new map, produced using machine learning, of rock cover for the United Kingdom and Ireland (chapter 1). This map can be used to improve quantitative assessments of potential seaweed cover in European waters. Chapter 2 then reports an analysis of eelgrass connectivity in Danish waters to improve the identification of suitable sites for eelgrass restoration. We show that this modelling tool can identify connectivity between different eelgrass regions and thus sites most suitable for restoration.

Chapter 3 summarizes the climate change scenarios and climate models used in the future projections for seagrasses and seaweeds in chapters 4 and 5. We summarize the 3 climate change scenarios used and how a large 14 model suite of global climate models was statistically downscaled to be suitable for seagrass and seaweed modelling.

We summarize the projections of climate change impacts on the seagrass species *P. oceanica* and *Z. marina* in chapter 4. First, we summarize how an existing seagrass population model was modified so that we could model *P. oceanica* and *Z. marina*. We then show the projected impacts on seagrass biomass under 3 climate change scenarios and with the seagrass models being driven by changes from a large suite of climate models. We show that there is potential for *P. oceanica* meadows to decline dramatically this century in the absence of efforts to mitigate climate change; however, in a high-mitigation scenario *P. oceanica* meadows can potentially begin to recover in the late 21st Century. Further, we show that across the northwest European shelf, *Z. marina* populations are largely resilient to climate change, except in the most extreme scenario used.

Chapter 5 shows the projected impacts of climate change on the geographic distributions of the seaweed species *S. latissima*, *L. hyperborea* and *L. digitata*. Northward shifts of all species appear certain this century. However, while the direction of change is highly certain, we find that the magnitude of change is not, and reducing uncertainty in how European waters respond to rising greenhouse gas emissions is critical if we are to fully anticipate future changes in seaweed distributions. Importantly, we find that without significant global action on climate change the extinction of *S. latissima* and *L. hyperborea* on the Spanish and Portuguese coasts, and *L. digitata* on the French coasts is possible.

Defining the Challenge

There are two commonly used approaches to modelling the impacts of climate change on marine species. The first approach is to use statistical modelling, which uses the statistical relationship between, for example presence and absence of species, and environmental variables such as sea surface temperature and nutrients. The second approach is to use mechanistic mathematical models, which will model ecological outcomes as the emergent outcome of processes such as the influence of temperature on growth.

Mechanistic models offer the ability to provide a more realistic representation of future impacts of climate change (Kearney and Porter, 2009) and, thus, represent the developing ambition for species distribution modelling for ocean species that may lead to more robust projections (Silber et al., 2017). For many seagrass and seaweed species, the influence of temperature and other variables on key processes is now well established. It is possible,

therefore, to develop credible models that represent populations on the basis of how environmental conditions influence temporal patterns of growth rate and mortality.

Approach

Mechanistic models were developed and used to project change in the spatial distributions of seaweeds and on seagrass productivity. Projections are provided for the scenarios SSP126, SSP245 and SSP585. SSPs (Shared Socioeconomic Pathways) are scenarios developed within the core of activities of the IPCC, that express potential future progressions of greenhouse gases (O'Neill et al., 2014). These scenarios are used as the forcing in biogeochemical models simulating future ocean conditions, the outputs of which are then used to drive the models developed and employed in this task. We used multiple climate models, as physical-biogeochemical models display different sensitivity to scenarios, and using multiple models is a more robust approach to climate projections (Payne et al., 2016).

Seaweed distributions are estimated using a growth model which represents seasonal growth on the basis of temperature, light and nutrient levels. In this framework, the species move north due to rising temperatures causing mortality when temperature-driven increases in respiration exceed photosynthesis for an extended period. We modelled seagrass populations using population models which represent seagrass growth and mortality on the basis of instantaneous temperature and light.

Contribution to the project

The work in this report will feed in directly to Storylines 1, 2, 3, 5, 6, 11, 15, 20, 21, 22, 23, 25, 26, 27, 28, 29, 30, 31, 36. The projections will be useful for ecosystem modelling applied in T4.4 and will be further used in T6.1.

Dissemination and Exploitation

The projections are available through Zenodo to all FutureMARES colleagues. The seagrass and seaweed model projections will form the basis of papers to be submitted to scientific journals in 2023. One paper will provide projections of the impacts of climate change on seagrasses and a second paper will focus on wild kelp populations. The third paper will provide projections of the impacts of climate change on aquaculture and carbon dioxide removal potential (carbon sequestration).

The work in this task has been referred to in presentations by WP4 lead Ana Queirós, including talks at the General Conference of the International Atomic Energy Agency 2020, the UK Blue Carbon Conference 2021, and at COP27. This work has also underpinned stakeholder engagement at the North Devon UNESCO Biosphere. The eelgrass connectivity work was presented by Ane Pastor Rollan at the 2022 ICES WPIG Meeting and the 2021 iMarCO meeting.

1. Chapter one

1.1. Using machine learning to map rock habitat in the UK and Ireland

Kelp species require hard substrate, typically rock or boulders to attach to and grown on. Estimates of the spatial extent of kelp habitat, therefore, require maps of hard substrate cover. However, the accuracy and spatial extent of maps across Europe remain a key barrier to precise quantification of potential kelp habitat.

Rock habitat is typically mapped in a binary fashion, with rock presence or absence mapped instead of rock fraction. This creates ambiguities because it is often unclear if there is a one-to-one relationship between total rock area mapped and total area of the seabed covered by rock. Furthermore, it is often unclear if historical maps of rock cover do, in fact, relate clearly to suitable hard substrate for seaweeds and other species. For example, the European rock map produced by the European Marine Observation and Data network (EMODnet) originally used a UK hard substrate map produced by the British Geological Survey (Gafeira et al., 2010), which defined hard substrate as the presence of objects of similar size or larger than cobbles within 0.5 metres of the seabed, and a later revision dramatically reduced rock cover in the UK.

A second problem is weaknesses in spatial coverage. Currently, the EMODnet spatial map of rock extends throughout most European regional seas and coasts, with the exception of a large part of the Irish coast. Furthermore, it is unclear if habitat map coverage is sufficient to cover the coastal regions occupied by kelp. This analysis uses machine learning (ML) to map rock cover across the Irish coast using historical data for the UK and Ireland, and to point to future directions for how to use big data and ML to improve our understanding of the extent of suitable kelp habitat.

1.2. Rock mapping methodology summary

Rock was mapped in the UK and Ireland's Exclusive Economic Zones using a ML approach similar to that by Wilson et al. (2018). Gridded predictor data was derived from historical datasets. Near-coast observations of rock presence/absence were derived from EMODnet historical observations for the UK and Ireland. Rock presence/absence data for the UK shelf waters were derived from historical British Geological Survey (BGS) sediment core records in a similar way to Wilson et al. (2018), but only considering rock/boulder presence when they occur at the seabed. Rock presence was predicted using the ML algorithm Catboost (Hancock et al., 2020). Cross-validation showed that the method was able to impute rock values in new areas with high accuracy.

We identified a large number of potential predictors of rock occurrence. Bathymetry at 1/16-minute resolution was taken from the EMODnet 2020 product. A series of bathymetric properties were derived using the Whitebox software. These were edge density, maximum downslope elevation change, minimum downslope elevation change, number of upslope neighbours, tangential curvature, number of downslope neighbours, hill shade, relative topographic position, ruggedness index, elevation percentile, and downslope index. Further bathymetric properties were derived using the Python package richdem: aspect, curvature, planform curvature, slope, profile curvature. We also derived distance from the coast from the high resolution EMODnet bathymetry product.

Water clarity is likely to be predictive of rock cover due to the relationship between mud content and suspended sediment. We therefore used monthly mean light attenuation (KD490) from the OCCCI initiative (at 4km resolution). Each monthly mean from February to November was used as a candidate predictor. Rock is more likely to occur in regions with high natural disturbance to waves and tides. We therefore derived candidate predictors based on wave and tide data. Annual mean and maximum depth averaged and bottom velocity were derived from the 1.5 km resolution CMEMS product NORTHWESTSHELF_ANALYSIS_FORECAST_PHY_004_013. Data from 2019 and 2020 were used to calculate tidal velocities. Waves were accounted for by using the climatological annual maximum and annual mean significant wave height. Annual maximum was calculated as the mean of the annual maximum SWH over the period 2010-2019. We used the 1.5 km CMEMS product NWSHELF_REANALYSIS_WAV_004_015 for SWH data.

In total, 34 candidate predictors were derived. This number was reduced using feature elimination by applying a simple, backward stepwise selection approach (James et al., 2013). First, we split the data into 66% for training and the rest for testing. We started by training a model with all 34 variables, calculating validation statistics. The best 33, 32,…, 1 member(s) were iteratively evaluated by calculating the least valuable and then dropping it from the predictors. This process indicated that a model with 9 variables performed as well as any model with a greater number of variables. A model was used with the following nine predictors: average KD490 in May and June, elevation percentile of bathymetry, bathymetry, downslope index of bathymetry, climatological maximum significant wave height, climatological average significant wave height, distance from the coast, depth-averaged velocity.

Typical approaches to validating the ability of ML/statistical models to predict environmental parameters are to split the models randomly into training and test data, and to train a model on the training data and to then compare predictions with test data. However, this approach risks exaggerating the predictive performance of models, and can in fact result in concluding that models with no predictive ability have good predictive ability due to spatial-autocorrelation (Ploton et al., 2020). We therefore used a version of spatial-leave-one-out-cross validation (SLOOCV) to validate the predictive ability of the model because of spatio-autocorrelation. SLOOCV is an approach where test data is spatially separated from training data to ensure that spatio-autocorrelation does not impact estimates of predictive performance. In our case, we adapted the approach previously taken by Wilson et al. (2018). First, we divided the observations into 0.125 by 0.125-degree bins, only considering bins with at least 10 rock observations. We then iteratively moved through each 0.125 by 0.125-degree bin and created a training and test data set. The test data set are the rock observations within the bin, and the training dataset are the fully rock dataset, excluding data in the bin and within 1 degree of that bin. This resulted in 1096 cells for cross-validation. For each cell, we independently created Catboost models using that cell's training data and predicted rock cover within the cell.

Results

The cross-validation of the rock mapping method is shown in Figure 1.1. Spatial agreement between predicted rock cover and observed rock cover is reasonably high. The R^2 of the SLOOCV is 0.54. We note this is likely an underestimate of the predictive performance of the model at the spatial scale considered because of the likely considerable variance due to uncertainty in observed rock cover in heterogeneous regions caused by the binary nature of the raw data.

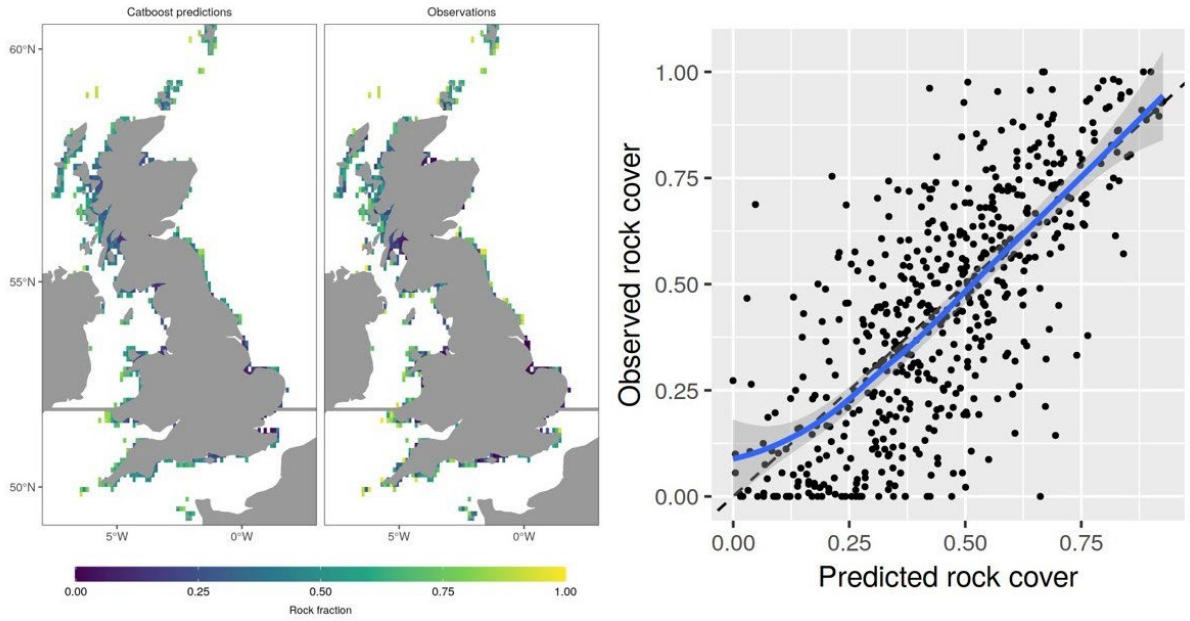

Figure 1.1: Spatial-leave one out cross validation of rock prediction using ML. Left: Mapped predictions of rock cover in each cell were carried out iteratively, where in each 0.125 by 0.125-degree coastal cell a Catboost model was trained using all available observational data, except that in the cell and within 1 degree of that cell. Results shown are averages in each cell. Right: comparisons of predicted and observed rock cover in SLOOCV.

The final rock map for the UK and Ireland is shown in figure 1.2. The total hard substrate cover in the UK EEZ was 30,100 km^2. This is approximately 10% higher than recent estimates based on EMODnet outputs 26,854 km^2 (Duarte et al., 2022b). Total hard substrate cover for the Irish EEZ was 10,800 km2. This is notably lower than recent estimates, indicating that historical rock cover maps for Ireland could over-estimate rock levels. This is in line with the reduction in rock cover observed for the UK in the EU Seamap between 2016 and 2019 due to a switch to ML-based mapping of rock habitat for the UK.

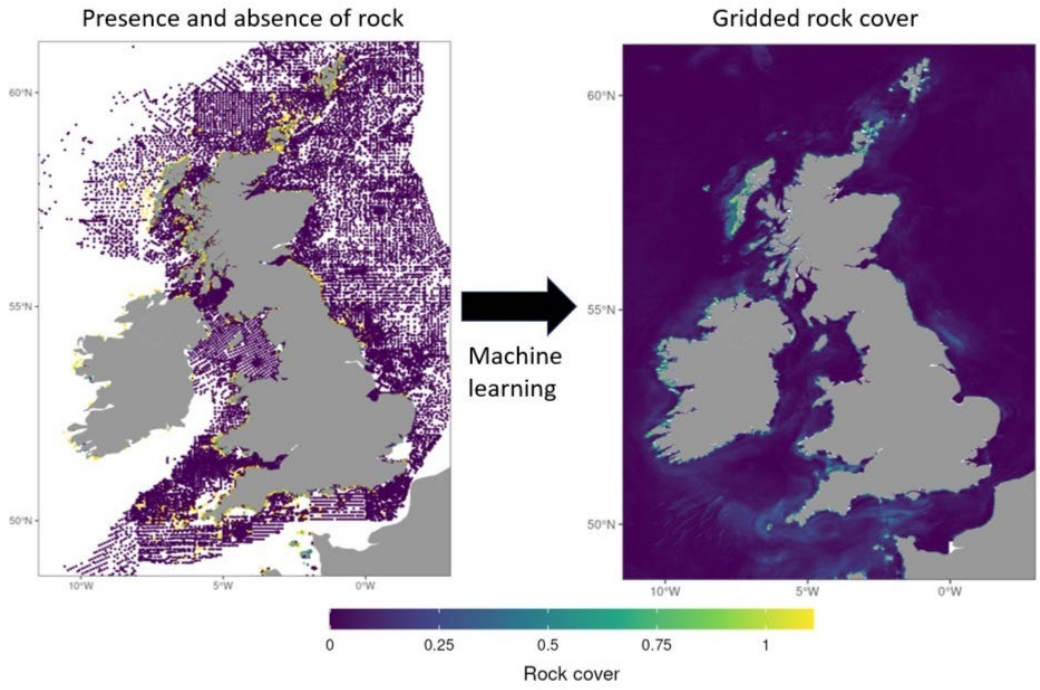

Figure 1.2: Schematic of ML method for mapping rock cover. Left: Legacy samples of presence and absence compiled from EMODnet and the British Geological Survey. Right: Predicted rock cover (fraction) using the machine learning algorithm Catboost. The model was trained using legacy rock data and environmental predictors such as bathymetry, distance from the coast, light attenuation and significant wave height.

Discussion of rock mapping

A critical caveat in the rock mapping is that the data used for the mapping potentially suffer from sampling bias. The historical sediment data from the British Geological Survey are almost exclusively from systematic surveys that aimed to objectively map seabed habitats, and we do not expect any serious sampling bias. However, the nearshore samples taken from EMODnet potentially contain sampling bias in some locations. These data are largely composed of benthic sampling which, in some cases, would have been explicitly targeting specific habitats, such as kelp. The large volume of data available from EMODnet and the relatively heterogeneous nature of benthic sampling indicates that sampling bias is not likely to have a large impact on EEZ-levels of rock cover. However, future work should focus on reducing the impact of sampling on fine-scale rock mapping.

Our analysis highlights the benefits of open data to habitat mapping across Europe. A decade ago, this work would have been extremely challenging, if not impossible to undertake. However, the continued growth in openly available benthic habitat data in EMODnet and expansion of environmental data available from services such as the Copernicus Marine Service continue to transfer how large-scale habitat mapping can be carried out. While we acknowledge that data limitations limit the ability to extend the approach used here across all of Europe, ongoing improvements in open and big data are likely to change that.

1.3. Data availability

The rock cover map is available for download at https://doi.org/10.5281/zenodo.7681699. Data are provided in netCDF format with fully self-describing meta-data.

2. Chapter 2: Eelgrass connectivity analysis to improve identification of restoration site identification

2.1. A network analysis of connected biophysical pathways to guide eelgrass (Zostera marina) restoration

Eelgrass (*Zostera marina* L.) is a subtidal marine angiosperm, a seagrass, that grows in temperate waters, often forming extensive underwater meadows. Eelgrass is widely distributed across the northern hemisphere, where it occurs in shallow sheltered settings to maximum depths ultimately set by water clarity. Eelgrass and other seagrasses are habitat forming species with an essential role in shaping the community structure and the ecosystem functioning in marine environments. They provide food resources, habitat or nursery areas for a wide range of aquatic organisms, such as invertebrates, fish and birds, thereby stimulating biodiversity. They also play a role in carbon and nutrient sequestration and coastal protection.

Seagrass meadows are one of the most affected ecosystems during the Anthropocene geological era. The North Sea and Baltic Sea, and especially Danish coastal waters, have experienced a drastic decline in eelgrass (*Zostera marina*) coverage during the past century. Around 1900, eelgrass meadows covered about 6700 km^2 while the current potential distribution area is only about 1/3 of this (Pastor et al., 2022). In some areas, the potential distribution area is far from realized, and restoration efforts are needed to assist recovery. Such efforts are challenging, and resource-demanding and careful site selection is, therefore, important. In the present study, we aim to identify the connectivity of eelgrass populations as a basis for guiding site selection for restoration (Pastor et al., 2022).

2.2. Methodology for eelgrass network analysis

In order to identify the potential connectivity of the eelgrass populations to guide restoration efforts in the Kattegat (Figure 2.1), we 1) developed a dispersal model of the eelgrass (*Z. marina*) by coupling a hydrodynamic and an individual-based model (IBM), 2) analysed the dispersal potential and connectivity of seagrass patches over time, and 3) used network analysis and calculated centrality measures to identify eelgrass patches that act as key areas promoting system connectivity. This approach can identify key sinks and keystone areas that prevent network fragmentation, pointing to where restoration efforts should be directed.

The Kattegat 3D hydrodynamic model was developed in the FlexSem framework using an orthogonal computational mesh (Larsen et al., 2020; Pastor et al., 2022). The mesh consisted of 2840 polygons with a high resolution of 200 m in the Aalborg Bay and a lower resolution of 4.5 km towards Sweden. The model implemented 20 vertical z-layers ranging in thickness from 2 m in the top 10 layers to 10 m in the bottom layers. Open boundary forcing of water level, temperature, salinity and velocities were interpolated from Copernicus Marine Environment Monitoring Service (CMEMS https://marine.copernicus.eu). Because the Copernicus data generally underestimates the salinity in the deep water, salinity and temperature data was adjusted using measured data from the Danish National Monitoring Database (ODA) https://odaforalle.au.dk. Meteorological forcing data of wind velocities, temperature, cloud cover and precipitation was downloaded from the Copernicus ERA5 hourly data (https://cds.climate.copernicus.eu). River discharges of freshwater from 14 sources were obtained from the High-resolution pan-European water model (E-HYPE, https://hypeweb.smhi.se/explore-water/). The model was run for the years 2017, 2018 and 2019, each year initialized with temperature and salinity values from the Copernicus data.

The dispersal of seed-bearing eelgrass shoots was simulated with a Lagrangian IBM coupled to the hydrodynamic model. Particles represented suspended seeds with a short dispersal phase and reproductive shoots containing seeds with a longer dispersal phase. Shoots are

positively buoyant and particles in the model drifted in the surface, whereas the seeds sink fast and disperse only a few metres around the shoots from where they are released. Particles were given different dispersal days (1, 5, 10, 20 and 30) to account for the different sinking times. The flowering season was set to range from July to September with a peak occurring in August. A total number of 200.000 particles were released in each simulation. The release was made at the beginning of each month, 20% in July, 50% in August and 30% in September. The release area was determined from the habitat model by Staehr et al. (2019). In the first scenario, we used the assumption that the historical distribution of eelgrass corresponds to the areas with a probability of >10% of encountering eelgrass (light green polygons in Figure 2.1). This map compares well with historical records of eelgrass in the area. In the second scenario, we used current eelgrass distribution shown as dark green polygons (defined as >50% probability of eelgrass cover (Staehr et al., 2019)). Particles were released randomly within the historical area as a surface release and drifted according to their assigned number of drift days.

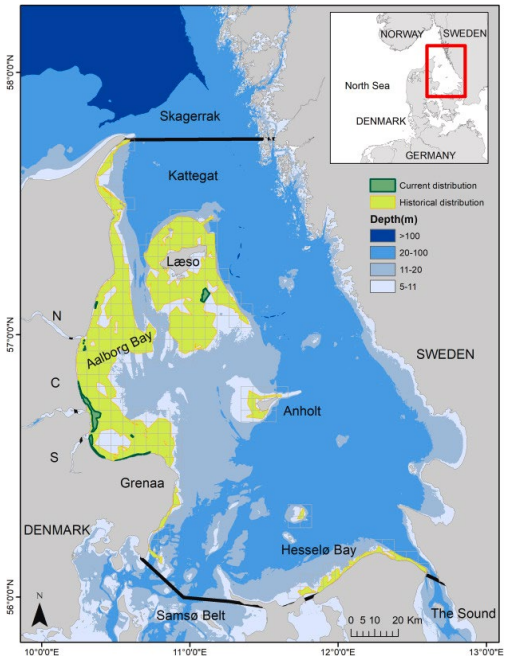

Figure 2.1: *Study area and bathymetry in the Kattegat (Denmark). Eelgrass historical distribution is shown as light green polygons and current distribution as dark green polygons. Model boundaries are shown as black lines, and the grid used for the graph theory analysis is shown in grey. Aalborg Bay is divided into 3 regions: North (N), centre (C) and South (S). From Pastor et al. (2022).*

In order to assess connectivity at a regional scale, the study area was divided into a 5 km grid. For the graph theory metrics, the potential and realized connectivity matrices were calculated, but only the grid cells with occurrence of eelgrass were used in the assessment (Figure 2.1). Potential connectivity is defined as the probability of seed transport from a release area *j* to a destination area *i*, and realized connectivity is defined as the number of seeds that are been transported from *j* to *i*. In the potential connectivity matrices, the quantity does not mean actual dispersal, but the probability that it will occur given seed production.

To identify the areas that contribute most to the distinct levels of potential and realised connectivity, three centrality measures: Betweenness, In-strength and Eigenvector centrality were calculated for each node in the network. In an ecological context, nodes with the highest betweenness scores represent fragile nodes that would otherwise fragment or disconnected parts of the network (Figure 2.2), acting as key stepping stone patches for movement. Nodes with high In-strength scores can act as important settlement areas for eelgrass seeds.

Eigenvector centrality can assist to identify the most resilient patches with strong and quality links to other patches or guide the selection of optimal protected networks with respect to population growth and persistence.

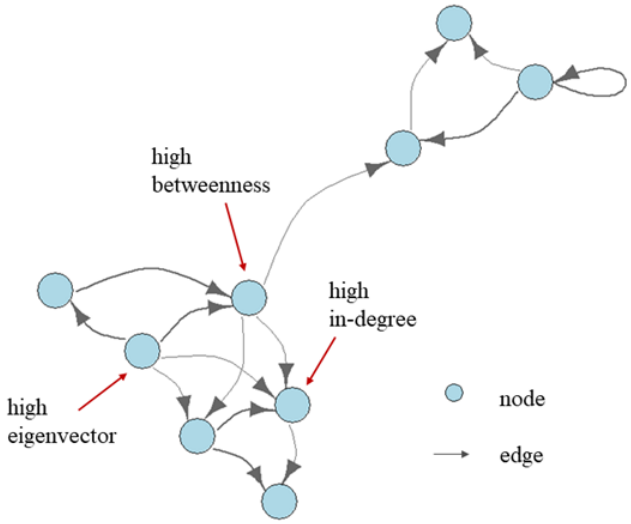

Figure 2.2: *Example of a graph represented by nodes and edges. Direction of the graph is represented with an arrow and the thickness of the arrow reflects the weight or strength of the connection. The addressed centrality measures are shown in the figure: Betweenness centrality, Degree centrality (in-degree) and Eigenvector centrality. From Pastor et al. (2022).*

Detecting communities or clusters is of great importance in biology and ecology where systems of connected elements are often represented as graphs. Using information theory concepts, *Infomap* decomposes the network into a number of clusters that can define oceanic provinces (i.e. clusters of areas) well connected internally, but with minimal exchanges of particles between them.

2.3. Results of eelgrass connectivity analysis

For the current distribution of eelgrass (dark green areas in Figure 2.1), the three centrality measures were calculated as a mean of all three years. The nodes with the highest Betweenness centrality (>0.7 probability) were located mainly in the southern part of Aalborg Bay (#58, 41 and 82, Figure 2.3a). The nodes with high In-strength centrality were located in the central part of Aalborg Bay (#82, 98 and 86, Figure 2.3b), and the nodes with high Eigenvector centrality were located in the southern part of the bay (#57 Figure 2.3c). Node 82 in the central part of Aalborg Bay was highlighted in all three measures analysed. Using the current distribution and yearly average, there were no connections between Aalborg Bay and Læso, between Anholt and Hesselo/Hesselo Bay and between Anholt and Grenaa. Very few connexions still exist between Læso and Anholt.

A total of 6 clusters were detected with the *Infomap* algorithm for the studied years (Figure 2.4). Three clusters were located along the Danish coast, one in the central and coastal area of Aalborg Bay, another one expanding to the Northern coast and the last one in Grenaa. Two other clusters were detected around the islands of Læso and Anholt and the last one was detected in Hesselø Bay.

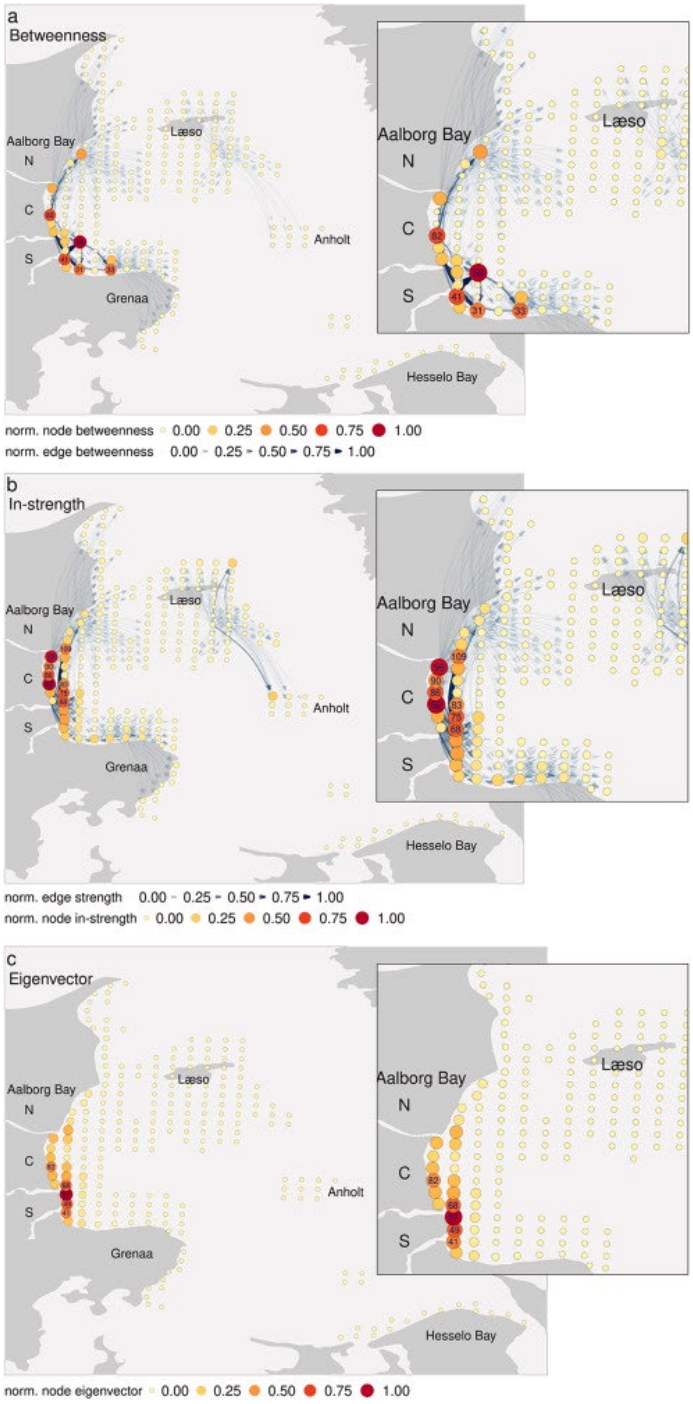

***Figure 2.3**. (a) Betweenness (b) in-strength and (c) eigenvector centrality for the simulations conducted in all three years, with a release of seeds from the current potential eelgrass distribution area. Node size and colour symbolises the normalized centrality score and edge width and colour symbolise normalised edge betweenness and strength respectively. From Pastor et al. (2022).*

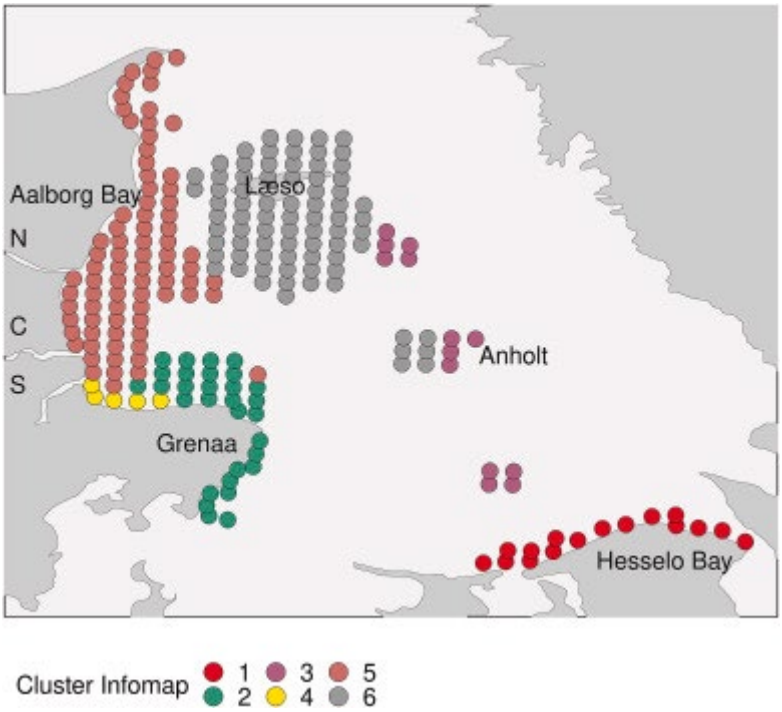

***Figure 2.4**: Oceanographic cluster detection through the Infomap algorithm for all years from the historical distribution network. The coloured dots represent the centroids from the release 5 km grid used. Dots with the same colour indicate areas that have an internal connectivity. From Pastor et al. (2022).*

2.4. Discussion of eelgrass connectivity analysis

This study investigated the dispersal and connectivity of eelgrass (*Z. marina*) in the Kattegat through an IBM to identify potential areas important for restoration from a graph theory perspective. Network analysis through graph theory provides a useful foundation for analysing connectivity because it efficiently handles very large and complex network topologies (Treml et al., 2008). Graph theory provides insights into the system's properties and identifies important or critical nodes with high in-degree (i.e. connected to many other areas) or clusters of well-connected nodes acting as bridges between distant populations (Ospina-Alvarez et al., 2020).

Using the historical and current distribution of eelgrass as a release area in the model, we were able to identify keystone areas in the network (Betweenness centrality) as well as the potential pathways for shoot transportation (edge-Betweenness) (Figure 2.3). We found a fragmentation of the current system and the loss of connections compared to the historical distribution. The results identified the central part of the Aalborg Bay as an important area for potential seed- and shoot dispersal (in-strength and eigenvector centrality measures), but this area does not have the potential to colonize bare areas in for example Hesselo Bay, Læso and Anholt. Hence, these three clusters would require restoration efforts outside Aalborg Bay to recover (Figure 2.4). Much of the shallow Aalborg Bay is currently devoid of eelgrass, although habitat conditions are suitable across the Bay and historical information documents that eelgrass was widely distributed in the area in the past.

In conclusion, the proposed modelling tools can help guide the selection of priority areas for restoration as an extra tool in the restoration toolbox. Because of their ability to buffer environmental stress and support biodiversity and climate change mitigation and adaptation, the restoration of eelgrass meadows and other seagrasses have gained increasing focus as

management actions serving multiple benefits. Therefore, all available tools should be implemented to assist manage and restore these important ecosystems (Pastor et al., 2022).

3. Chapter 3: Summary of climate change models and scenarios used for seagrasses and seaweed projections

3.1. Scenarios used for projections

The mechanistic modelling approach developed here for seaweeds and seagrasses used a large-ensemble of climate models, to increase our ability to understand how uncertainties in future climate feed through to uncertainties in ecological change.

Three climate change scenarios were used in the projections: SSP1-2.6, SSP2-4.5, and SSP5-8.5 (Figure 3.1). These represent potential future climates with both varying severity and mitigation levels, with SSP1-2.6 leading to a mean global warming of 2.0°C degrees by the end of the 21st century, SSP2-4.5 leading to 2.4°C degrees, and SSP5-8.5 leading to 4.3°C degrees (Masson-Delmotte et al., 2018). It is critical that the scenarios should not be viewed in a highly probabilistic fashion, and no particular scenario should be viewed as a "business-as-usual" scenario. We note that SSP 126 is broadly consistent with the maximum atmospheric CO_2 concentration required under the Paris Climate Agreement, which sets the ambition to "substantially reduce global greenhouse gas emissions to limit the global temperature increase in this century to 2 degrees Celsius while pursuing efforts to limit the increase even further to 1.5 degrees".

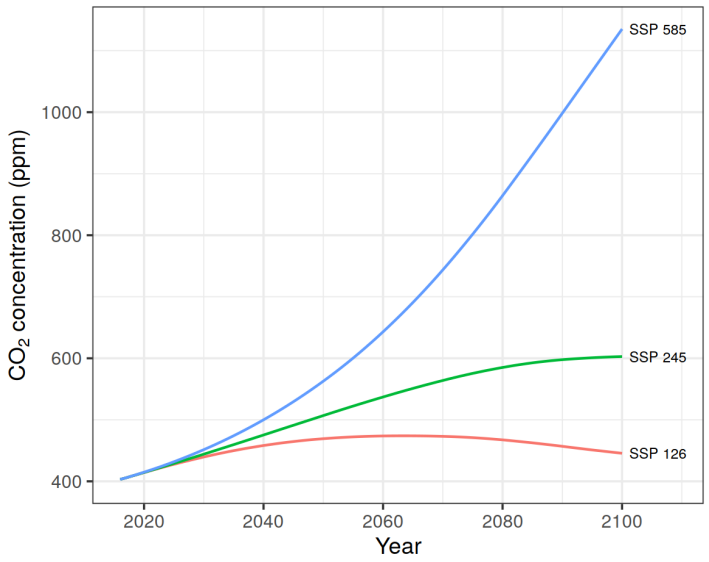

Figure 3.1: Atmospheric carbon dioxide concentrations assumed in the three climate change scenarios for seagrasses and seaweeds projections. Data taken from Meinshausen et al. (2020).

3.2. Climate models used for projections

We used a large ensemble of global climate models from the Coupled Model Intercomparison Project Phase 6 (CMIP6) for the projections (Table 3.1). These models were selected on the basis that they had available data (e.g. sea temperature and nitrate concentration) at sufficient temporal scales. Data was downloaded from the Earth System Grid Federation (ESGF) for all models.

The ensemble used was the largest available given the following requirements. Seagrass models required daily SST and shortwave radiation, and seaweed models required daily SST and shortwave radiation, and monthly nitrate concentration. Shortwave radiation was used to project future changes in PAR.

Table 3.1: List of global climate models used for projecting climate change impacts on seagrasses and seaweeds. Columns Seagrasses and Seaweeds indicate whether a model was for seagrass or seaweed projections. The equilibrium climate sensitivity (ECS) is taken from Scafetta (2022). The IPCC assesses that the credible range for ECS is between 1.5 and 4.5 °C. Models coloured red are those which were part of the FutureMARES T4.1 ensemble.

Model	**ECS (°C)**	**Reference**	**Seagrasses**	**Seaweeds**
CanESM5	5.62	Swart et al., 2019	X	
HadGEM3-GC31-LL	5.55	Roberts et al., 2019	X	
HadGEM3-GC31-MM	5.42	Roberts et al., 2019	X	
UKESM1-0-LL	5.34	Sellar et al., 2019	X	X
CESM2	5.16	Danabasoglu et al., 2020	X	
CESM2-WACCM	4.75	Gettelman et al., 2019	X	
NESM3	4.72	Yang et al., 2020	X	
ACCESS-CM2	4.72	Bi et al., 2020	X	
IPSL-CM6A-LR	4.56	Boucher et al., 2019	X	X
ACCESS-ESM1-5	3.87	Ziehn et al., 2020	X	X
CMCC-ESM2	3.57	Lovato et al., 2022	X	X
CMCC-CM2-SR5	3.52	Cherchi et al., 2019	X	
MRI-ESM2-0	3.15	Yukimoto et al., 2019	X	X
BCC-CSM2-MR	3.04	Wu et al., 2019	X	
MPI-ESM1-2-LR	3	Müller et al., 2018	X	X
MPI-ESM1-2-HR	2.98	Mauritsen et al., 2019	X	X
MIROC6	2.61	Tatebe et al., 2019	X	
NorESM2-LM	2.54	Seland et al., 2020	X	X
NorESM2-MM	2.5	Seland et al., 2020	X	X

Users of the seagrass and seaweed projections should note that a so-called “hot-model” problem exists within the CMIP6 projections. Overall, climate sensitivity is typically measured using the Equilibrium Climate Sensitivity (ECS), which is the average global air surface temperature increase when greenhouse gas emissions are doubled beyond pre-industrial levels. The credible range for ECS has been assessed to be 1.5 to 4.5 °C by the International Panel on Climate Change. However, a disproportionate number of the newer more complex climate models have ECS outside this range, as discussed by Hausfather et al. (2022). This is reflected in the ensemble used here, with many models having a high ECS. We provide the ECS values in Table 3.1 so that the users of the projections can more easily interpret the varying projected outcomes more credibly.

Three approaches have been suggested by Hausfather et al. (2022) to deal with the “hot-model” problem. First, model projections can be weighted by model skill, which was the approach taken in the most recent International Panel on Climate Change (IPCC) report. Second, model projections can be compared at the same global warming level, not at the same time. They argued this was more meaningful in a policy context where climate targets are increasingly based on global warming level. Third, they argue that a simplistic, though effective, approach is to remove the “hot” models from any ensemble. In this report, we will report all results, however we will explicitly show which projections rely on hot models and which do not.

3.3. *Bias correction approach for climate models*

A bias-corrected ensemble of CMIP6 global climate models was used to drive the seagrasses and seaweeds projections. The required temporal resolution of the ecological model inputs is hourly. However, in most cases data is not available at that resolution either for historical data or CMIP6 projections. We therefore derived inputs at the most credible resolution available.

We used the “change-factor” (Ekstrom et al., 2015) method to bias-correct all CMIP6 projections. This is a method which uses the projected change that occurs within the climate model and a present-day value for each variable is then modified to account for the change projected. The “change-factor” approach ensures that climatological conditions in the climate model for a historical reference period match those from observations.

The general approach to bias-correction was to first derive a historical and CMIP6 climatology for the period 1995-2014. This is the final 20-year historical period in the CMIP6 runs which can be directly compared with historical data. The historical climatology is viewed as giving us a credible historical baseline, and the CMIP6 model output was viewed as giving credible projections of how much that baseline will change, either in absolute or relative terms. The projections were therefore derived by calculating a change factor, which compares the CMIP6 values at any time in the projection with the day/month in the CMIP6 climatology. The value in the historical climatology is then multiplied by or added to this change factor. For example, if the temperature is 10 °C in the historical climatology for the 1st of March, and the CMIP6 scenario is projecting the temperature on 1st March 2090 to be 2.3 °C higher than the average CMIP SST for 1st March between 1995-2014, the bias-corrected SST on 1st March 2090 will be 12.3 °C. We used an additive approach when calculating the change factors for SST, and a multiplicative approach when calculating them for nitrate concentration and shortwave radiation.

Historical temperature was derived from the Global Ocean OSTIA Sea Surface Temperature. Product User Manual (CMEMS-SST-PUM-010-011). Quality Information Document

(CMEMS-SST-QUID-010-011). A daily climatology covering the period 1995-2014 was derived. The raw geographic resolution is 0.05 by 0.05 degrees. SST is available for CMIP6 at daily resolution. The CMIP6 projections were then bias-corrected by first calculating change factors (°C) for each day between 1995 and 2099 and adding these to the daily climatology.

Historical photosynthetically active radiation (PAR) was derived from ERA5 Surface net solar radiation (SWR). This is available at hourly resolution at a spatial resolution of 0.25 by 0.25 degrees. We assumed that 48% of SWR is PAR. An hourly historical climatology was calculated for each day between 1995-2014. Short-wave radiation is available at daily resolution for CMIP6. We therefore applied change factors (relative change) to the hourly climatological values by calculating the relative value of the daily CMIP6 value compared with the 1995-2014 climatological value.

Climatological nitrate concentration was derived from biogeochemical model outputs, which were adjusted using coarser gridded observational data. Model predictions of nitrate concentration typically show systematic biases (e.g. Ciavatta et al., 2016), which will limit their ability to be used as direct inputs for seaweed growth models. We therefore bias-corrected outputs from four biogeochemistry models to derive a composite gridded nitrate climatology covering European seas from the Mediterranean to the Baltic. All products are openly available from the Copernicus Marine Service (CMEMS). The 7 km North West European Shelf product “Atlantic-European North West Shelf-Ocean Biogeochemistry Reanalysis” (QUID: https://catalogue.marine.copernicus.eu/documents/QUID/CMEMS-NWS-QUID-004-011.pdf) was used for the north-west European shelf, north of Spain. For the Atlantic Spanish and Portuguese coasts we used the “Atlantic-Iberian Biscay Irish- Ocean BioGeoChemistry NON ASSIMILATIVE Hindcast” product (QUID: https://catalogue.marine.copernicus.eu/documents/QUID/CMEMS-IBI-QUID-005-003.pdf). For the Mediterranean we used the “Mediterranean Sea Biogechemistry Reanalysis” product (QUID: https://catalogue.marine.copernicus.eu/documents/QUID/CMEMS-MED-QUID-006-008.pdf). For the Baltic Sea we used the “Baltic Sea Biogeochemistry Reanalysis” (QUID: https://catalogue.marine.copernicus.eu/documents/QUID/CMEMS-BAL-QUID-003-012.pdf). Nitrate concentrations were bias-corrected using the latest version of the NOAA World Ocean Atlas nitrate concentration which are available at 1 degree resolution and at monthly temporal resolution.

Light attenuation was derived from historical satellite estimates KD490. This was downloaded at daily resolution for the years 1997-2021 from the Ocean Colour Climate Change Initiative project using version 4.3. Due to cloud cover and spatiotemporal gaps in the data, we derived a daily climatology for KD490. Light attenuation is not available from CMIP6. We therefore had to use the same climatology in all years of the projections.

3.4. Caveats and limitations of climate model output

The global climate models used for seagrass and seaweed modelling have been statistically downscaled to best represent regional climate change. However, there are critical issues that should be kept in mind by users of the seagrass and seaweeds model outputs. First, the global models have coarse spatial scale, with 1 by 1 degree being a typical horizontal resolution. A consequence is that many important spatial features are poorly resolved by the global models. For example, the Balearic Islands are not represented in most of the climate models used here, and the models largely have open sea in this part of the Mediterranean. Similarly, such processes as the Iberian upwelling can be poorly represented by the global models.

However, it is important to note that improvements in resolution of global climate models are unlikely to result in dramatically different projections. We have included models which have low- and high-resolution versions in our ensemble, and there was no indication that the magnitude of projected change differed significantly in important model regions between low- and high-resolution projections.

An important caveat to the bias-correction approach outlined above is that, while it corrects the climatological temperatures over the reference period, any differences in inter-annual variability in the CMIP6 model will be preserved. It is expected, therefore, that the procedure will push ecological models driven by the bias-corrected CMIP6 models towards that expected when using the historical data, it is not expected that they will be identical. This is due to the impact temporal variation can have on ecological and biological processes. An example of this is the explicit or implicit impacts of marine heatwaves. A CMIP6 model with greater variability in temperature than in the observational record would have more extreme temperatures, which will alter how an ecological model behaves. It is therefore important to consider the future changes within one of the climate change modelling scenarios, instead of comparing future distributions of species with their observed present distributions.

4. Chapter 4: Projecting future impacts of climate change on seagrass

4.1. Modelling approach

The mechanisms that explain why climate change can have a negative impact on seagrass populations across European waters are now reasonably well understood. Seagrass growth shows a dome-shaped relationship with temperature. As a result, for many populations living near their temperature optimum, rising temperatures will result in a decline in population growth rates and will also likely reduce overall productivity. Furthermore, temperature extremes have been linked to mortality events. However, the magnitude of potential future impacts remains uncertain and poorly quantified. Here we use a modelling approach to provide the first mechanistic assessment of the range of potential future changes that could occur to the European seagrasses *Posidonia oceanica* and *Zostera marina*.

Both species were modelled using a framework adapted from Baird et al. (2016), who modelled the seagrass species *Zostera muelleri* and *Halophila ovalis*. Within this modelling framework there are two key state parameters: above-ground seagrass biomass (SG_A) and below-ground seagrass biomass (SG_B), with the effective projected area of seagrass (A_{eff}) being a critical derived variable influencing photosynthesis. Full details of the rationale behind the model are given in Baird et al. (2016). We summarize the equations used here in Table 4.1.

The model equations used are largely unchanged from Baird et al. (2016), except for a couple of simplifications and modifications. First, we ignored nutrient uptake from sediment pore waters. This choice was necessary because of the lack of relevant data either from the CMIP6 models used to drive the projections or at relevant spatial scales in the present day. This choice is reasonable given the high levels of sediment nutrients typically experienced by seagrass populations, making nutrient limitation unlikely to be a critical long-term influence. Second, we created species-specific relationships between temperature and growth for *P. oceanica* and *Z. marina*. Baird et al. (2016) assumed a Q10 relationship between growth and temperature. Although Q10 relationships are likely suitable to depict increases in metabolic rate, growth processes are an amalgam of energy intake (from photosynthesis) and costs (from metabolism). Experimental studies on seagrasses make it clear that there is a dome-shaped relationship between growth / productivity and temperature.

Table 4.1 State parameters of the seagrass model

Symbol	Unit	Variable
E_d	Wm^{-2}	Downwelling PAR at seabed
SG_A	gNm^{-2}	Above-ground seagrass biomass
SG_B	gNm^{-2}	Below-ground seagrass biomass
A_{eff}	m^2m^{-2}	Effective projected area of seagrass
T	$gNm^{-2}s^{-1}$	Translocation rate

Table 4.2: Model equations used to represent seagrass growth and mortality

Equation	Description
$\frac{\partial SG_A}{\partial t} = \mu_{SG_A} SG_A - \zeta_{SG_A}(SG_A) - \Upsilon$	Rate of above-ground biomass growth
$\frac{\partial SG_B}{\partial t} = \mu_{SG_B} SG_B - \zeta_{SG_B}(SG_B) + \Upsilon$	Rate of below-ground seagrass biomass growth
$\mu_{SG_A} = \left[\frac{30}{5500} \times 14 \times \frac{(0, k_l - k_{resp})}{SG_A}\right]$	Pre-loss and translocation above-ground biomass growth
$k_l = \frac{(10^9 hc)^{-1}}{A_V} E_d(1 - exp(-A_{L,\lambda}\Omega_{SG} SG_A sinB_{blade}))$	
$k_{resp} = 2\left(E_{comp} A_L \Omega_{SG} sinB_{blade} - \frac{5500}{30} \times \frac{1}{14} \times \zeta_{SG_A}\right) SG_A$	Seagrass respiration
$T = \left(f_{below} - \frac{SG_A}{SG_A + SG_B}\right)(SG_A + SG_B)\tau_{tran}$	Translocation rate

4.2. Seagrass model parameter derivation

The parameters used for the *P. oceanica* and *Z. marina* population models are shown in Table 4.3. These were derived from literature values.

Table 4.3: Parameters used for seagrass populations models

Parameter	Symbol	*Z. marina*	*P. oceanica*	Units
Max. growth rate of above-ground seagrass	μ_{SG}^{max}	0.4	0.05	d^{-1}
Nitrogen-specific area of seagrass	Ω_{SG}	1.15	1.5	$(gNm^{-2})^{-1}$
Leaf absorbance	$A_{L,\lambda}$	0.67	0.79	-
Fraction biomass below ground	f_{below}	0.55	0.6	-
Translocation rate	τ_{tran}	0.033	0.0055	d^{-1}
Compensation scale PAR irradiance	E_{comp}	2.6	4.5	mol photon $m^{-2}d^{-1}$

Parameter	Symbol	*Z. marina*	*P. oceanica*	Units
Leaf loss rate	ξ_{SG_A}	0.01	0.0046	d^{-1}
Root loss rate	ξ_{SG_B}	0.01	0.00046	d^{-1}
Sine of nadir blade angle	$\sin\beta_{blade}$	0.5	0.5	-
Q10 for mortality	Q_{10}^{m}	2	2	-

We followed Baird et al. (2016) by deriving maximum growth rate from the literature, and multiplied this by 2 to account for growth at night that is not represented and by a further 2 to account for the requirement to translocate growth in leaves to the roots.

Based on published studies, we chose a maximum growth rate for *Z. marina* of 0.4 day^{-1}. The assessed studies were: Zimmerman et al. (1995), Beta-Carretero et al. (2018), Kim et al. (2013), Zimmerman et al. (2001), Palacio et al. (2007), Foldager Pedersen and Borum (1992), Dennison and Alberte (1985), Dennison and Alberte (1986), Kim et al. (2015), Zimmerman et al. (1989), Holmer and Bondgaard (2001), Lent and Verschnure (1995), Ruesink et al. (2015), Kraemer and Alberte (1995), Zimmerman et al. (1996), Zimmerman et al. (2017), Young et al. (2018), Moreno-Marin et al. (2018), Rasmussen et al. (2012), Hauxwell et al. (2006), Kaldy and Lee (2007), Mascaro et al. (2009), Kaldy (2014), Moore and Wetzel (2000).

Using published studies, we chose a maximum growth rate for *P. oceanica* of 0.05 day^{-1}. The published studies found were Pazzaglia et al. (2020), Marin-Guiro et al. (2011), Olsen et al. (2012), Kirkman and Young (1981), Ruiz et al. (2009), Savva et al. (2018), Wittman and Ott (1982), Ruocco et al. (2019), Marin-Guirao et al. (2017)

Nitrogen-specific area of seagrasses was evaluated for both species. Leaf nitrogen content varies. However, we use fixed stoichiometry in our model. We derived the nitrogen-specific area of seagrass from published studies. The derivation for *Z. marina* was as follows. Leaf density estimates vary from 22.7 (Hansen et al., 2000) to 20-30 g m^{-2} of leaf area (Olesen and Sand-Jensen, 1993). We therefore assumed a typical *Z. marina* leaf density of 25 g m^{-2}. Published estimates of *Z. marina* leaf N content (%) varies from 1.2% to 3.3% (Moore and Wetzel, 2000; Pedersen and Borum, 1993; Birget et al., 2015; Lent et al., 1995; Liu et al., 2019; Paul and Santos, 2019; Rigollet et al., 1998), with an approximate median N content of 2.1%. Therefore, if we assume a leaf density of 25 g m^{-2} and a nitrogen content of 2.1%,the nitrogen density of leaves is 0.525 g m^{-2}. Therefore, the nitrogen specific area for Z. is 1.5 $(gNm^{-2})m^{-1}$.

Nitrogen-specific area of *P. oceanica* were derived using the leaf characteristics in Fourqurean et al. (2007) and Apostolaki et al. (2018). In Fourqurean et al. (2007), mean leaf area was 148.4 cm^2 $shoot^{-1}$. Leaf mass was 0.57 g $shoot^{-1}$ and nitrogen content was 1.63 %. This results in a leaf nitrogen density of 0.63 g N m^2 and a nitrogen-specific area of seagrass of 1.6 $(gNm-2)^{-1}$ for *P. oceanica.* Using the leaf characteristics given by Apostolaki et al. (2018) for six sites, there was mean and median nitrogen-specific area of seagrass of 1.46 and 1.45 $(gNm-2)^{-1}$. We therefore chose an approximate mid-range value from the two studies of 1.5 (gNm).

The light absorbance parameter was taken from published studies for both species. Mean absorbance of *Z. marina* in the 400-700 nm range is 0.67 (Vähätalo et al., 1998). Mean absorbance for *P. oceanica* in the PAR range is 0.79 (Marín-Guirao et al., 2011b). This is mid-way between the absorptance found for shallow and deep plants in (Sandoval-Gil et al., 2014). We therefore use an absorptance of 0.79 for *P. oceanica*.

In the modelling framework, respiration is represented using the compensation scalar PAR irradiance for both species. Here we summarize published estimates of this parameter. However, this parameter was viewed as a free parameter to enable the models to provide credible depth limits of seagrass. Seabed PAR was derived from sea surface PAR and satellite estimates of light attenuation. However, in the north-west European shelf light attenuation has a positive bias (based bias estimates provided by OCCCI) and in the Mediterranean light attenuation has a negative bias. Our seabed PAR estimates are therefore likely to be too low in *Z. marina* habitats, but too high in *P. oceanica* habitats. We therefore compensated for this bias by adjusting the compensation irradiance to reduce or increase light requirements.

Our preliminary estimate of compensation irradiance for *Z. marina* was based on literature values. Olesen and Sand-Jensen (1993) estimated compensation irradiance of 29 μ mol photons $m^{-2}s^{-1}$ at temperature of 21 °C. Dennison and Alberte (1986) estimated compensation irradiance of 18 and 29 μ mol photons $m^{-2}s^{-1}$ at temperatures at 20 °C. Dennison and Alberte (1982) have compensation irradiance of 10 μ mol photons $m^{-2}s^{-1}$ at temperatures between 20 and 23 °C. P. Beca-Carretero et al. (2018) have compensation irradiance of 40 μ mol photons $m^{-2}s^{-1}$ at a temperature of 20 °C. We therefore assume that compensation irradiance is a mid-range value 29 μ mol photons ms^{-2}, ie. 2.6 mol photons $m^{-2}day^{-1}$, at 20 °C. Model simulations indicated that this resulted in credible depth limits of *Z. marina*. We therefore did not modify the value.

The starting point for *P. Oceanica* was literature estimates of the compensation irradiance. Koopmans et al. (2020) estimated this to be an irradiance of 15 and 28 μ mol photons $m^{-2}s^{-1}$ at temperatures between 17.4 and 18.8 °C. We choose the open ocean value and scale the daily parameter to 2.63 as the starting point of simulations. This resulted in unrealistically large depth limits for *P. oceanica*. This was unsurprising given that 1) the satellite light attenuation used has a negative bias and therefore too much light is reaching the sea bed, and 2) *P. oceanica* has a large depth limit of over 40m, which means any bias in light attenuation can have a very large impact on the amount of light reaching the deepest population. We therefore manually tuned the compensation irradiance using simulations, comparing the predicted depth limits around the Balearic Islands, Malta and Sardinia and ensuring the resulting predictions are close to observations. As a result, we chose a parameter value of 4.5 mol photons m^{-2} day^{-1}.

We assumed that the fraction of biomass that is belowground was equal to a medium-range values from published studies for both species. The fraction of biomass below ground for *Z. marina* varies from 0.38 to 0.77 (Dahl et al., 2018; Beca-Carretero et al., 2019; Berg et al., 2019; Rohr et al. 2018). We therefore chose to use a mid-range value of 0.55.

The fraction of biomass below ground for *P. oceanica* varies from 0.34 to 0.87 (Olesen et al., 2002; Olsen et al., 2021; Apostolaki et al., 2018). We therefore chose a value of 0.6 as a representative mid-range value.

We found insufficient published data to provide estimates of translocation rates of surface to sub-surface biomass for either species. We therefore used the same assumptions as in Baird et al. (2016).

Leaf mortality rates for both species were assumed following prior modelling studies and based on published evidence. For *Z. marina*, leaf loss rates ranging from 0.005 to 0.018 day^{-1} have been assumed in prior modelling studies (Zharova et al., 2001). We therefore assumed that the leaf mortality rate at 20 °C was 0.01 for *Z. marina*.

For *P. oceanica* we derived the leaf loss rates from Marbà et al. (1996). They estimated a mean annual loss rate of leaves of 1.67, which scales linearly to a daily loss rate of 0.0046

day^{-1}. We assumed this is the mortality rate at 20 °C. For both species we assumed that mortality rate increases with temperature at a Q10 of 2.

Based on published estimates of blade angle (Fonseca et al., 1982; Hendriks et al., 2008) we assumed that there were no inter-species differences in this parameter and that it took the same value as in Baird et al. (2016).

The mathematical relationship between temperature and growth rate was derived from the literature for both species. The relationship between growth and temperature for *P. oceanica* was taken from Bennett et al. (2022) who measured *P. oceanica* growth over multiple temperatures and sites. We used the average parameter from their estimates. We relied solely on the study of Bennett et al. (2022) due to the lack of data from other studies on growth rates below the optimal temperature of approximately 20 ℃.

For *Z. marina* we derived the temperature-growth relationship from published studies (Abe et al., 2008; Beca-Carretero et al., 2018; Hoffle et al., 2011; Kaldy, 2014; Nejrup and Pedersen, 2008; Zimmerman et al., 2019). These studies measured the growth rate of *Z. marina* across multiple temperatures, but used different units (Figure 4.1).

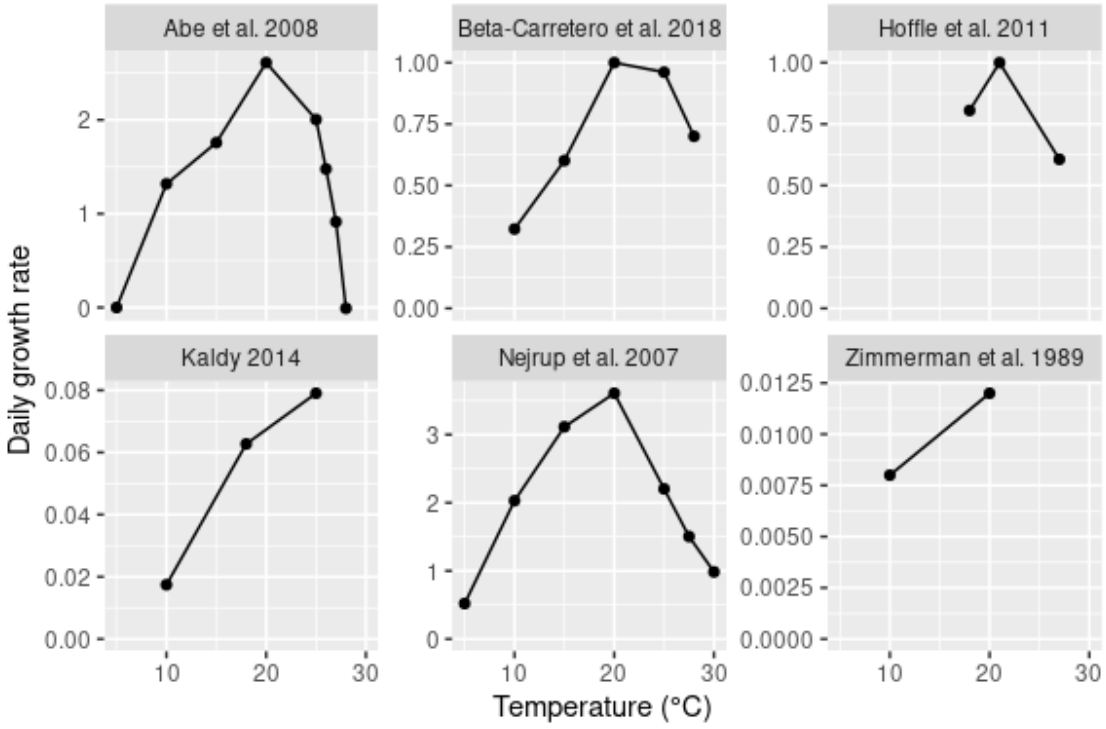

Figure 4.1. Growth rates of Z. marina from published studies used to parameterize the relationship between Z. marina growth rate and temperature. Note: growth rates scales do not have the same units in the studies, and should not be directly compared. See references for units.

Maximum growth rate of *Z. marina* (scaled to 1 at the optimum temperature) was related to temperature using the temperature cardinal model with inflexion (CTMI) from Ras et al. (2013):

$$(T - T_{max}) * (T - T_{min}) ** 2 / \left((T_{opt} - T_{min}) * \left((T_{opt} - T_{min}) * (T - T_{opt}) - (T_{opt} - T_{max}) * (T_{opt} + T_{min} - 2 * T) \right) \right)$$

The growth model was fitted to the published data using a procedure that optimized the fit between observed growth rates and modelled growth rates when the observed growth rates were rescaled to the same scale. For each potential model, the growth rate from each study was rescaled as a fraction of the maximum growth and the model growth rates were similarly

rescaled as a fraction of the model growth rate at the temperature of the maximum observed growth rate. To prevent giving excessive weight to individual studies with multiple treatments, each individual study was averaged. Figure 4.2 shows the relationship between growth and temperature for *P. oceanica* and *Z. marina*.

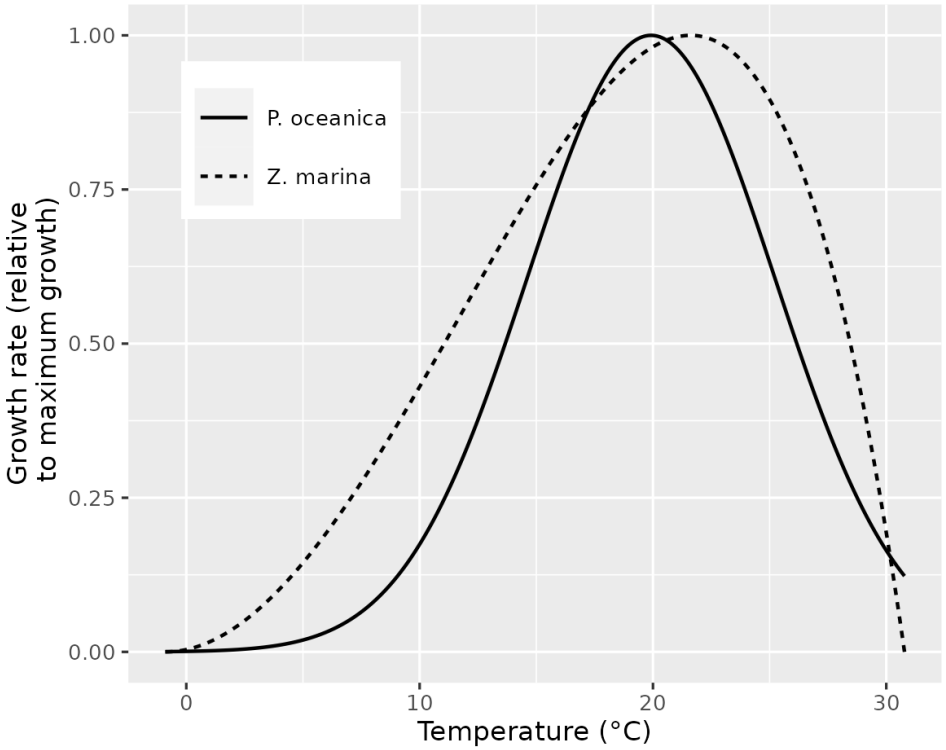

Figure 4.2. Relationship between temperature and growth rate for P. oceanica and Z. marina. Derived from experimental studies.

4.3. Seagrass model simulation grid setup

The populations of *P. oceanica* and *Z. marina* were modelled using suitable grids and appropriate spatial resolutions. In each case, a model grid was defined and populations were seeded at the start of the simulation period.

The approach taken to simulating future changes in *P. oceanica* was as follows. Our target question was the impact of climate change on existing populations, and we therefore only simulated populations in areas known to have *P. oceanica* meadows. First, we created a high-resolution map of present-day *P. oceanica* distribution. This was created using EMODnet's benthic habitat map, which compiles regional *P. oceanica* distribution maps. This was regridded initially to 100 metre resolution. We then resampled the grid to 200 metre resolution, with the bathymetry being that in the middle of each 200 by 200 metre grid cell. Model simulations then began in January 1975, which enabled sufficient spin-up to the beginning of the 1995-2100 run period used for the study. The *P. oceanica* populations were then simulated using hourly temperature and seabed PAR values from 1975 to 2100.

We took a similar approach for projecting changes in *Z. marina*, with one critical exception. Due to the large historical impact of wasting disease, *Z. marina* seagrass cover may, in some areas, be below potential levels because of the lack of mother populations. Apart from wasting disease, the reduced distribution of eelgrass relative to the past in some regions is likely due to negative impacts of multiple pressures including eutrophication and physical disturbance. We therefore sought to model potential *Z. marina* cover and biomass and how

that could change in future. We therefore first created a high-resolution map of seabed bathymetry at 500 by 500 metre resolution, but only considering areas shallower than 15 metres for the northwest European shelf as eelgrass is confined to shallow waters typically less than 10 m depth. As with *P. oceanica*, model simulations began in 1975, and the *Z. marina* population changes were driven by hourly temperature and seabed PAR from 1975 to 2100.

In all grid cells, PAR reaching the seabed was estimated using sea surface PAR, the bathymetry of the cell, and the instantaneous light attenuation.

Adjustment of surface temperatures to seabed temperature for *P. oceanica*

Mediterranean Sea temperatures can have strong vertical gradients, and surface temperatures may not reflect those experienced by the deepest *P. oceanica* meadows, which can extend to over 40 metres below the surface. We therefore adjusted the surface temperature to account for this. CMIP6 models poorly resolve the Mediterranean spatially, in particular they typically do not resolve most of the islands. We therefore assumed that the difference between surface temperature and seabed temperature in the present day would be reflective of that throughout the 21st Century. We took a simplified approach to adjusting SST to approximate that at the seafloor, by calculating the climatological difference in the present day and adding that to the projected SSTs. We derived the climatology from the CMEMS product "Mediterranean Sea Physics Reanalysis" (QUID: https://catalogue.marine.copernicus.eu/documents/QUID/CMEMS-MED-QUID-006-004.pdf). First, a monthly climatology was derived for all depths. We then calculated the difference between the temperature at each depth from the surface. These differences were then spatially interpolated to the *P. oceanica* model grid and added to the projected SSTs to estimate the projected seabed temperature.

4.4. Seagrass modelling results

Validation and tuning for P. oceanica model

As discussed in the previous section, the *P. oceanica* model's light compensation point parameter was tuned so that overall, the model provided a reasonable representation of the present-day distribution of the model. We targeted the *P. oceanica* populations across the Balearic Islands, Malta and Sardinia, as this would ensure that the model gave credible depth distributions across the model's geographic domain. Satellite light attenuation has a general negative bias across the region, and therefore seabed PAR is higher than it should be. Furthermore, we use modelled reanalysis temperature to adjust accurate satellite estimates of surface SST to provide seabed temperatures. However, the reanalysis temperatures will typically have significant spatial biases. We therefore expect the ability to represent broad-scale patterns in distribution, but due to biases in model inputs we expect poorer fine-scale patterns.

Figures 4.4-4.8 show present day modelled *P. oceanica* biomass compared with observed *P. oceanica* occurrences. Overall, depth limits of the model are in reasonable agreement with the historical maps. Notably, model inputs such as seabed temperature are too poorly resolved to further resolve features in the *P. oceanica*, as shown in the southwest of Ibiza (Figure 4.6).

Levels of surface biomass are somewhat lower than typically recorded. However, this is a result of the negative bias in the light attenuation product used to estimate seabed PAR. The impact of any bias on seabed PAR will increase exponentially with depth. Therefore, this bias

has a much larger impact on marginal deep meadows than productive shallow meadows. As a result, to get the depth distribution of *P. oceanica* meadows correct we have to over-penalize shallow meadows by increasing the light compensation point significantly.

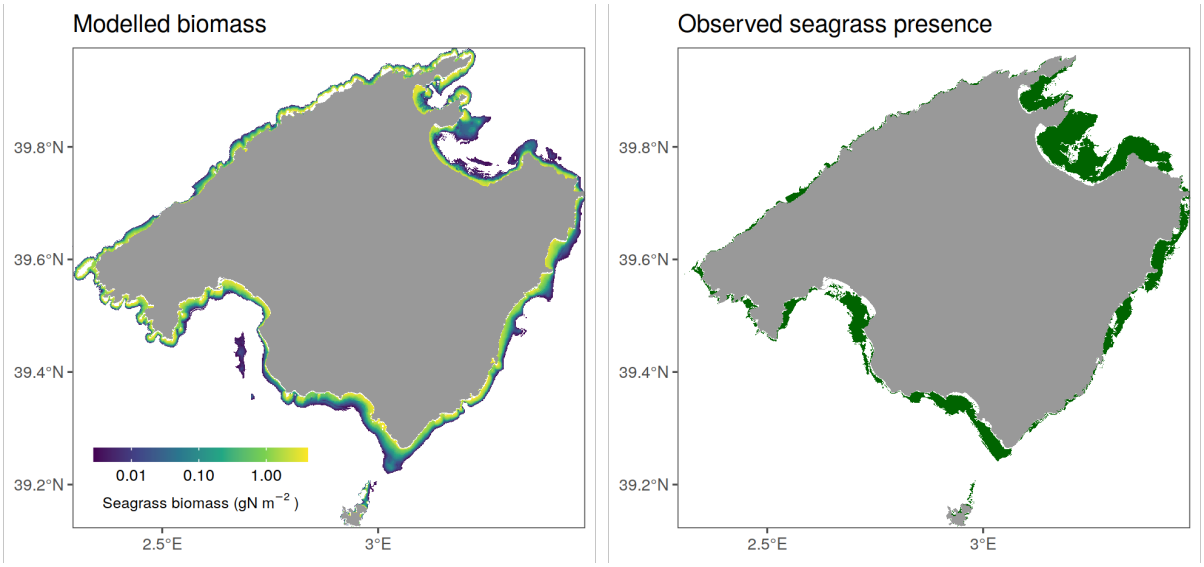

Figure 4.4. Modelled P. oceanica biomass in Mallorca and observed seagrass presence. FutureMARES storyline of interest: 25.

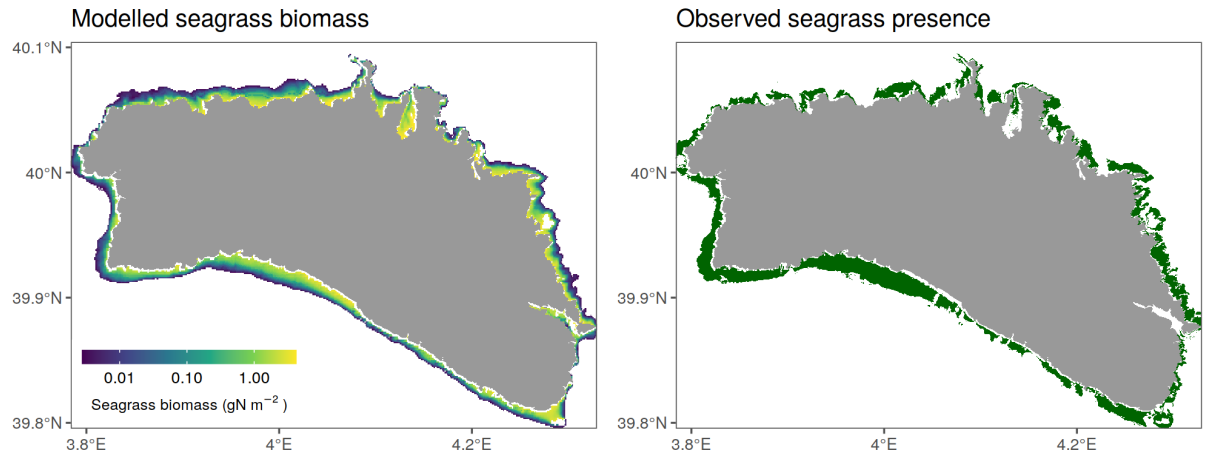

Figure 4.5. Modelled P. oceanica biomass in Menorca and observed seagrass presence. FutureMARES storyline of interest: 25.

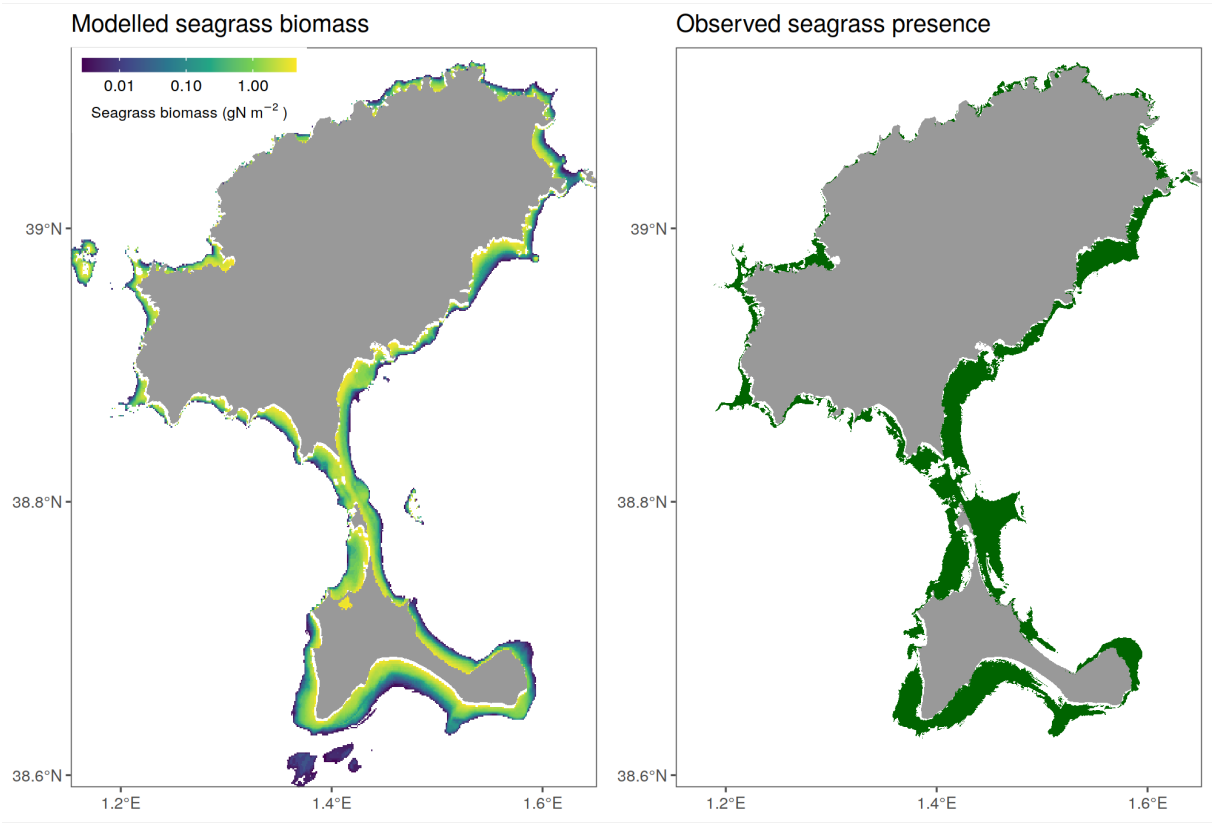

Figure 4.6. Modelled P. oceanica biomass in Ibiza and observed seagrass presence. FutureMARES storyline of interest: 25.

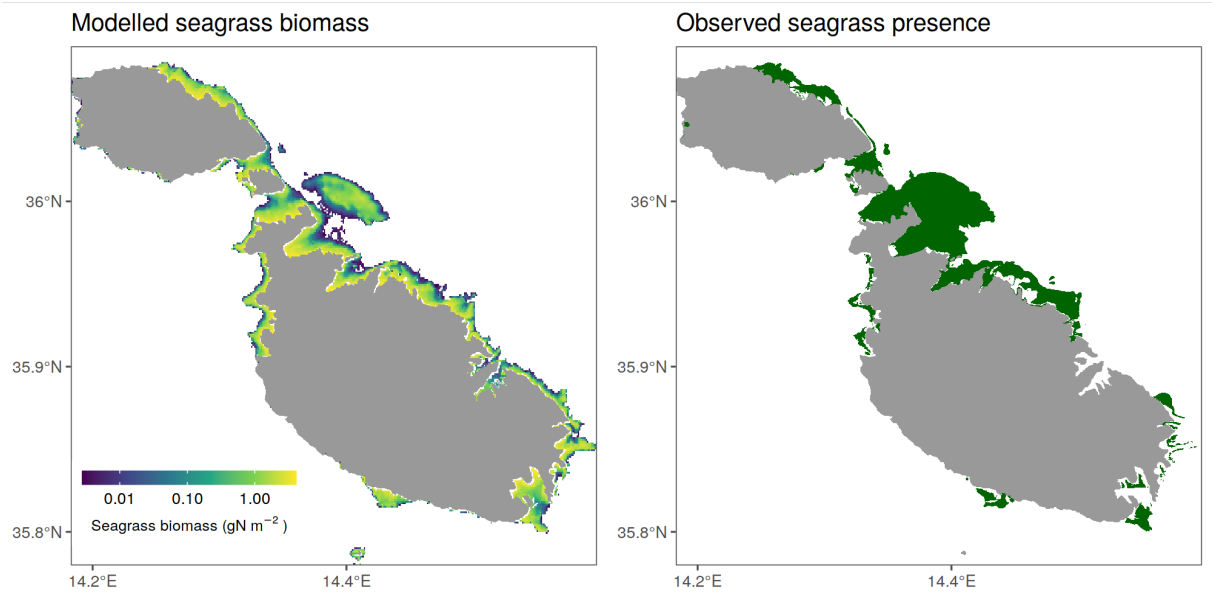

Figure 4.7. Modelled P. oceanica biomass in Malta and observed seagrass presence.

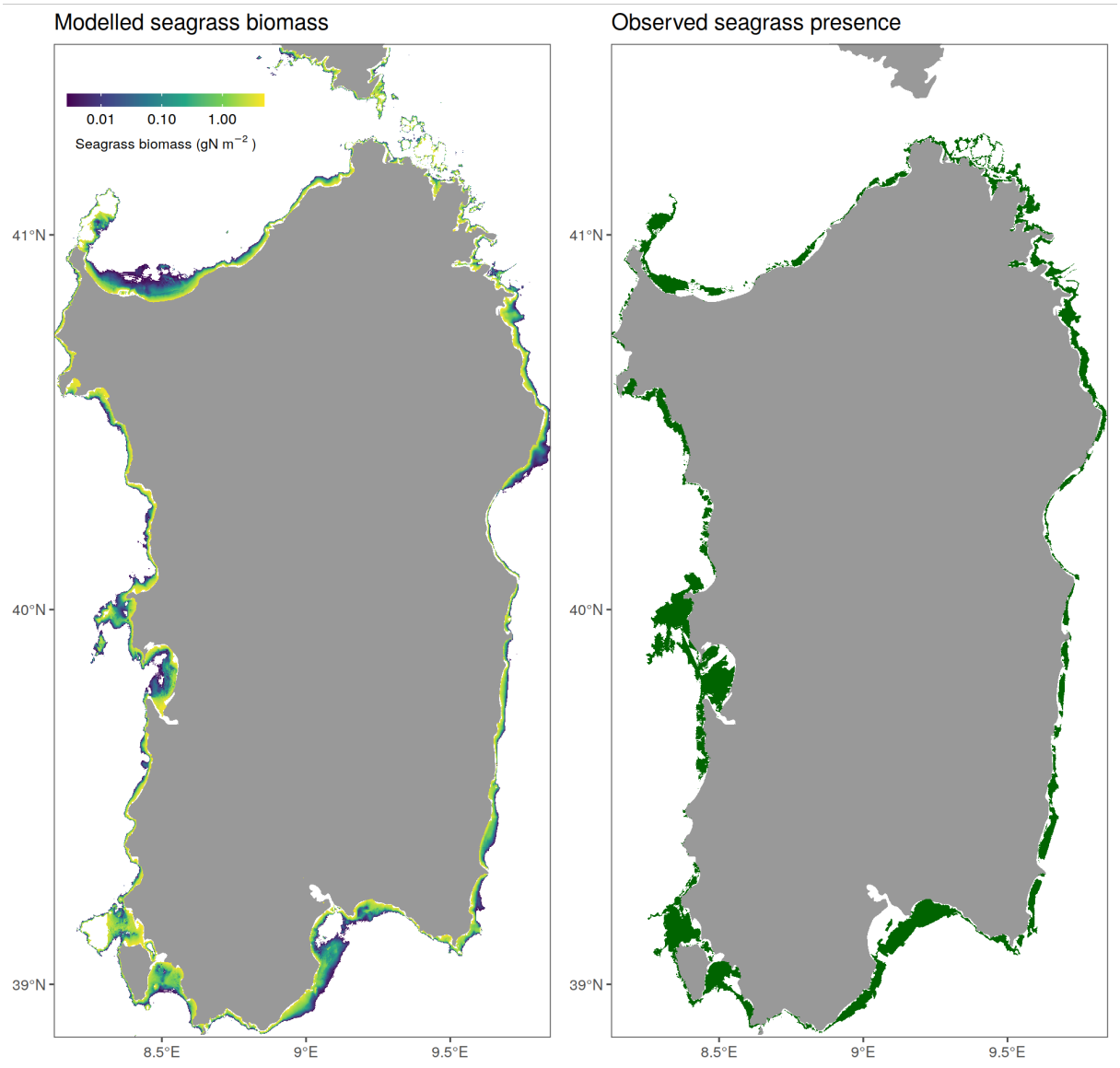

Figure 4.8. Modelled P. oceanica biomass in Sardinia and observed seagrass presence.

Projections for seagrass

P. oceanica

Figure 4.9 shows mapped changes in *P. oceanica* biomass between the present day (1995-2014) and mid-century (2040-59). And end-of-century (2080-99), while Figure 4.10 shows projected changes within Mediterranean countries Exclusive Economic Zones across the full seagrass model ensemble.

All models show clear agreement that there will be a widespread decline in *P. oceanica* biomass this century, with the projected decline increasingly dramatic in higher emissions scenarios.

Spreads within the model ensemble are large, with the magnitude of decline varying by a factor of 2 or 3 across regions in SSP 245.

A dramatic decline in the SSP 585 scenario is possible, and functional extinction is projected in some regions in some ensemble members. However, these dramatic declines are much more likely within the “hot” members of the ensemble, which have climate sensitivity above the IPCC’s credible range. Despite this uncertainty, a decline in Mediterranean wide biomass of over 70% is projected across the ensemble for SSP 585.

A number of the ensemble members within SSP 126 show increasing *P. oceanica* biomass in the second half of the century. This reflects the positive effects of reducing atmospheric carbon dioxide levels (Figure 3.1) that occur after 2060 in this scenario. The scenarios were not extended beyond 2100. However, it is notably that individual ensemble members are trending towards a reversal of climate impacts in the early 2100s.

The changes within the ensemble are notably larger if you do not exclude the “hot” models (Figure 4.10), and there is a clear relationship between impacts on *P. oceanica* and the overall equilibrium climate sensitivity of the global model used in the projections.

Z. marina

Projected changes in *Z. marina* populations are not as dramatic as those of *P. oceanica*, reflecting that these populations are unlikely to move far from their temperature optima (Figures 4.11 and 4.12). Overall, the model simulations indicate little within-ensemble agreement about the direction of change in more northern populations in SSP 126. However, there are indications that warmer and more southerly regions on the Spanish and Portuguese coasts could experience declines this century.

Widespread and potentially impactful declines only occur in the SSP 585 scenario, with clear agreement within the ensemble that *Z. marina* biomass will decline this century.

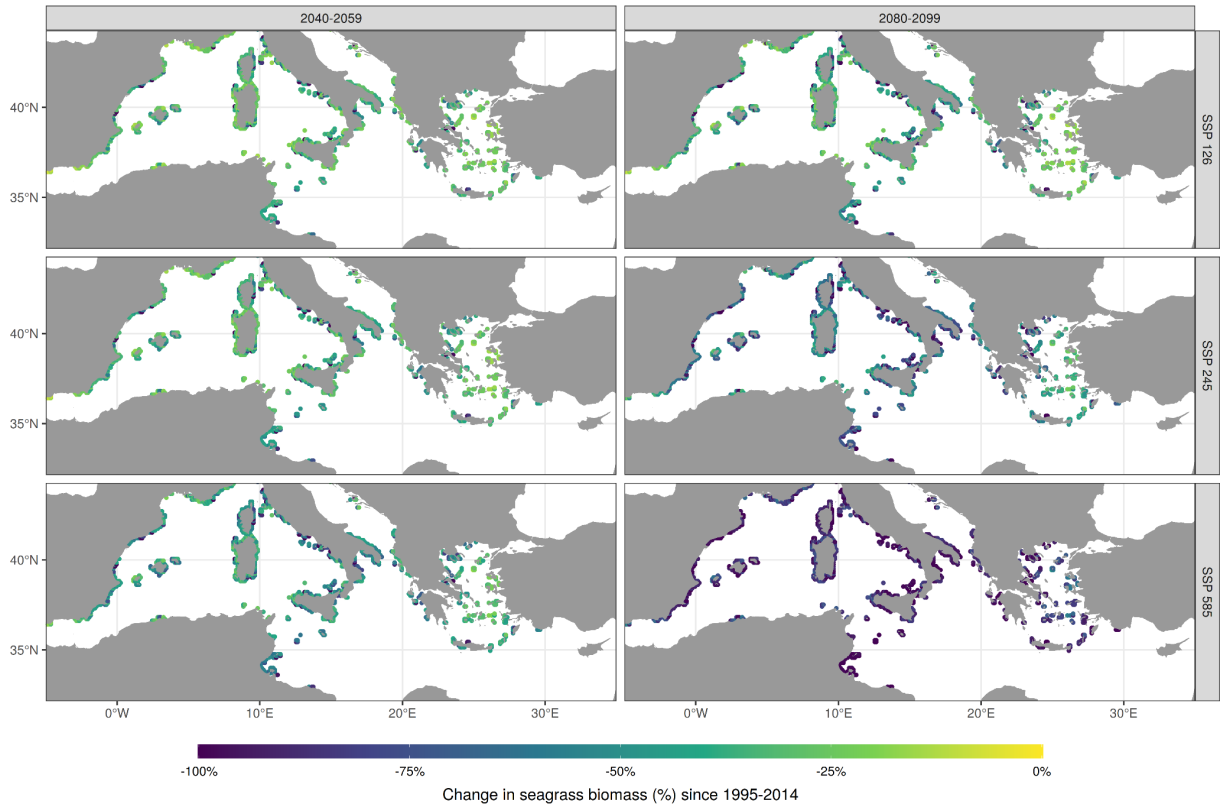

Figure 4.9: Median modelled projected changes in surface Posidonia oceanica biomass between early 2000’s (1995-2014) and mid-2100 Century (2040-59, left panels) and end-2100 Century (2080-99, right panels) under three different GHG-emission scenarios (top,

mid, and lower panels). Projections are based on a large climate model ensemble and a mechanistic seagrass population model. FutureMARES storylines of interest 25, 26, 27, 28.

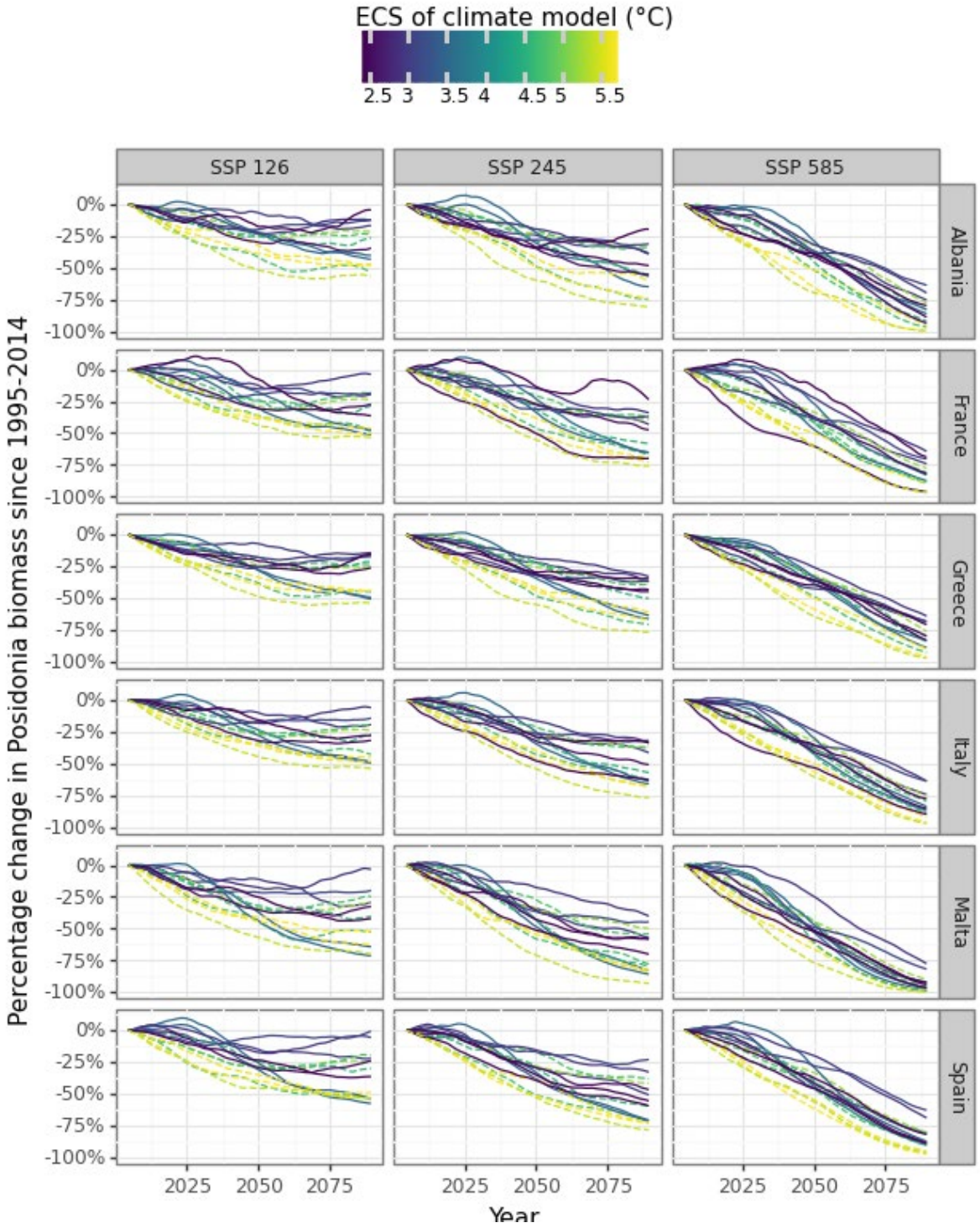

Figure 4.10: Projected changes in EEZ-wide Posidonia biomass using a seagrass population model and a large ensemble of climate models. Each line represents the outcome when driven by a specific global climate model. Line colour represents the equilibrium climate sensitivity (ECS). Global models with ECS outside the IPCC's assessed credible range (1.5-4.5) have dashed lines. Each column represents a different climate change scenario. FutureMARES storylines of interest 25, 26, 27, 28.

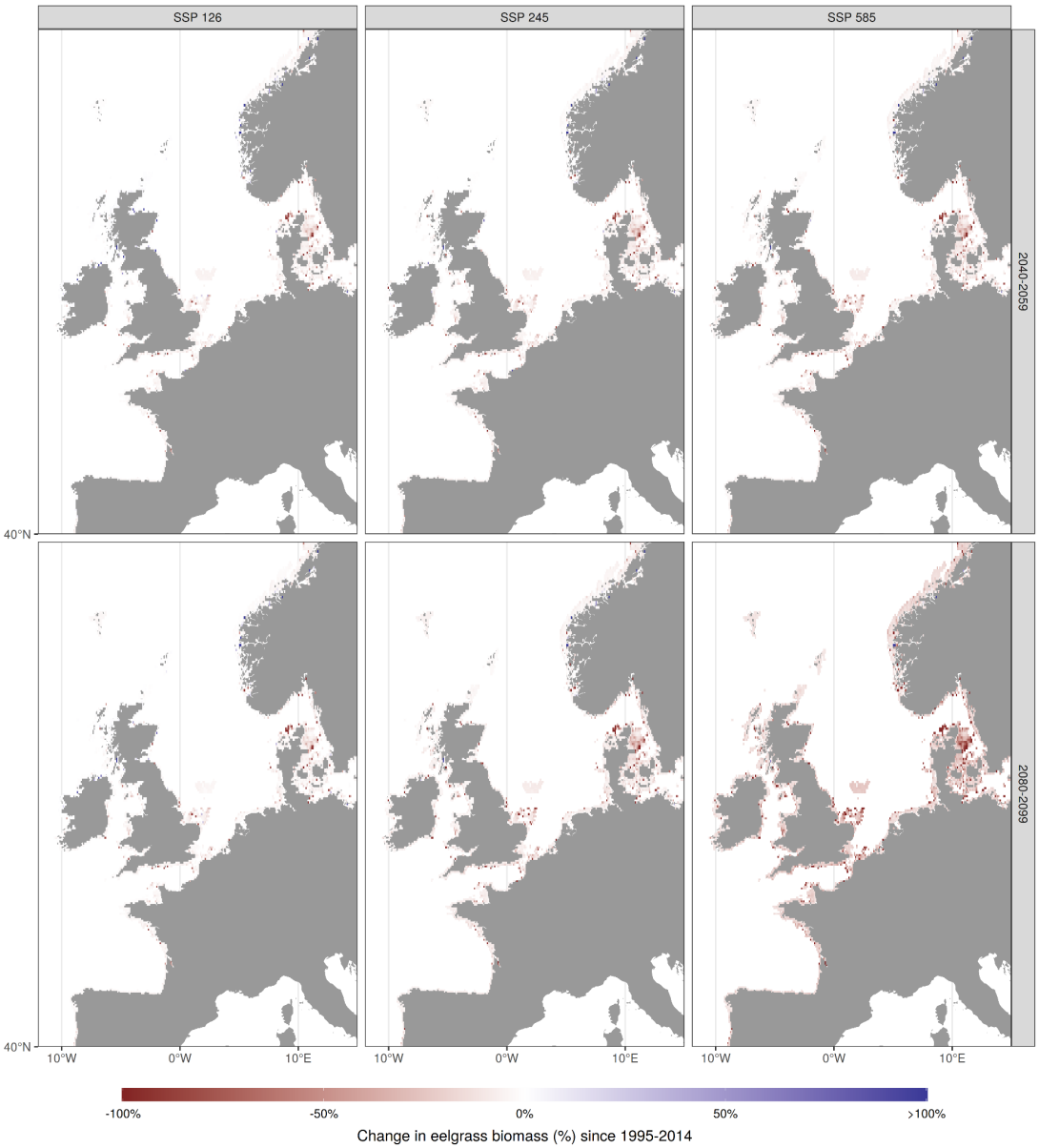

Figure 4.11: Median modelled projected changes in surface Zostera marina biomass between 1995-2014 and 2040-59 and 2080-99 using a large climate model ensemble and a mechanistic seagrass population model. FutureMARES storylines of interest: 14, 26, 51.

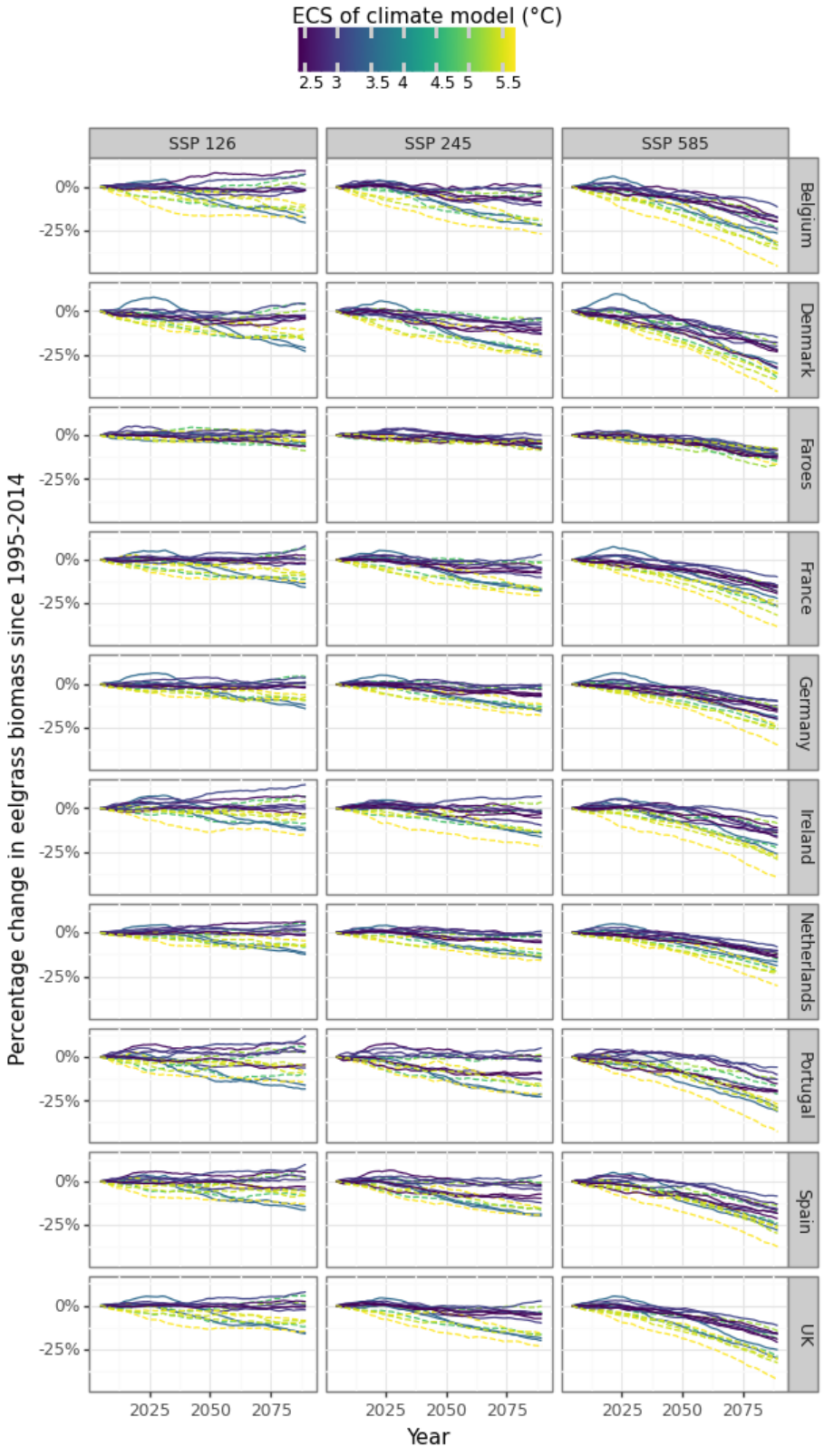

Figure 4.12: Projected changes in EEZ-wide potential eelgrass biomass using a seagrass population model and a large ensemble of climate models. Solid grey lines represent projections using individual climate models. Black lines represent the median change from models. Each column represents a different climate change scenario. FutureMARES storylines of interest: 14, 26, 51.

4.5. Discussion of seagrass projections

This study represents the first use of mechanistic models to make projections of the impacts of climate change on seagrasses in European waters. Our conclusions are reasonably clear. Climate change is likely to cause reductions in *P. oceanica* meadows across the Mediterranean Sea and in the more extreme scenario, it will cause dramatic reductions in biomass. In contrast, populations of *Z. marina* across the northwest European shelf are relatively resilient to climate change, reflecting their present-day temperature regime in relation to this species' temperature optimum.

As the first study to use mechanistic mathematical modelling to project changes in seagrass populations in Europe, we made simplifications and modelling assumptions that have the potential to result in projections that are either too optimistic or pessimistic. Here, we will discuss some key issues that need future exploration to refine the model projections.

Seagrass has a positive impact on water clarity due to its reduction in bed shear stress and thus a reduction in levels of re-suspension of sediment in the water column. We therefore expect that a reduction in seagrass cover will result in an increase in bed shear stress, reduced water clarity and less light reaching seagrass meadows. This feedback mechanism has the potential to accelerate the impacts of climate change on *P. oceanica* meadows in some locations.

Users of the seagrass model projections should be cautious when looking at fine spatial-scale changes and patterns. Because of our relatively robust understanding of impacts of climate change on growth, we can be broadly confident of the direction of large-scale changes. However, at finer scales (< 10km), model inputs are typically too poorly resolved or uncertain to provide highly credible regional projections or present-day understanding. For example, comparisons (unshown) between the light attenuation product we used had poor agreement with in-situ measurements for Danish waters, which potentially limit the ability of the model to identify specific seagrass habitats for restoration purposes. Another challenge is the often large vertical gradient in temperature between the deepest *P. oceanica* meadows and surface waters. While we used a regional Mediterranean physics model to generate seabed temperatures, the resolution of this model is too low in regions such as the Balearic Islands to have high confidence in temperatures in the deepest seagrass meadows.

Future versions of the modelling framework shown here will improve the representation of seagrass mortality, which is currently influenced largely by temperature. For example, mortality is likely to be influenced by events such as disturbance due to waves and tides, and hypoxia. Due to the reliance on CMIP6 data and the large spatial scales considered, these influences were not considered. However, future use of regional climate driving models would enable their representation and potentially significantly improve fine-scale representation of seagrass populations.

Due to the poor spatial resolution of the global CMIP6 models, we chose to assume present-day differences between surface and seabed temperatures to adjust SST to give estimated seabed temperatures for *P. oceanica*. However, modelling projections (Pagès et al., 2020) have indicated that thermal stratification will increase in the Mediterranean during this century. It is therefore plausible that some of the negative impacts of climate change on deeper *Posidonia oceanica* meadows could be partially, though not largely, offset by increasing stratification that reduces the temperature increases in deeper waters.

Our model projections used present-day light attenuation when calculating the amount of PAR reaching the seabed. However, changes in light attenuation are expected to occur due to alterations in primary production patterns and the wave regime. Historically, large declines in water clarity have occurred in much of the northwest European shelf, with increasing wave

height the likely cause (Wilson et al., 2019). Future changes of this nature could have large impacts on *Z. marina*. However, future projections of significant wave height point towards declining wave height being more likely in the 21st Century (Casas-Prat et al., 2018). The magnitude of these changes is unlikely to be significant in the Mediterranean Sea. However, a partial or large reversal of negative changes in the northwest European shelf could have significant positive impacts on *Z. marina* restoration efforts.

4.6. Data availability

The seagrass projections are available for the 3 scenarios at https://doi.org/10.5281/zenodo.7681219. Data is provided at yearly resolution in netcdf format with fully self-describing meta-data.

5. Chapter 5: Projecting future impacts of climate change on seaweeds

5.1. Summary of kelp distribution modelling

Laminaria kelp species play critical roles in coastal ecosystems across the northwest European shelf, providing hotspots for biodiversity of species that inhabit the canopy, including commercially important fish species, and making important contributions to carbon fluxes in this region (Pessorodona et al., 2022) and providing trophic subsidy to distal habitats (Queiros et al., 2019). *L. hyperborea* plays a dominant role in coastal kelp communities in this region, and there is rapidly growing interest in the use of *S. latissima* (commonly called sugar kelp) and *L. digitata* for use in growing aquaculture and carbon dioxide removal (CDR).

However, climate change is now impacting kelp communities, with marine heat waves clearly linked to mass mortality events at the population limits of some species in the North Atlantic region (Filbee-Dexter et al., 2020). Critically, statistical models (which use correlations between present-day distributions of species and environmental variables to project future changes) indicate that large future changes are likely to occur, and the extinction of *S. latissima* and *L. hyperborea* in Spain and Portugal, and *L. digitata* in France is possible this century (Assis et al., 2018). However, statistical-based models ignore physiological constraints on the response of species to environmental conditions, and are not expected to produce reliable results in long-term projections (Kearney and Porter, 2009).

The present-day geographic distributions of *S. latissima*, *L. hyperborea* and *L. digitata* are shown in figure 5.1. The southern limits of *S. latissima* and *L. hyperborea* are similar, with populations existing on the northwestern Spanish and mid-Portuguese coasts, whereas the southern limit of *L. digitata* is on the western coast of France (Assis et al., 2018).

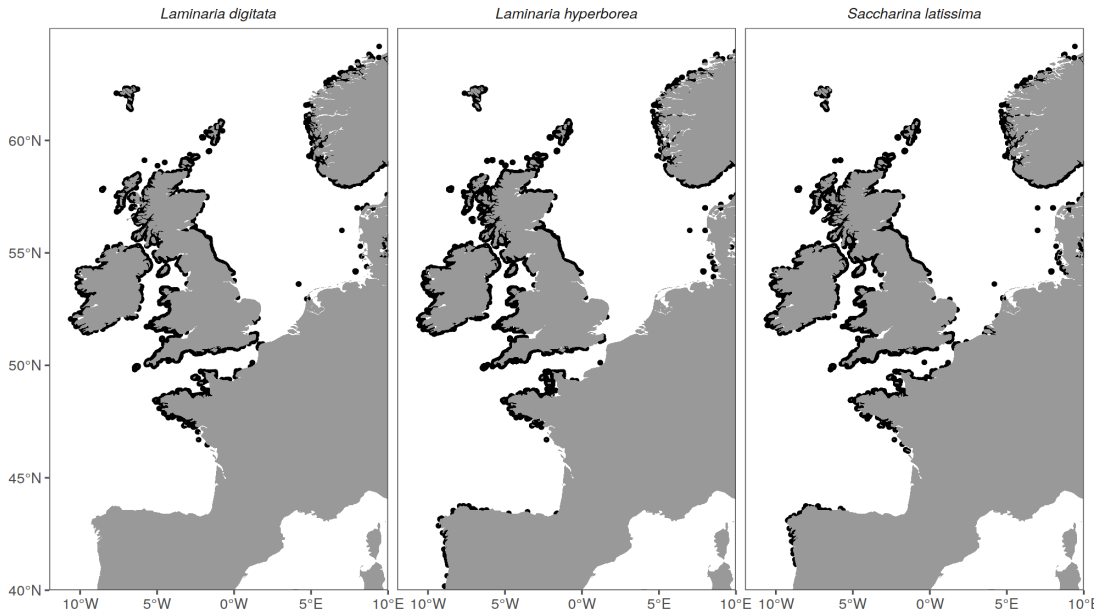

Figure 5.1: Present-day distribution of L. digitata, L. hyperborea and S. latissima. Records of observed occurrences compiled by Assis et al. (2020) are shown. Note: there are probable false positives due to mistakes in biogeographical databases. For example, species occurrences in the eastern North Sea are highly improbable due to the lack of hard substrate. Furthermore, L. hyperborea occurrences on the northeastern coast of Spain are likely due to errors in databases.

Here, we use a mechanistic modelling framework to project future changes in kelp distributions in the 21st Century. We take an ensemble approach that accounts for uncertainty in both future greenhouse gas emissions and the response of the climate system to those emissions.

Future changes in the geographic distribution of the kelp species *Saccharina latissima*, *Laminaria hyperborea* and *Laminaria digitata* were projected for the northwest European shelf. The innovative modelling approach taken uses a dynamic energy budget model (DEB) to explicitly model seasonal growth of kelp on the basis of environmental conditions. The biogeographic limits of each species are determined by whether an organism's energy reserves will be depleted, which is linked either with mortality or low-reproductivity.

Table 5.1 provides details of the climate model ensemble used to drive the kelp models. A total of 9 models were used for projections. 2 models, MPI-ESM2 and NorESM2, were available at different spatial resolutions. We provide those outputs in the supplementary data, but only report results from the higher resolution models here. Bias-corrected projections of SST, PAR and nitrate concentration were taken from the climate models for the kelp projections. See chapter 3 for full details for the derivation of climate model driving data.

Table 5.1: List of climate models used for projecting future kelp distributions. Columns indicate whether the model was available for a specific Shared Socioeconomic Pathway (SSP)

Model	SSP 126	SSP 245	SSP 585
ACCESS-ESM1-5	Y	Y	Y
CMCC-ESM2	Y	Y	Y
IPSL-CM6A-LR	Y	Y	Y
MPI-ESM1-2-HR	Y	Y	Y
MPI-ESM1-2-LR	Y	Y	Y
MRI-ESM2-0	N	N	Y
NorESM2-LM	N	Y	Y
NorESM2-MM	Y	Y	Y
UKESM1-0-LL	Y	Y	Y

5.2. Modelling approach to seaweeds

Mechanistic models have rarely been used to understand the biogeography of kelp species due to the historical lack of data required to create a complete set of robust parameter estimates. However, in recent years a growing body of literature has used growth models to understand the potential for seaweed aquaculture across European seas for sugar kelp (*S. latissima*). This growth model approach has been used to map the potential of seaweed aquaculture across European waters (Westmeijer et al., 2019). Here we extend this approach to develop a mechanistic niche model where the occurrence of a species is determined by its annual growth and whether kelp can survive without depleting their energy reserves.

The foundation model used is that of Broch et al. (2012), who used a dynamic energy budget model (DEB) to model seasonal growth of individual *S. latissima* organisms. The approach of Broch et al. (2012) explicitly divides kelp biomass into structural biomass and reserve biomass. This enables a proper understanding of seasonal growth of kelp, for which growth is not entirely dependent on instantaneous conditions, and which build up large carbohydrate reserves during summer and nutrients during winter. Here, we made minor adaptations to the model of Broch et al. (2012) for *S. latissima* and extended it to *L. hyperborea* and *L. digitata*.

In the approach taken, annual growth of individual kelp is modelled, which enables us to understand rates of productivity and how they might change in future. Second, the annual growth model can explicitly model death of kelp due to the depletion of energy reserves. We can therefore identify how patterns of modelled kelp mortality will determine the future of kelp biogeography.

Model starting point and modifications

The DEB models used for kelp are based on Broch et al. (2012), who modelled seasonal growth of sugar kelp based on the following environmental variables: temperature, irradiance, water current speed and nitrate concentration. Minor modifications were made to this model for *S. latissima* and parameterizations were created for *L. hyperborea* and *L. digitata*. Full details of the model were given in Broch et al. (2012). Here we summarize modifications to the Broch at al. approach.

Broch et al. (2012) included the influence of water currents on nutrient uptake. This influence was excluded from the model because of difficulties in acquiring reliable data in the present day and the lack of velocity data from the CMIP6 projections.

The Broch et al. (2012) model did not have a mechanism for kelp mortality. Mortality within a DEB model is typically related to reserves, with death occurring when kelp crosses a lower threshold. We deal with mortality as follows. First, following Broch et al. (2012) we allow “extreme carbon limitation”. When reserves fall to their “minimum” levels we initially allow kelp to use structural mass to fuel respiration requirements. However, extreme carbon limitation is only allowed to reduce the total size of the structural mass of the kelp to a certain extent, and we assumed that once more than 5% is lost the kelp will die.

An additional model mechanism was added for the *L. digitata* model. Model simulations indicated that the Broch et al. framework was unable to successfully extend *L. digitata* to the southern Brittany coast without simultaneously extending it to the Spanish and Portuguese coasts. However, recent work has indicated that instantaneous growth rates of *L. digitata* and *S latissima* are dependent on temperatures experienced during previous growth phases, with individuals grown at lower temperatures experiencing higher growth rates at high temperatures (i.e. ecological stress memory, Scheschonk et al. (2022)). We therefore adjusted the *L. digitata* model so that it tracks the average temperature experienced when kelp fronds actually grew, which is significantly lower on the Brittany Coast than the northern Portuguese coast. We then assume that photosynthetic rates were lower for individuals grown at higher temperatures.

The model used three state variables (Table 5.2): frond area *A* (one side, projected area), nitrogen reserves *N* and carbon reserves *C,* with the *L. digitata* model having a fourth state variable: T_{exp}, the average temperature kelp was exposed to during frond growth. Area *A* is measured in dm^2, while *N* (resp. *C*) is measured in g N (resp. g *C*) per gram structural mass (sw). By structural mass, we mean the mass of the kelp frond minus the water and the nitrogen (*N*) and carbon (*C*) reserves. Note that we actually model only the kelp frond.

Table 5.2: State variables used in kelp models

Symbol	Unit	Description
A	dm^2	Frond area, state variable
C	$gC(gsw)^{-1}$	Carbon reserves, relative to W_s, state variable
N	$gN(gsw)^{-1}$	Nitrogen reserves, relative to W_s, state variable
μ	day^{-1}	Specific growth rate, derived variable
W_w	g	Total wet weight of sporophyte, derived variable
W_d	g	Total dry weight, derived variable
W_s	g	Dry weight of structural mass, derived variable
β	$gO_2dm^{-2}h^{-1}(\mu mol\ photons\ m^{-2}s^{-1})^{-1}$	Photoinhibition parameter, auxiliary variable
P_S	$gO_2dm^{-2}h^{-1}$	Photosynthesis parameter, auxiliary variable
I	$\mu mol\ photons\ m^{-2}s^{-1}$	Irradiance (PAR), environmental variable
T	°C	Water temperature, environmental variable
T_{exp}	°C	Average temperature frond exposed to during growth. *L. digitata* only parameter.
N	$mmol\ L^{-1}$	Nutrient concentration, environmental variable

The model follows DEB theory and makes the assumption that the structural mass and each reserve has separate and fixed chemical compositions, but overall, the C/N ratio will vary. Growth and composition of kelp in the models are influenced by the following: temperature (*T*), irradiance (*I*), and nitrate concentration (*X*) in the water. As in Broch et al. (2012), we assume that the species have “flat” absorption in the photosynthetic range 400–650 nm, so only consider irradiance without taking into account the spectral distribution of light. This is a reasonable assumption, and furthermore we are only able to capture irradiance from CMIP6 projections. The main model equations, with a short description of their meaning, are listed in Table 5.3.

Table 5.3: Model equations used for kelp models.

Equation		Description
1	$\frac{dA}{dt} = (\mu - \nu)A$	Rate of change of frond area
2	$\mu = f_{area} f_{photo} f_{temp} \left\{1 - \frac{N_{min}}{N}, 1 - \frac{C_{min}}{C}\right\}$	Specific growth rate
3	$f_{area} = m_1 \, exp\left(-\left(\frac{A}{A_0}\right)^2\right) + m_2$	Effect of size on growth rate
4	$f_{temp}(T) = (T - T_{max})(T - T_{min}) \cdot 2\Big((T_{opt} - T_{min}) \cdot \big((T_{opt} - T_{min}) \cdot (T - T_{opt}) - (T_{opt} - T_{max}) \cdot (T_{opt} + T_{min} - 2 \cdot T)\big)\Big)$	Effect of temperature on growth
5	$f_{photo}(n) = a_1 \left[1 + sgn(\lambda(n))\lvert\lambda(n)\rvert^{\frac{1}{2}}\right] + a_2$	Seasonal influence on growth
6	$\nu(A) = \frac{10^{-6} \, exp\,(\varepsilon A)}{\left(1 + 10^{-6}(exp\,(\varepsilon A) - 1)\right)}$	Frond erosion
7	$\frac{dN}{dt} = k_A^{-1} J - \mu(N + N_{struct})$	Rate of change in nitrogen reserves
8	$J = J_{max} \frac{X}{K_X + X}\left(\frac{N_{max} - N}{N_{max} - N_{min}}\right)$	Nitrate uptake rate
9	$\frac{dC}{dt} - k_A^{-1}\left[P(I,T)(1 - E(C)) - R(T)\right] - (C + C_{struct})\mu$	Rate of change in carbon reserves
10	$P(I,T) = P_S\left(1 = exp\left(-\frac{\alpha I}{P_S}\right)\right) exp\left(-\frac{\beta I}{P_S}\right)$	Gross photosynthesis
11	$P(I,T) = P(I,T)(0.06T_{exp} + 1.6)$	Additional adjustment of photosynthesis in *L. digitata* for temperature history
12	$R(T) = r_1 Q_{10}^{\frac{(T - T_1)}{10}}$	Temperature dependent respiration
13	$E(C) = 1 - exp\,[\gamma(C_{min} - C)]$	Carbon exudation

We carried out an extensive literature search to identify inter-species differences between *L. hyperborea* and *S. latissima*. The starting point of the model parameter sets was the work on *S. latissima* by Broch et al. (2012). We found no evidence of inter-species differences or improved parameterizations; we used the same parameters as Broch et al. (2012). The critical differences we found were in maximum growth rate, apparent seasonal growth strategy and the influence of temperature on growth and likely photosynthesis. *L. hyperborea* appears to have a growth strategy that involves slower overall growth rates and a greater reduction in growth during summer than *S. latissima* (Lühning, 1979). However, for *L. hyperborea* the relationship between growth and temperature appears to be broadly similar to that of *S. latissima,* which reflects its similar geographic distribution.

The relationship between temperature and growth rate was derived from the work of Bolton and Lüning (1982) who calculated specific growth rates across a temperature range of 0-23 °C for each species under the same set of controlled conditions. The relationship between temperature and growth is different from that in Broch et al. (2012) for *S. latissima*, which assumed that *S. latissima* could not grow at temperatures above 19 °C. However, extensive evidence indicates that this is not the case, with experimental work growing *S. latissima* at 20 °C. Equation 4 (Table 5.3) was fitted using the data of Bolton and Luning (1982) for the three species, and optimal temperature for growth of the species were 14.25 °C, 14.96 °C and 10.4 °C for *S. latissima*, *L. hyperborea* and *L. digitata* respectively.

We carried out an extensive search of published values of growth rate (day^{-1}). Published studies assessed for *L. hyperborea* were Dring et al. (1996), Bolton and Luning (1982), Kregting et al. (2013), Sjotun et al. (1996). For *L. digitata* the following studies were assessed: Liesner et al. (2022), Bolton and Luning (1982), Millar et al. (2020), Dring et al. (1996), Makarov et al. (1996), Pedersen et al. (2010), Kregting et al. (2015), Liesner et al. (2022), Kregting et al. (2016), Ageuilera et al. (1999), Schmid et al. (1999), Wilson et al. (2020), Nitschke and Stengel (2014). Published values for *S. latissima* were found in Chapman et al. (1978), Dring et al. (1996), Qi and Rorrer (1994), Iniguez et al. (2016), Zhi and Rorrer et al. (1996), Olischlager et al. (2017), Gerard (1988), Forbord et al. (2021), Freitas et al. (2016), Azevedo et al. (2016), Stedt et al. (2022), Nielsen et al. (2016), Luning and Fortes (1980), Makarov et al. (1999), Forbord et al. (2020), Li et al. (2020), Bruhn et al. (2016), Stedt (2017), Fieler et al. (2021), Grandorf (2019), Aguilera et al. (2019), Fossberg et al. (2018), Nepper-Davidsen et al. (2019), Mattson et al. (2021), Bolton and Luning (1982).

This review showed that the maximum published growth rate was 0.18 day^{-1} for *S. latissima* (Chapman et al., 1978), 0.07 day^{-1} for *L. hyperborea* (Dring et al., 1996) and 0.13 day^{-1} for *L. digitata* (Liesner et al., 2022). The figure for *S. latissima* is the same as the assumption in the Broch et al. Model. Within the model, maximum growth rate is determined by the m1 and m2 parameters. We therefore used the Broch et al. (2012) parameters for *S. latissima* and multiplied them by 0.13/0.18 for *L. digitata* and by 0.07/0.18 for *L. hyperborea* to provide maximum growth rates that are consistent with published maximums.

Respiration rates are poorly constrained for the species. Therefore, we made minor modifications to the respiration parameters for each species to ensure the geographic distribution of each species related clearly to that of predicted kelp survival.

A minor modification was made to the model specifically for *L. digitata*. Model experiments indicated that modelling growth purely from instantaneous environmental conditions could not ensure that *L. digitata* could exist on the western French coast, but not on the Spanish and Portuguese coasts due to their similar average conditions. However, frond growth largely occurs in winter and spring when temperatures are much lower on the French coast than the Spanish coast. Experimental work shows that *L. digitata* growth at lower temperature has higher photosynthetic rates than when growth at higher temperatures. This provides an explanation for the occurrence of *L. digitata* on the western French coast, but absence on the Spanish and Portuguese coasts. Following recent (Liesner et al., 2020) and historical work (Davison et al., 1991) which suggests lower growth temperature can increase photosynthetic rate, we used a simplified equation (equation 11, table 5.3), which will reduce photosynthetic rates for *L. digitata* when growth temperatures are higher. The model tracks a state variable, T_{exp}, which is the average temperature experienced across the frond during growth.

Kelp simulations description

New frond growth of juvenile or adult kelp begins from late winter to spring. We therefore simulated an annual cycle of growth for each month from January to the end of December through a full 12 months of growth. New fronds were seeded at the start of January using the same starting conditions as in Broch et al. (2012): A(0) = 0.1, C(0) =0.3, N(0) = 0.022.

For historical validation simulations, we used historical SST, nitrate, PAR and light attenuation data described in chapter 3 for the years 1995-2014. Models were run at hourly resolution. SST was available at daily resolution. PAR was available at hourly resolution. We used a daily climatology of light attenuation to drive the historical simulations. For historical simulations, kelp were placed at a depth of 2m in coastal locations with recorded rock cover. This 2m depth was chosen because the aim of the historical simulations was to ensure that the geographic distribution was correct, and typically fringe populations are at shallower depths.

For future simulations, we created a high-resolution map of northwest European shelf rock habitat (100 m resolution) by combining the map generated as part of this task for the UK and Ireland (Figure 1.2) and the EMODnet seabed habitat map. For the UK and Ireland, we only used model cells where rock cover was greater than 70%. Depth within each cell was taken from the 100 by 100 m EMODnet 2020 elevation product. We took the simple approach that PAR reaching kelp in each cell can be calculated using the depth of the cell, surface PAR and the instantaneous light attenuation.

5.3. *Kelp modelling results*

Present day validation

Figure 5.2 shows the fraction of years (1995-2014) the model predicts kelp survival across the NW-shelf. Regions with high kelp survival overlap with those with observed kelp occurrence, with warmer southern locations seeing low survival. Highly turbid areas such as the Bristol Channel in England see low kelp survival due to the reduced PAR levels reaching simulated kelp.

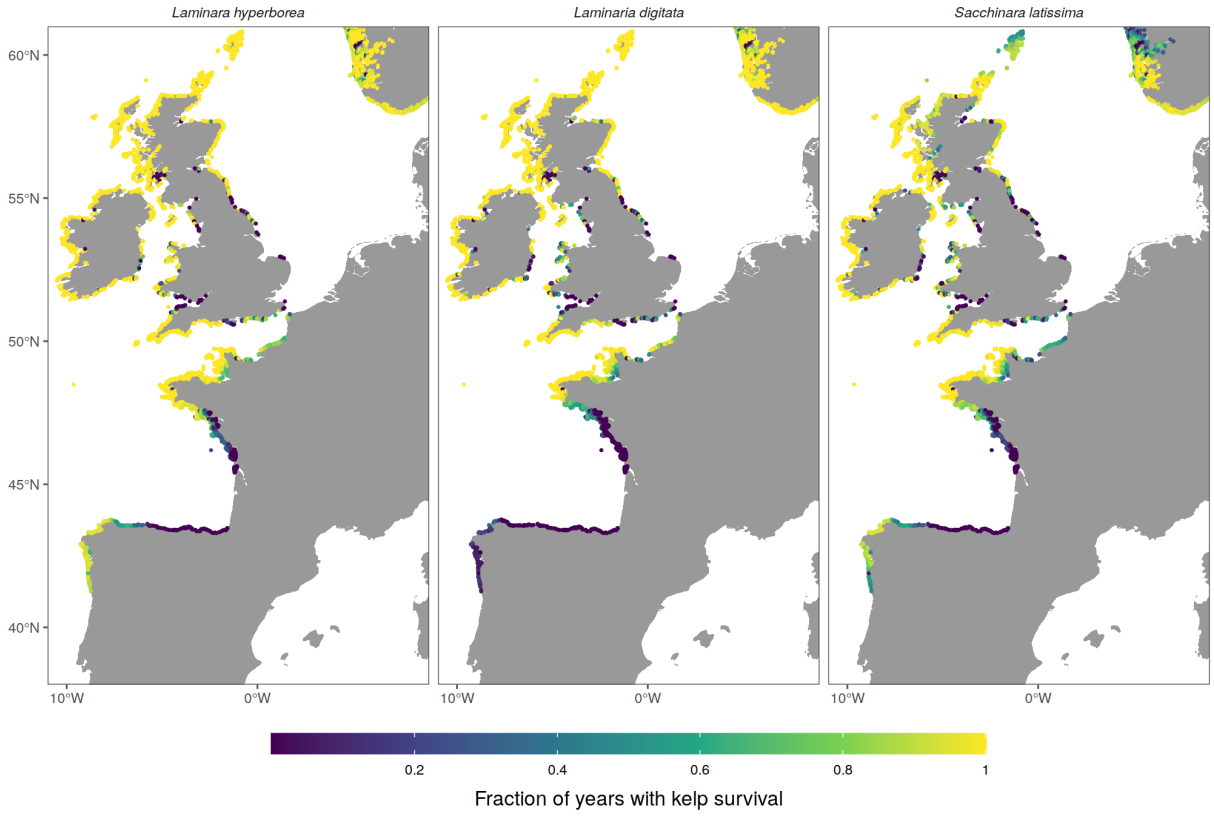

Figure 5.2: Modelled fraction of years (1995-2014) where kelp fronds can survive. Annual kelp was simulated at a depth of 2m in coastal locations with rock cover using historical SST, PAR, light attenuation and nitrate concentration.

The historical simulations broadly reproduce the biogeography of the species. Historical kelp occurrences are broadly predicted by whether kelp can survive in more than 50% of the years between 1995-2014 (Figure 5.3).

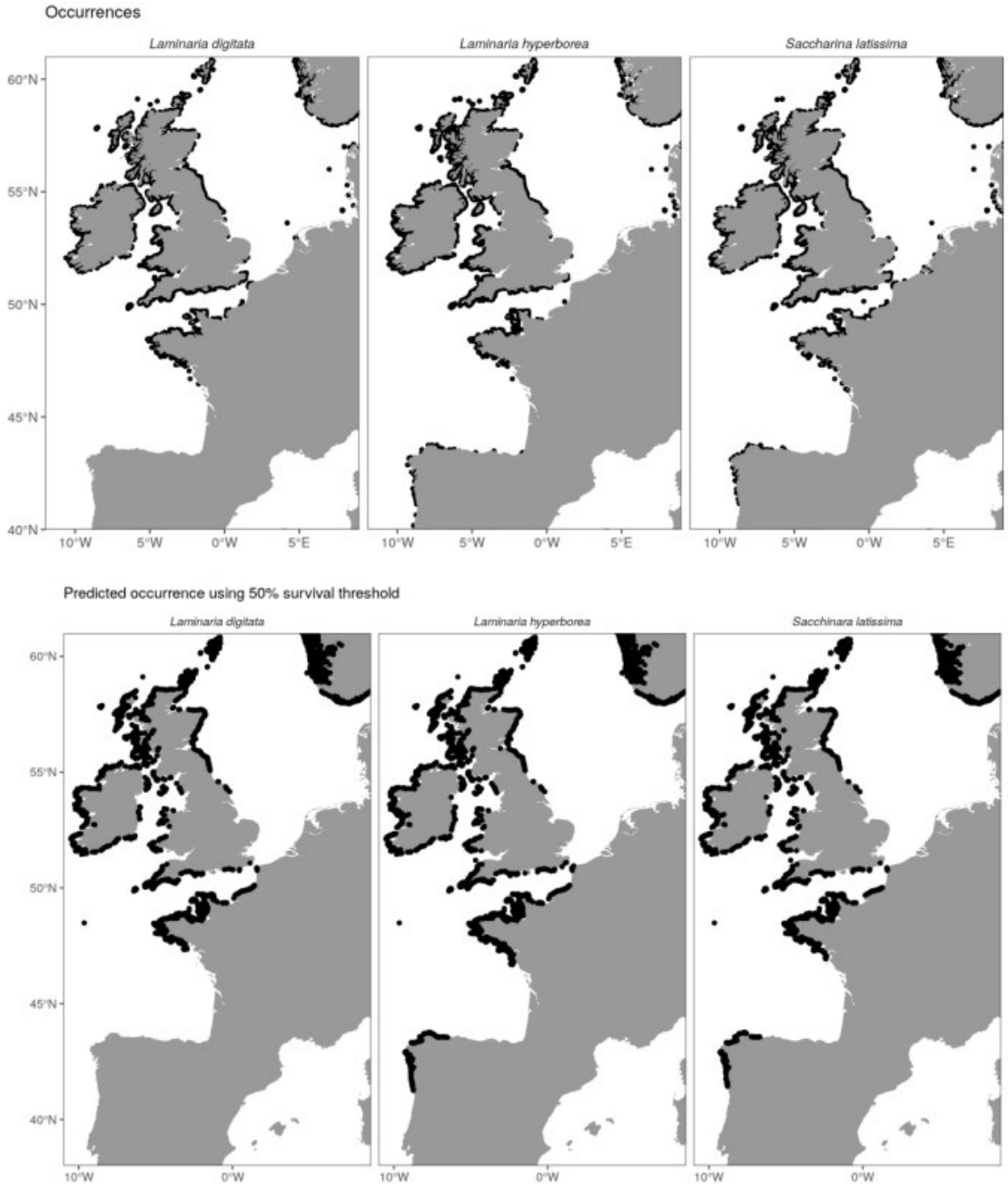

Figure 5.3: Top: historical observations of Laminaria species (Assis et al., 2020). Bottom: predicted occurrences using a 50% kelp survival percentage.

Projected changes in kelp distribution

Figures 5.4-5.10 show projected changes in kelp survival for 2040-59 and 2080-99 under SSP 126, SSP 245 and SSP 585. A northward shift in species' distribution is projected across all scenarios and models. However, the magnitude of that shift has high uncertainty,

reflecting uncertainty both in levels of greenhouse gases within each scenario and the increase in regional temperature projected by each climate model.

Projected changes for *L. hyperborea* and *S. latissima* are similar, which is unsurprising given their similar present-day distributions and similar temperature responses. Under SSP 126, persistence of *S. latissima* populations on the Spanish and Portuguese coasts is uncertain. Low *S. latissima* survival levels are projected by 3 of the 6 ensemble members for 2080-2099. For *L. hyperborea,* 2 or the 6 ensemble members are projecting rare survival for 2080-2099. However, of those, UKESM1-0-LL has very high ECS, and the other, CMCC-ESM2 has high warming levels in the region under SSP 126.

Inter-ensemble comparisons of projections of *S. latissima* and *L. hyperborea* for SSP 245 and SSP 585 (Figures 5.5, 5.6, 5.8 and 5.9) indicate that future changes under higher emissions scenarios, above the Paris agreement, are highly dependent on model climate sensitivity. Under SSP 245, 2 of 6 of the ensemble members are projecting kelp survival exceeding 50% of years in 2080-99 on the Spanish and Portuguese, and therefore likely *S. latissima* persistence. A similar ensemble spread occurs for *L. hyperborea* under SSP 585.

Domain-wide extinction of kelp occurs in SSP 585 in the projections using the model UKESM-0-LL. Similarly, there is extremely widespread extinction using the models ACCESS-ESM1-5 and IPSL-CM6A-LR. It is important to note that, as discussed, the equilibrium climate sensitivity of UKESM-0-LL and IPSL-CM6A-LR are outside the credible range assessed by the IPCC. Furthermore, ACCESS-ESM1-5 has similar warming levels in the region to UKESM-0-LL and IPSL-CM6A-LR.

The projections for *L. Digitata* indicate that projected future changes are potentially large, but uncertain. All projections indicate northward range shifts are expected this century (Figures 5.12-5.14). Persistence of *L. digitata* on the French coast appears probably in SSP 126 (Figure 5.10), but uncertain to unlikely in SSP 245 and 585 (Figures 5.13-5.14), beyond the Paris agreement warming target.

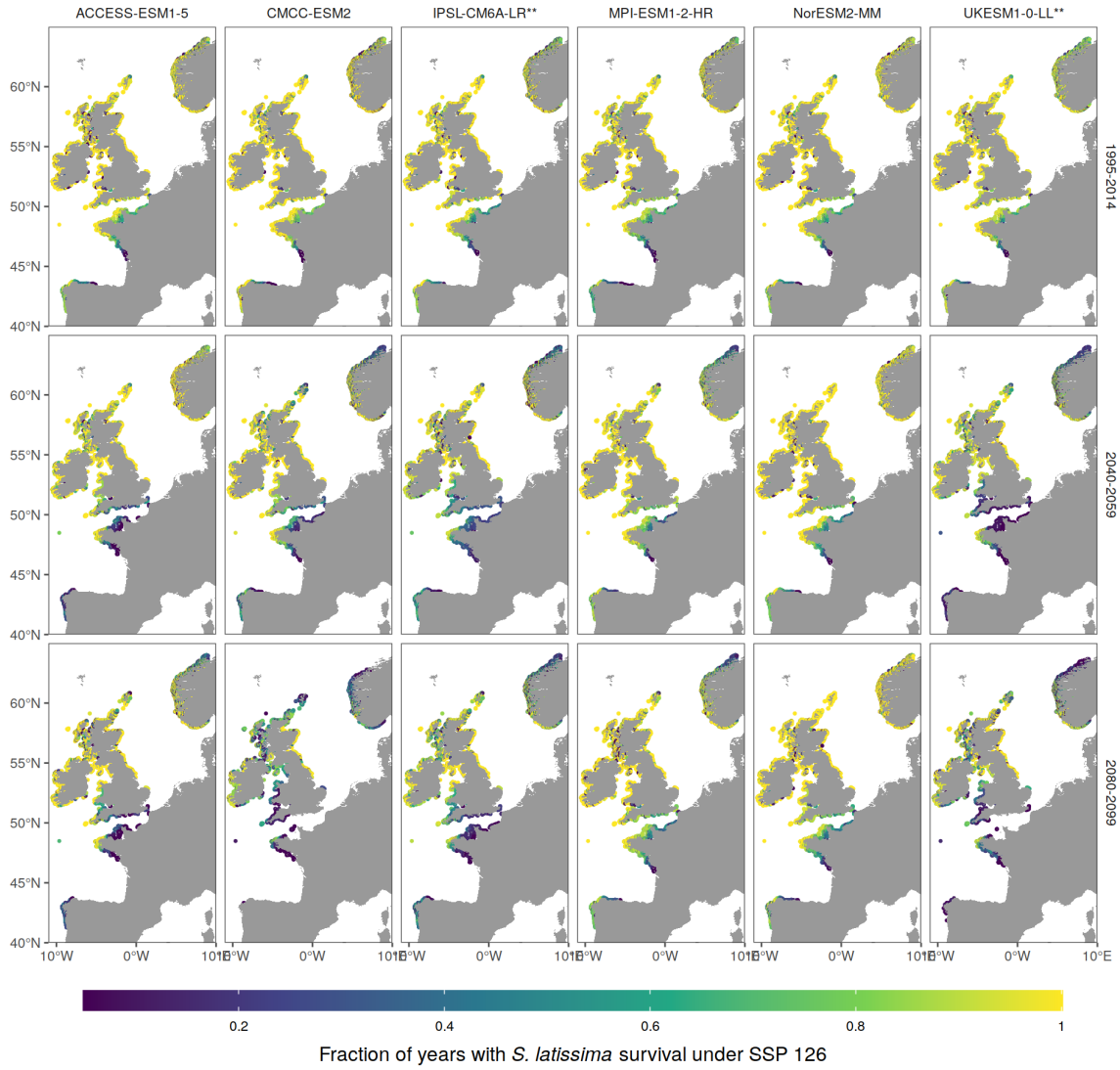

Figure 5.4: Projected impacts on annual patterns of S. latissima kelp survival under SSP 126. Note: only regions where annual kelp survival occurs are shown for time periods. FutureMARES storylines of interest: 1, 2, 3, 5, 11, 15, 21, 23.

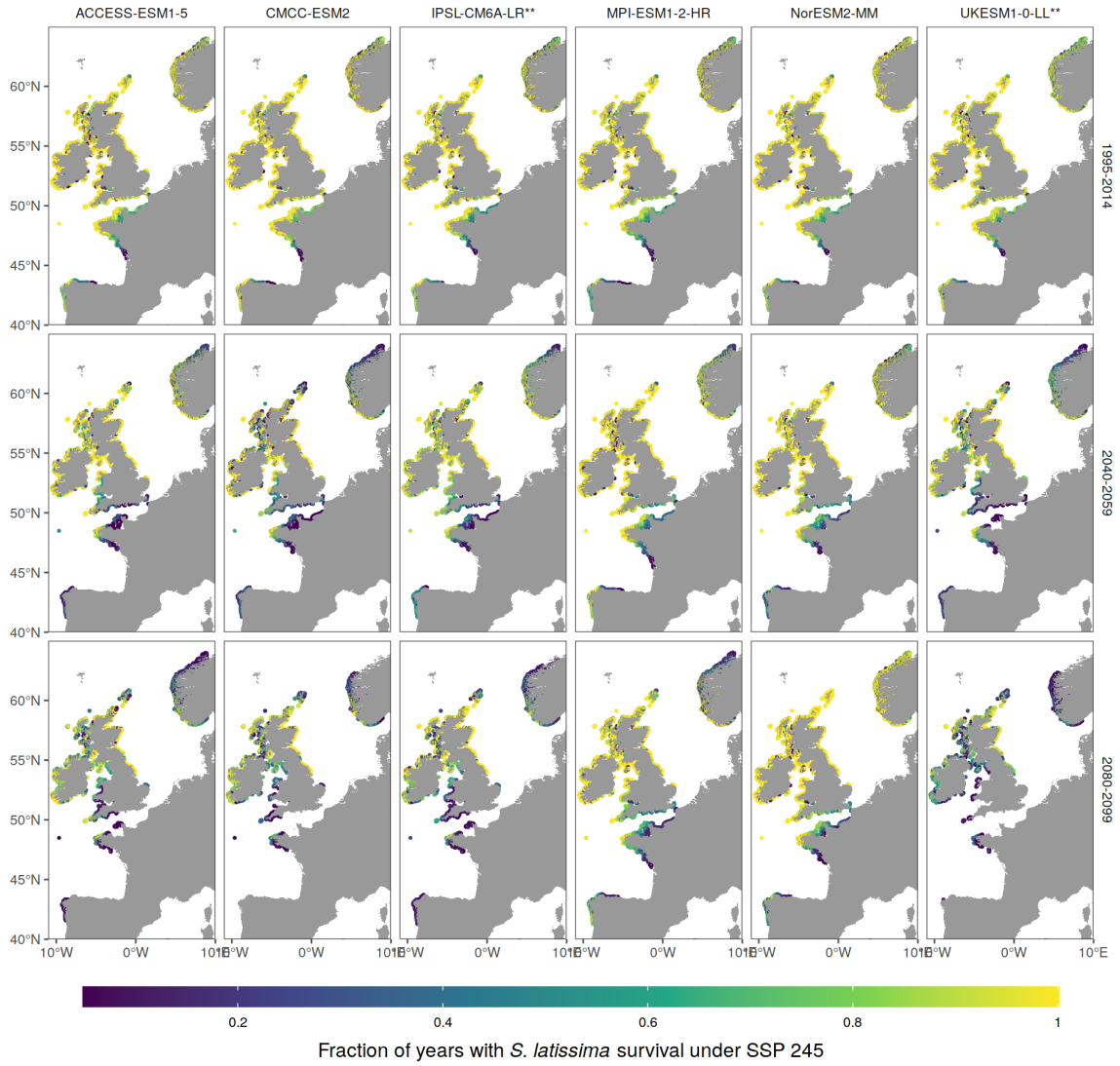

Figure 5.5: Projected impacts on annual patterns of S. hyperborea kelp survival under SSP 245. Note: only regions where annual kelp survival occurs are shown for time periods. FutureMARES storylines of interest: 1, 2, 3, 5, 11, 15, 21, 23.

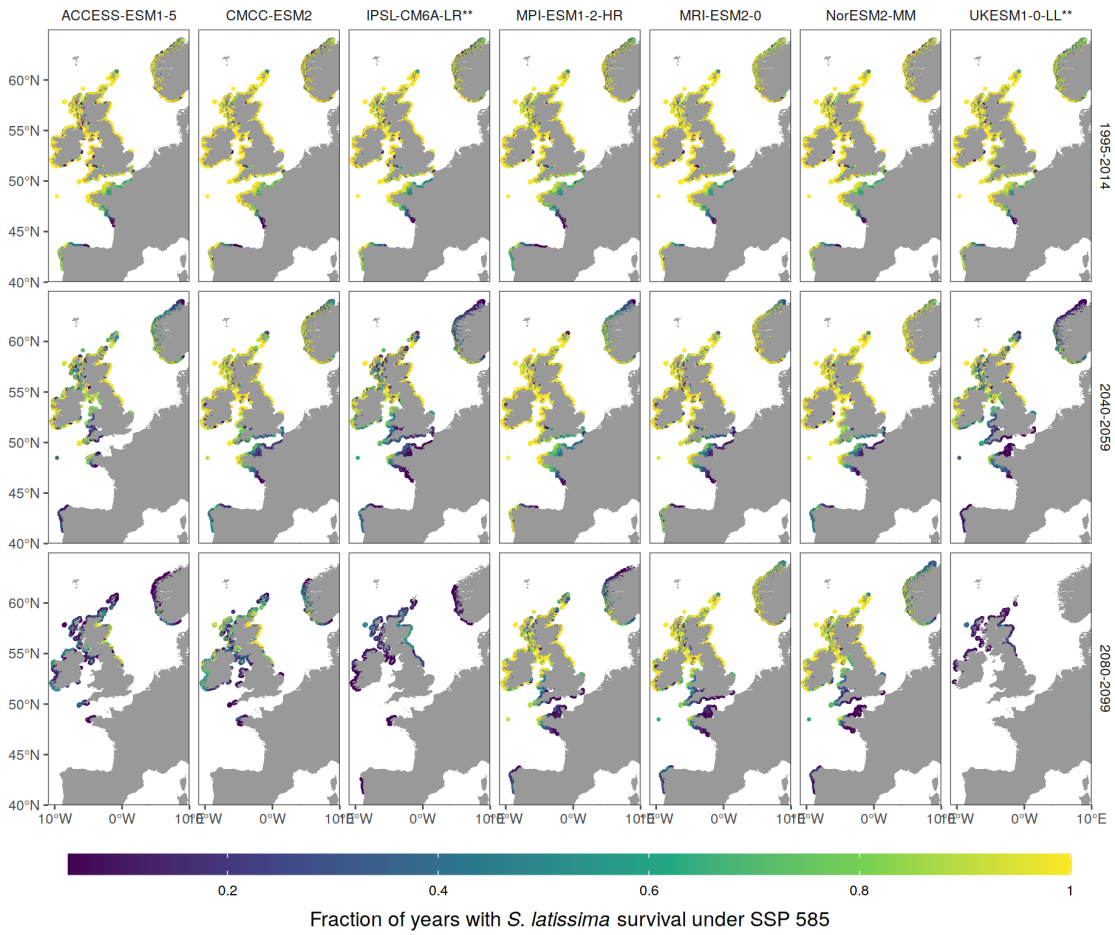

Figure 5.6: Projected impacts on annual patterns of S. hyperborea kelp survival under SSP 585. Note: only regions where annual kelp survival occurs are shown for time periods. FutureMARES storylines of interest: 1, 2, 3, 5, 11, 15, 21, 23.

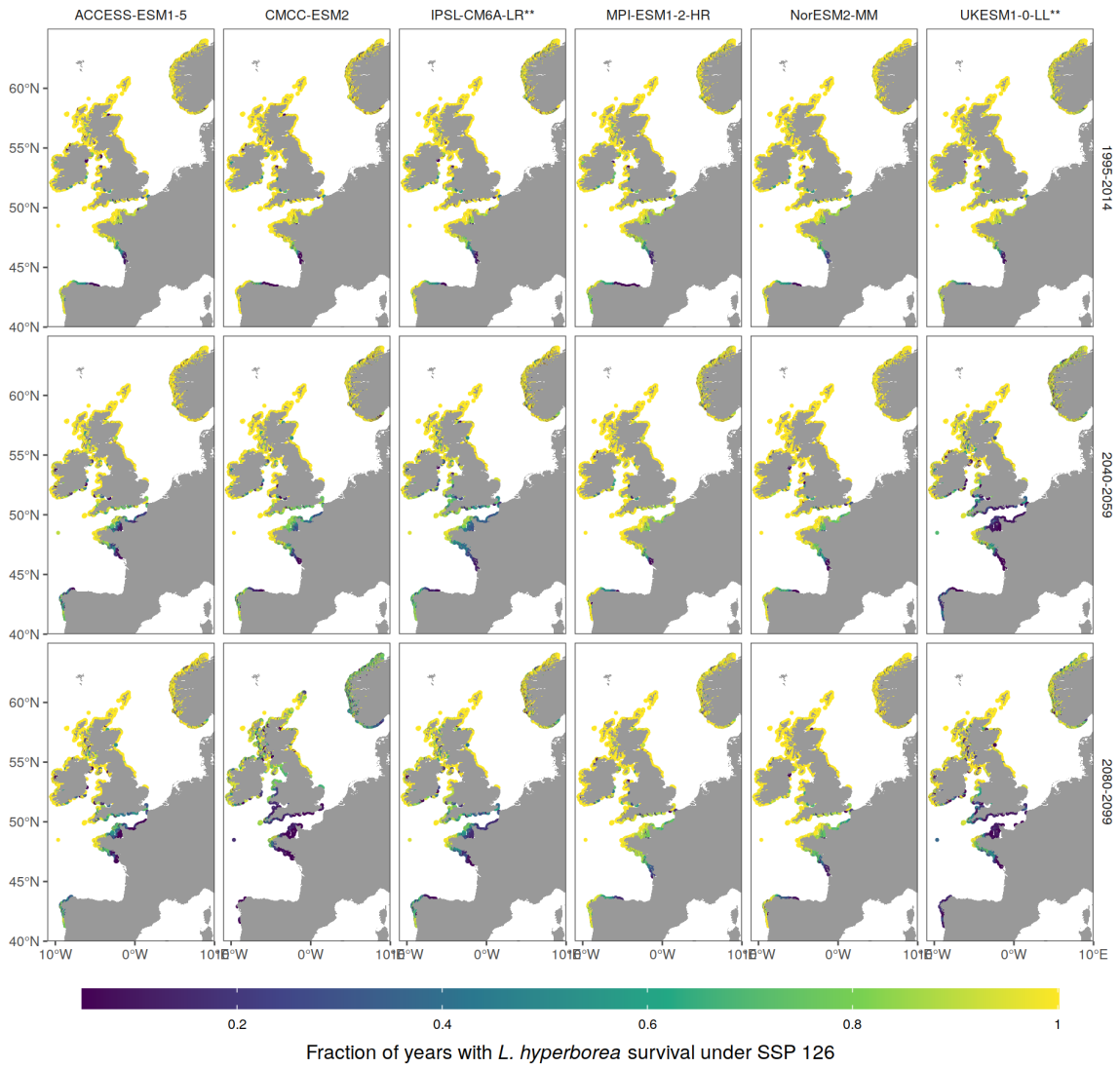

Figure 5.7: Projected impacts on annual patterns of L. hyperborea kelp survival under SSP 126. Note: only regions where annual kelp survival occurs are shown for time periods. FutureMARES storylines of interest: 1, 2, 3, 5, 11, 15, 21, 23.

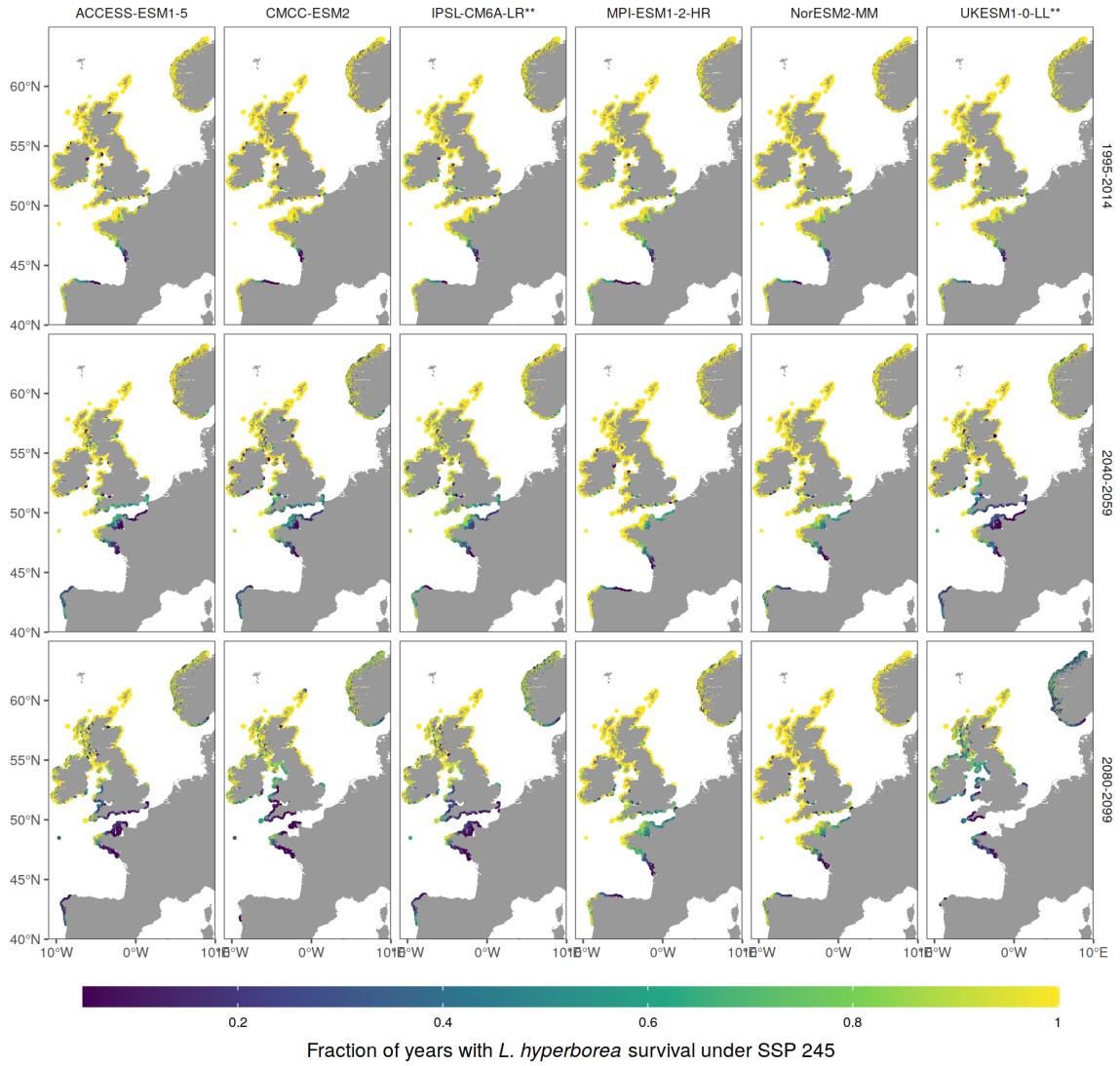

Figure 5.8: Projected impacts on annual patterns of L. hyperborea kelp survival under SSP 245. Note: only regions where annual kelp survival occurs are shown for time periods. FutureMARES storylines of interest: 1, 2, 3, 5, 11, 15, 21, 23.

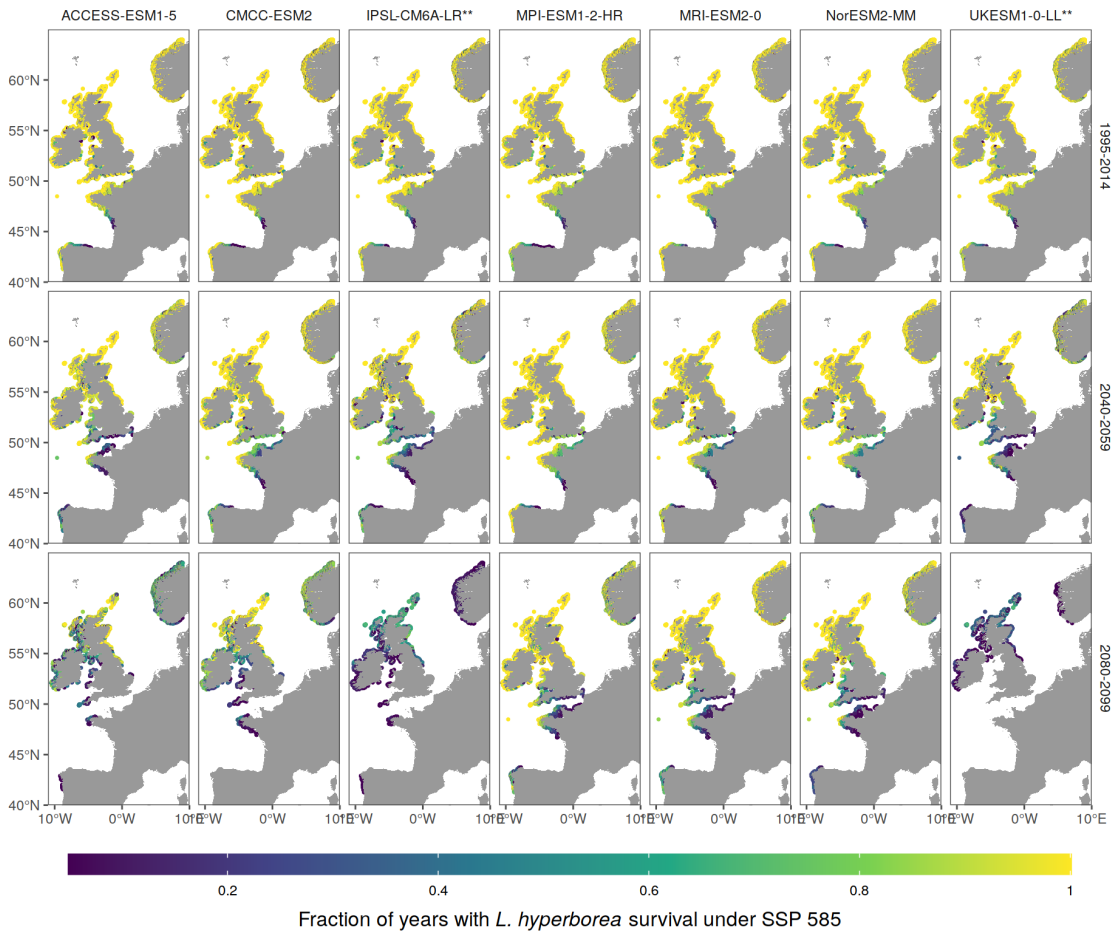

Figure 5.9: Projected impacts on annual patterns of L. hyperborea kelp survival under SSP 585. Note: only regions where annual kelp survival occurs are shown for time periods. FutureMARES storylines of interest: 1, 2, 3, 5, 11, 15, 21, 23.

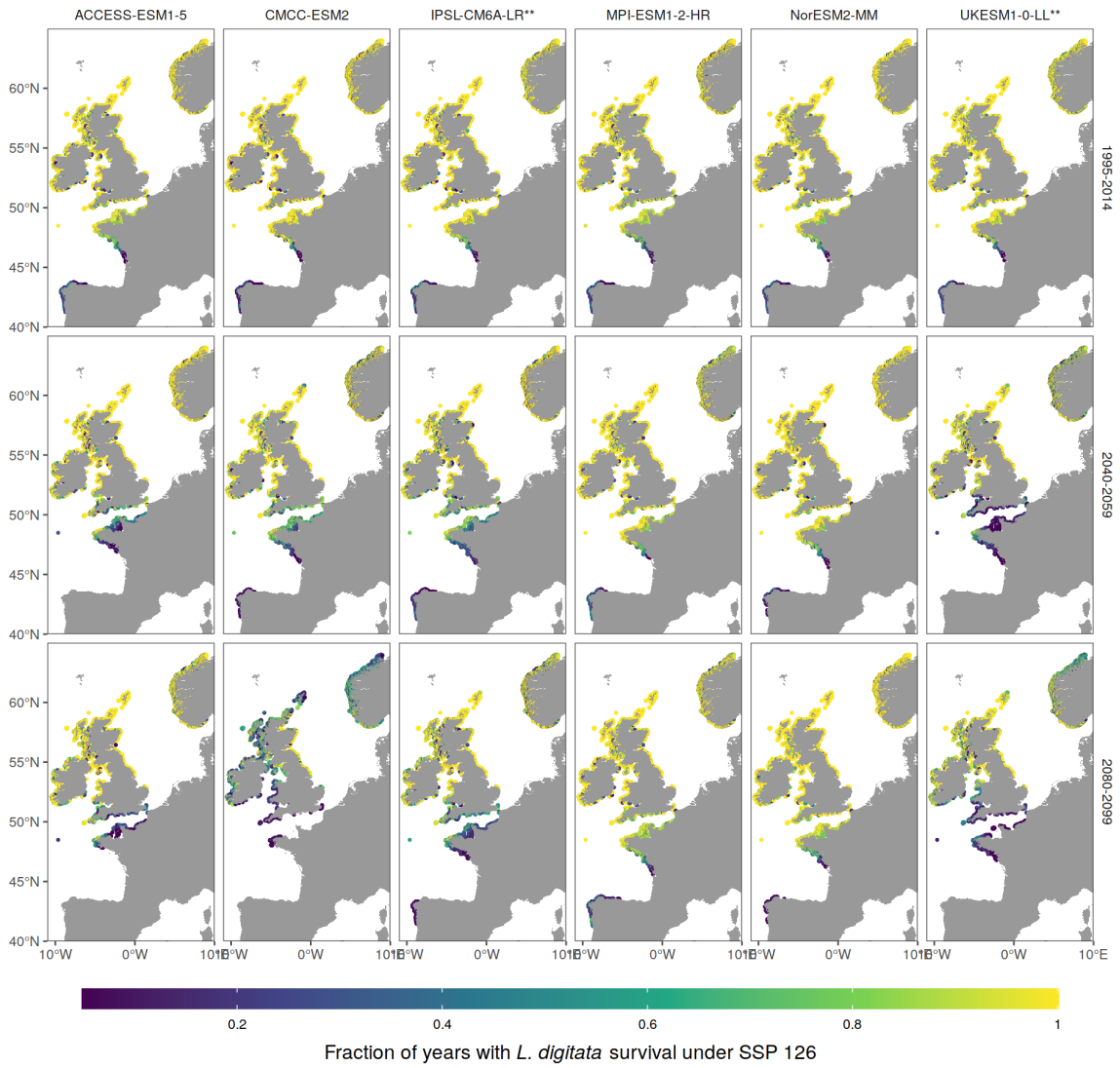

Figure 5.10: Projected impacts on annual patterns of L. digitata kelp survival under SSP 126. Note: only regions where annual kelp survival occurs are shown for time periods. FutureMARES storylines of interest: 1, 2, 3, 5, 11, 15, 21, 23.

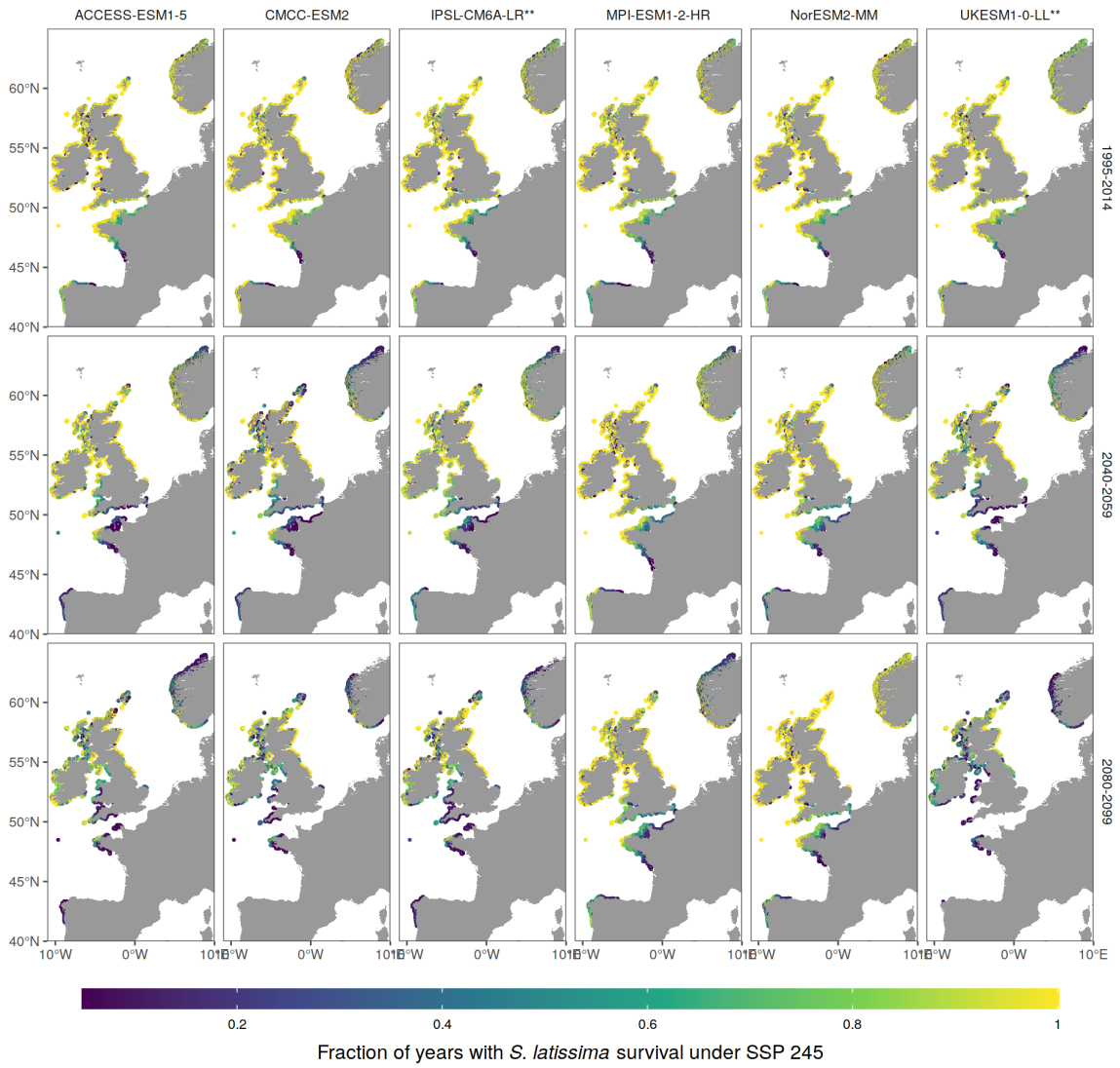

Figure 5.11: Projected impacts on annual patterns of L. digitata kelp survival under SSP 245. Note: only regions where annual kelp survival occurs are shown for time periods. FutureMARES storylines of interest: 1, 2, 3, 5, 11, 15, 21, 23.

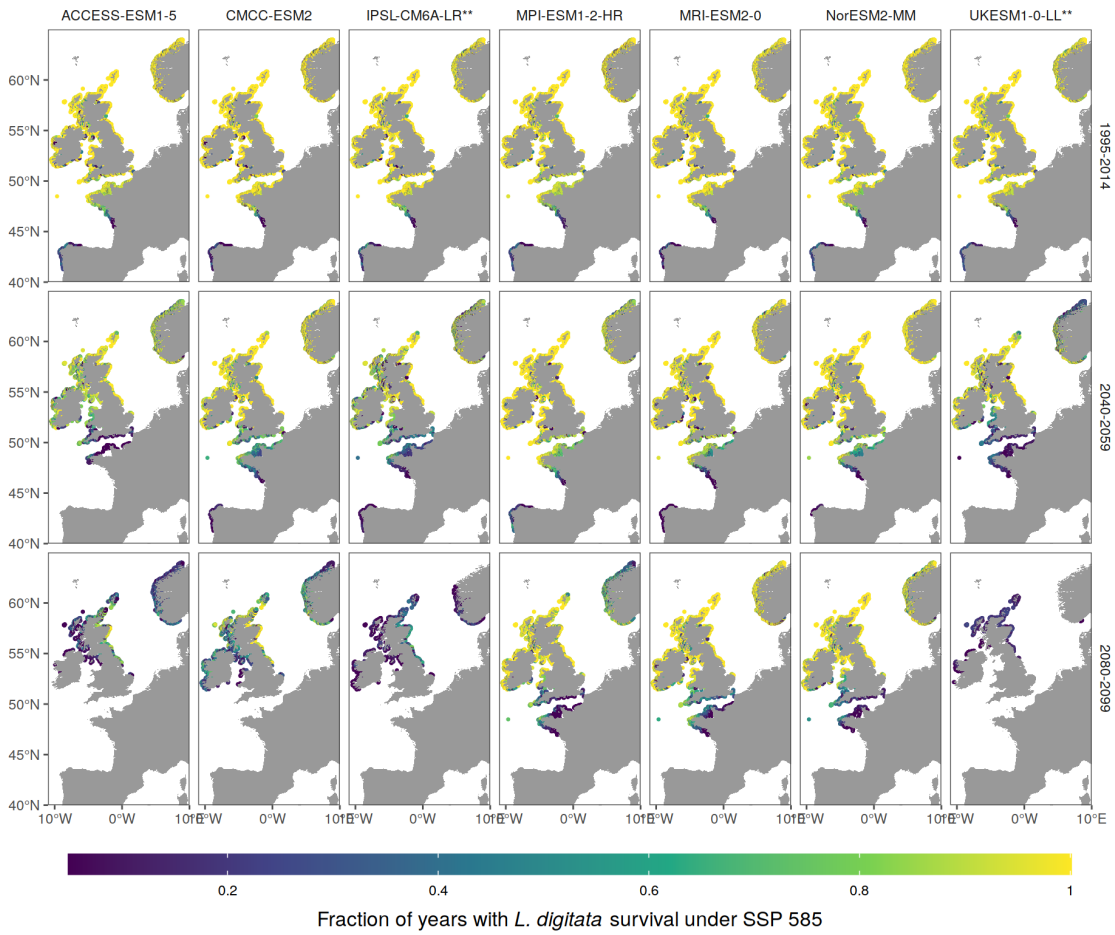

Figure 5.12: Projected impacts on annual patterns of L. digitata kelp survival under SSP 585. Note: only regions where annual kelp survival occurs are shown for time periods. FutureMARES storylines of interest: 1, 2, 3, 5, 11, 15, 21, 23.

Conclusions and discussion of kelp projections

Our projections for kelp indicate that large biogeographic shifts should be anticipated this century, and widespread extinctions cannot be ruled out. Critically, we have shown that there is a widespread difference in the sensitivity and risk to kelp populations depending on the global climate model used, and this results in potential future changes in kelp populations being highly uncertain. However, while the magnitude of change is uncertain, we are much more confident in the direction of change.

A critical uncertainty is whether kelp populations will be able to acclimate to future climate change and whether temperature responses are the same in different regions. Regional adaptation to rising temperatures has the potential to partially offset the impacts of rising temperature projected here. However, such adaptations remain poorly understood, and work on the influence of growth temperatures on photosynthesis (Davison, 1986) indicates that rising temperatures could actually have a further negative impact on species that are not fully captured here.

Marine heatwaves are known to have caused mortality events in kelp species (Filbee-Dexter et al., 2020). However, the explicit impacts of heat waves on kelp were not represented within the model framework. Experimental work (Nepper-Davidsen et al., 2019) has suggested that extreme heat will have a long-term impact on kelp functioning and can induce tissue loss (Simonson et al., 2015), with reduced photosynthetic and growth rates long after exposure to extreme heat. For example, a recent study shows varying response of *S. latissima* to heatwaves across latitudes (Diehl et al., 2021). Future modelling work should consider how to integrate such impacts and whether they result in a significant increase in climate impacts. Ecological stress memory may also improve resistance to heat stress as was reported under experimental conditions for *S. latissima* (Scheschonk et al., 2022; Niedzwiedz et al., 2022). The extent to which this physiological mechanism would enable persistence of wild populations is uncertain and likely not sufficient to counter long-term warming impacts projected in our work. Indeed, the relentless impact of heatwaves on kelp populations in Australia suggests that this may be an unlikely mechanism leading to successful outcomes for kelp under stronger regimes of heatwaves projected in a future climate (Smale et al., 2020).

A key outcome of our projections is the clear benefit of using climate ensembles for projecting the future fate of kelp species and populations. Typically, published studies only use one climate model in their projections. However, our results underline that this can result in misleading conclusions due to the diverging responses of climate models particularly in different scenarios of greenhouse gas emissions. Furthermore, the existence of the “hot model” problem in CMIP6 (where a large number of models have equilibrium climate sensitivity outside the credible range assessed by the IPCC) makes it critically important to provide a nuanced view of projected changes.

5.4. Data availability

The kelp projections are available for the 3 scenarios at https://doi.org/10.5281/zenodo.7682052. Data is provided for annual kelp survival/mortality in netCDF format with fully self-describing meta-data.

Acknowledgements

We thank Jacob Carstensen of Aarhus University for providing in-situ light attenuation data for Danish waters and seagrass occurrence data. We further thank Antonios Mazaris and Ignacio Catalán for highlighting distribution data for *P. oceanica*.

We acknowledge the World Climate Research Programme's Working Group on Coupled Modelling, which is responsible for CMIP.

Indexes

Index of figures

Index of tables

References

Abe, M., Akira K., Miyuki M. (2008). Temperature requirements for seed germination and seedling growth of *Zostera marina* from central Japan. *Fisheries Science, 74* (3), 589–93. https://doi.org/10.1111/j.1444-2906.2008.01562.x.

Assis, J., Fragkopoulou, E., Frade, D., Neiva, J., Oliveira, A., Abecasis, D., et al. (2020). A fine-tuned global distribution dataset of marine forests. *Scientific Data, 7(1)*, 1–9. https://doi.org/10.1038/s41597-020-0459-x.

Aguilera, J., Karsten, U., Lippert, H., Vögele, B., Philipp, E., Hanelt, D., Wiencke, C. (1999). Effects of solar radiation on growth, photosynthesis and respiration of marine macroalgae from the Arctic. *Marine Ecology Progress Series, 191*, 109–19. https://doi.org/10.3354/meps191109.

Apostolaki, E.T., Holmer, M., Santinelli, V., Karakassis, I. (2018a). Species-specific response to sulfide intrusion in native and exotic Mediterranean seagrasses under stress. *Marine Environmental Research, 134*, 85–95. https://doi.org/10.1016/j.marenvres.2017.12.006.

Araújo, R., Vázquez Calderón, F., Sánchez López, J., Azevedo, I. C., Bruhn, A., Fluch, S., et al. (2021). Current status of the algae production industry in Europe: an emerging sector of the blue bioeconomy. *Frontiers in Marine Science, 7*, 626389. https://doi.org/10.3389/fmars.2020.626389.

Assis, J., Araújo, M. B., Serrão, E. A. (2018). Projected climate changes threaten ancient refugia of kelp forests in the North Atlantic. *Global Change Biology, 24(1)*, e55-e66. https://doi.org/10.1111/gcb.13818.

Assis, J., Fragkopoulou, E., Frade, D., Neiva, J., Oliveira, A., et al. (2020). A fine-tuned global distribution dataset of marine forests. *Scientific Data, 7(1)*, 119. https://doi.org/10.1038/s41597-020-0459-x.

Assis, J., Serrão, E.A., Duarte, C.M., Fragkopoulou, E., Krause-Jensen, D. (2022). Major expansion of marine forests in a warmer Arctic. *Frontiers in Marine Science, 9*. https://doi.org/10.3389/fmars.2022.850368.

Azevedo, I.C., Marinho, G.S., Silva, D.M., Sousa-Pinto, I. (2016). Pilot scale land-based cultivation of *Saccharina latissima* Linnaeus at southern European climate conditions: Growth and nutrient uptake at high temperatures. *Aquaculture, 459*, 166–72. https://doi.org/10.1016/j.aquaculture.2016.03.038.

Baird, M.E., Adams, M.P., Babcock, R.C., Oubelkheir, K., Mongin, M., Wild-Allen, K.A., Skerratt, J., et al. (2016). A biophysical representation of seagrass growth for application in a complex shallow-water biogeochemical model. *Ecological Modelling, 325*, 13–27. https://doi.org/10.1016/j.ecolmodel.2015.12.011.

Beca-Carretero, P., Olesen, B., Marbà, N., Krause-Jensen, D. (2018). Response to experimental warming in northern eelgrass populations: Comparison across a range of temperature adaptations. *Marine Ecology Progress Series, 589*, 59–72. https://doi.org/10.3354/meps12439.

Beca-Carretero, P., Stanschewski, C.S., Julia-Miralles, M., Sanchez-Gallego, A., Stengel, D.B. (2019). Temporal and depth-associated changes in the structure, morphometry and production of near-pristine *Zostera marina* meadows in western Ireland. *Aquatic Botany, 155*, 5–17. https://doi.org/10.1016/j.aquabot.2019.02.003.

Bennett, S., Vaquer-Sunyer, R., Jordá, G., Forteza, M., Roca, G., Marbà, N. (2022). Thermal Performance of Seaweeds and Seagrasses Across a Regional Climate Gradient. *Frontiers in Marine Science, 9*, 1–11. https://doi.org/10.3389/fmars.2022.733315.

Berg, P., Delgard, M.L., Polsenaere, P., McGlathery, K.J., Doney, S.C., Berger, A.C. (2019). Dynamics of benthic metabolism, O_2, and pCO_2 in a temperate seagrass meadow. *Limnology and Oceanography, 64*, 2586–2604. https://doi.org/10.1002/lno.11236.

Bi, D., Dix, M., Marsland, S., O'Farrell, S., Sullivan, A., Bodman, R., Law, R., et al. (2020). Configuration and spin-up of ACCESS-CM2, the new generation Australian Community Climate and Earth System Simulator Coupled Model. *Journal of Southern Hemisphere Earth Systems Science, 70(1)*, 225–251. https://doi.org/10.1071/ES19040.

Bolton, J.J., Lüning, K. (1982). Optimal growth and maximal survival temperatures of Atlantic *Laminaria* species (Phaeophyta) in culture. *Marine Biology, 66 (1)*, 89–94. https://doi.org/10.1007/BF00397259.

Boucher, O., Servonnat, J., Albright, A. L., Aumont, O., Balkanski, Y., et al. (2020). Presentation and Evaluation of the IPSL-CM6A-LR Climate Model. *Journal of Advances in Modeling Earth Systems, 12(7)*, 1–52. https://doi.org/10.1029/2019MS002010.

Campbell, I., Macleod, A., Sahlmann, C., Neves, L., Funderud, J., et al. (2019). The environmental risks associated with the development of seaweed farming in Europe-prioritizing key knowledge gaps. *Frontiers in Marine Science, 6,* 107. https://doi.org/10.3389/fmars.2019.00107.

Casas-Prat, M., Wang, X.L., Swart, N. (2018). CMIP5-based global wave climate projections including the entire Arctic Ocean. *Ocean Modelling, 123*, 66-85. https://doi.org/10.1016/j.ocemod.2017.12.003.

Champman, A.R.O., Markham, J.W., and Luning, K. (1978). Effects of nitrate concentration on the growth and physiology of *Laminaria saccharina* (PHAEOPHYTA) in culture. *Journal of Phycology, 14 (2)*, 195–98. https://doi.org/10.1111/j.1529-8817.1978.tb02448.x.

Cherchi, A., Fogli, P. G., Lovato, T., Peano, D., Iovino, et al. (2019). Global Mean Climate and Main Patterns of Variability in the CMCC-CM2 Coupled Model. *Journal of Advances in Modeling Earth Systems, 11(1)*, 185–209. https://doi.org/10.1029/2018MS001369.

Ciavatta, S., Kay, S., Saux-Picart, S., Butenschön, M., Allen, J.I. (2016). Decadal reanalysis of biogeochemical indicators and fluxes in the North West European shelf-sea ecosystem. Journal of Geophysical Research. *Oceans, 121(3)*, 1824–1845. https://doi.org/10.1002/2015JC011496.

Dahl, M., Infantes, E., Clevesjö, R., Linderholm, H.W., Björk, M., Gullström, M. (2018). Increased current flow enhances the risk of organic carbon loss from *Zostera marina* sediments: Insights from a flume experiment. *Limnology and Oceanography, 63 (6)*, 2793–2805. https://doi.org/10.1002/lno.11009.

Danabasoglu, G., Lamarque, J.F., Bacmeister, J., Bailey, D.A., DuVivier, A.K., et al. (2020). The Community Earth System Model Version 2 (CESM2). *Journal of Advances in Modeling Earth Systems, 12(2)*, 1–35. https://doi.org/10.1029/2019MS001916.

Davison, I.R. (1986). Adaptation of photosynthesis in *Laminaria Saccharina* (Phaeophyta) to changes in growth temperature. *Journal of Phycology, 23*, 273–283. https://doi.org/10.1111/j.1529-8817.1987.tb04135.x.

Davison, I.R., Greene, R.M., Podolak, E.J. (1991). Temperature acclimation of respiration and photosynthesis in the brown alga *Laminaria saccharina*. *Marine Biology, 110 (3)*, 449–54. https://doi.org/10.1007/BF01344363.

Dennison, W.C, Alberte, R.S. (1985). Role of daily light period in the depth distribution of *Zostera marina* (eelgrass). *Marine Ecology Progress Series, 25*, 51–61. https://doi.org/10.3354/meps025051.

Dennison, W.C., Alberte, R.S. (1982). Photosynthetic Responses of *Zostera marina* L. (Eelgrass) to in situ Manipulations of Light Intensity. *Oecologia, 55(2)*, 137–44. https://doi.org/10.1007/BF00384478.

Dennison, W.C., Alberte, R.S. (1986). Photoadaptation and growth of *Zostera marina* L. (eelgrass) transplants along a depth gradient. *Journal of Experimental Marine Biology and Ecology, 98 (3)*, 265–82. https://doi.org/10.1016/0022-0981(86)90217-0.

Diehl, N., Roleda, M.Y., Bartsch, I., Karsten, U., Bischof, K. (2021). Summer heatwave impacts on the European kelp *Saccharina latissima* across its latitudinal distribution gradient. *Frontiers in Marine science, 1433*. https://doi.org/10.3389/fmars.2021.695821.

Dring, M.J., Makarov, Schoschina, V.E., Lorenz, M., Lüning, K. (1996). Influence of ultraviolet-radiation on chlorophyll fluorescence and growth in different life-history stages of three species of *Laminaria* (phaeophyta). *Marine Biology, 126 (2)*, 183–91. https://doi.org/10.1007/BF00347443.

Duarte, C.M., Bruhn, A., Krause-Jensen, D. (2022a). A seaweed aquaculture imperative to meet global sustainability targets. *Nature Sustainability, 5(3),* 185-193. https://doi.org/10.1038/s41893-021-00773-9.

Duarte, C.M., Gattuso, J.P., Hancke, K., Gundersen, H., Filbee-Dexter, K., et al. (2022b). Global estimates of the extent and production of macroalgal forests. *Global Ecology and Biogeography*, *31*(7), 1422–1439. https://doi.org/10.1111/geb.13515.

Ekstrom, M., Grose, M.R., Whetton, P.H. (2015). An appraisal of downscaling methods used in climate change research. *Wiley Interdisciplinary Reviews: Climate Change*, *6*(3), 301–319. https://doi.org/10.1002/wcc.339.

Filbee-Dexter, K., Wernberg, T., Grace, S.P., Thormar, J., Fredriksen, S., et al. (2020). Marine heatwaves and the collapse of marginal North Atlantic kelp forests. *Scientific Reports*, *10*(1), 1–11. https://doi.org/10.1038/s41598-020-70273-x.

Foldager Pedersen, M.F., Borum, J. (1992). Nitrogen dynamics of eelgrass *Zostera marina* during a late summer period of high growth and low nutrient availability. *Marine Ecology Progress Series, 80 (1)*, 65–73. https://doi.org/10.3354/meps080065.

Fonseca, M.S., Fisher, J.S., Zieman, J.C., Thayer, G.W. (1982). Influence of the seagrass, *Zostera marina* L., on current flow. *Estuarine, Coastal and Shelf Science, 15 (4)*, 351–64. https://doi.org/10.1016/0272-7714(82)90046-4.

Forbord, S., Steinhovden, K.B., Solvang, T., Handå, A., Skjermo, J. (2020). Effect of seeding methods and hatchery periods on sea cultivation of *Saccharina latissima*

(Phaeophyceae): a Norwegian case study. *Journal of Applied Phycology, 32 (4)*, 2201–12. https://doi.org/10.1007/s10811-019-01936-0.

Fourqurean, J.W., Marbà, N., Duarte, C.M., Diaz-Almela, E., Ruiz-Halpern, S. (2007). Spatial and temporal variation in the elemental and stable isotopic content of the seagrasses *Posidonia oceanica* and *Cymodocea nodosa* from the Illes Balears, Spain. *Marine Biology, 151 (1)*, 219–32. https://doi.org/10.1007/s00227-006-0473-3.

Freitas, J. R., Salinas Morrondo, J. M., Cremades Ugarte, J. (2016). *Saccharina latissima* (Laminariales, Ochrophyta) farming in an industrial IMTA system in Galicia (Spain). *Journal of Applied Phycology, 28 (1)*, 377–85. https://doi.org/10.1007/s10811-015-0526-4.

Gafeira, J., Green, S., Dove, D., Morando, A., Cooper, R., et al. (2010). Developing the necessary data layers for Marine Conservation Zone selection - Distribution of rock / hard substrate on the UK Continental Shelf. British Geological Survey Report MB0103.

Gerard, V.A. (1988). Ecotypic differentiation in light-related traits of the kelp *Laminaria saccharina*. *Marine Biology, 97 (1)*, 25–36. https://doi.org/10.1007/BF00391242.

Gettelman, A., Mills, M.J., Kinnison, D.E., Garcia, R.R., Smith, A.K., et al. (2019). The Whole Atmosphere Community Climate Model Version 6 (WACCM6). *Journal of Geophysical Research: Atmospheres, 124(23)*, 12380–12403. https://doi.org/10.1029/2019JD030943.

Hancock, J.T., Khoshgoftaar, T.M. (2020). CatBoost for big data: an interdisciplinary review. *Journal of Big Data*, *7(1)*. https://doi.org/10.1186/s40537-020-00369-8.

Hansen, J.W., Pedersen, A.G.U., Berntsen, J., Rønbøg, I.S., Hansen, L.S., Lomstein, B.A.. (2000). Photosynthesis, respiration, and nitrogen uptake by different compartments of a *Zostera marina* community. *Aquatic Botany, 66 (4)*, 281–95. https://doi.org/10.1016/S0304-3770(99)00078-9.

Hasselström, L, Thomas, J. B., Nordström, J., Cervin, G., Nylund, G. M., et al. (2020). Socioeconomic prospects of a seaweed bioeconomy in Sweden. *Scientific Reports, 10.1*, 1610. https://doi.org/10.1038/s41598-020-58389-6.

Hausfather, Z., Marvel, K., Schmidt, G. A., Nielsen-Gammon, J. W., Zelinka, M. (2022). Climate simulations: recognize the 'hot model' problem. *Nature, 605(7908)*, 26–29. https://doi.org/10.1038/d41586-022-01192-2.

Hauxwell, J., Cebrian, J., Valiela, I. (2006). Light dependence of *Zostera marina* annual growth dynamics in estuaries subject to different degrees of eutrophication. *Aquatic Botany, 84 (1)*: 17–25. https://doi.org/10.1016/j.aquabot.2005.05.014.

Hawkins, S.J., Moore, P.J., Burrows, M.T., Poloczanska, E., Mieszkowska, N., et al. (2008). Complex interactions in a rapidly changing world: responses of rocky shore communities to recent climate change. *Climate Research, 37(2-3),* 123-133. https://doi.org/10.3354/cr00768.

Hendriks, I.E., Sintes, T., Bouma, T.J., Duarte, C.M. (2008). Experimental assessment and modeling evaluation of the effects of the seagrass *Posidonia oceanica* on flow and particle trapping. *Marine Ecology Progress Series, 356*, 163–73. https://doi.org/10.3354/meps07316.

Höffle, H., Thomsen, M.S., Holmer, M. (2011). High mortality of *Zostera marina* under high temperature regimes but minor effects of the invasive macroalgae *Gracilaria vermiculophylla*. *Estuarine, Coastal and Shelf Science, 92 (1)*, 35–46. https://doi.org/10.1016/j.ecss.2010.12.017.

Holmer, M., Bondgaard, E.J. (2001). Photosynthetic and growth response of eelgrass to low oxygen and high sulfide concentrations during hypoxic events. *Aquatic Botany, 70 (1)*, 29–38. https://doi.org/10.1016/S0304-3770(00)00142-X.

Iñiguez, C., Carmona, R., Rosario Lorenzo, M., Xavier Niell, F., Wiencke, C., Gordillo, F.J.L. (2016). Increased temperature, rather than elevated CO_2, modulates the carbon assimilation of the Arctic kelps *Saccharina latissima* and *Laminaria solidungula*. *Marine Biology, 163 (12)*. https://doi.org/10.1007/s00227-016-3024-6.

James, G., Witten, D., Hastie, T., Tibshirani, R. (2013). An introduction to statistical learning (Vol. 112, p. 18). New York: *Springer*.

Kaldy J.E. (2014). Effect of temperature and nutrient manipulations on eelgrass *Zostera marina L*. from the Pacific Northwest, USA. *Journal of Experimental Marine Biology and Ecology 453*, 108–15. https://doi.org/10.1016/j.jembe.2013.12.020.

Kaldy, J.E., Lee, S. (2007). Factors controlling *Zostera marina L.* growth in the eastern and western Pacific Ocean: Comparisons between Korea and Oregon, USA. *Aquatic Botany, 87 (2)*, 116–26. https://doi.org/10.1016/j.aquabot.2007.03.008.

Kearney, M., Porter, W. (2009). Mechanistic niche modelling: combining physiological and spatial data to predict species' ranges. *Ecology Letters, 12(4),* 334-350. https://doi.org/10.1111/j.1461-0248.2008.01277.x.

Kim, J.B., Lee, W.C., Lee, K.S., Park, J.I. (2013). Growth dynamics of eelgrass, *Zostera marina*, in the intertidal zone of Seomjin Estuary, Korea. *Ocean Science Journal, 48 (3)*, 239–50. https://doi.org/10.1007/s12601-013-0021-2.

Kim, Y.K., Kim, S.H., Lee, K.S. (2015). Seasonal Growth Responses of the Seagrass *Zostera marina* under Severely Diminished Light Conditions. *Estuaries and Coasts, 38 (2)*, 558–68. https://doi.org/10.1007/s12237-014-9833-2.

Kirkman, H., Young, P.C. (1981). Measurement of health, and echinoderm grazing on *Posidonia oceanica* (L.) Delile. *Aquatic Botany, 10 (C)*, 329–38. https://doi.org/10.1016/0304-3770(81)90031-0.

Koopmans, D., Holtappels, M., Chennu, A., Weber, M., de Beer, D. (2020). High Net Primary Production of Mediterranean Seagrass (*Posidonia oceanica*) Meadows Determined With Aquatic Eddy Covariance. *Frontiers in Marine Science, 7 (March)*, 1–13. https://doi.org/10.3389/fmars.2020.00118.

Kraemer, G.P., Alberte, R.S. (1995). Impact of daily photosynthetic period on protein synthesis and carbohydrate stores in *Zostera marina* L. (eelgrass) roots: implications for survival in light-limited environments. *Journal of Experimental Marine Biology and Ecology, 185 (2)*, 191–202. https://doi.org/10.1016/0022-0981(94)00145-4.

Krause-Jensen, D., Archambault, P., Assis, J., Bartsch, I., Bischof, K., et al. (2020). Imprint of climate change on pan-Arctic marine vegetation. *Frontiers in Marine Science, 7,* 617324. https://doi.org/10.3389/fmars.2020.617324.

Kregting, L., Blight, A., Elsäßer, B., Savidge, G. (2013). The influence of water motion on the growth rate of the kelp *Laminaria hyperborea*. *Journal of Experimental Marine Biology and Ecology, 448*, 337–45. https://doi.org/10.1016/j.jembe.2013.07.017.

Kregting, L.T., Hepburn, C.D., Savidge, G. (2015). Seasonal differences in the effects of oscillatory and uni-directional flow on the growth and nitrate-uptake rates of juvenile *Laminaria digitata* (Phaeophyceae). *Journal of Phycology, 51 (6)*, 1116–26. https://doi.org/10.1111/jpy.12348.

Kregting, L., Blight, A.J., Elsäßer, B., Savidge, G. (2016). The influence of water motion on the growth rate of the kelp *Laminaria digitata*. *Journal of Experimental Marine Biology and Ecology, 478*, 86–95. https://doi.org/10.1016/j.jembe.2016.02.006.

Larsen, J., Mohn, C., Pastor, A., Maar, M. (2020). A versatile marine modelling tool applied to arctic, temperate and tropical waters. *PLoS One, 1–18*. https://doi.org/10.1371/journal.pone.0231193.

van Lent, F., Verschnure, J.M. (1995). Comparative study on populations of *Zostera marina* L. (eelgrass): experimental germination and growth. *Journal of Experimental Marine Biology and Ecology, 185 (1)*, 77–91. https://doi.org/10.1016/0022-0981(94)00132-W.

van Lent, F., Verschuure, J.M., van Veghel., M.L.J. 1995. Comparative study on populations of *Zostera marina* L. (eelgrass): in situ nitrogen enrichment and light manipulation. *Journal of Experimental Marine Biology and Ecology, 185 (1)*, 55–76. https://doi.org/10.1016/0022-0981(94)00131-V.

Liesner, D., Pearson, G.A., Bartsch, I., Rana, S., Harms, L., et al. (2022). Increased Heat Resilience of Intraspecific Outbred Compared to Inbred Lineages in the Kelp *Laminaria digitata*: Physiology and Transcriptomics. *Frontiers in Marine Science, 9 (March): 1–20*. https://doi.org/10.3389/fmars.2022.838793.

Liesner, D., Shama, L.N.S., Diehl, N., Valentin, K., Bartsch, I. (2020). Thermal Plasticity of the Kelp *Laminaria digitata* (Phaeophyceae) Across Life Cycle Stages Reveals the Importance of Cold Seasons for Marine Forests. *Frontiers in Marine Science, 7 (June)*. https://doi.org/10.3389/fmars.2020.00456.

Liu, X., Zhou, Y., Liu, B., Zhang, X. (2019). Temporal Dynamics of the Natural and Trimmed Angiosperm *Zostera marina* L. (Potamogetonales:Zosteraceae), and an Effective Technique for Transplantation of Long Shoots in a Temperate Tidal Zone (Northern China). *Wetlands, 39 (5)*, 1043–56. https://doi.org/10.1007/s13157-019-01157-8.

Lovato, T., Peano, D., Butenschön, M., Materia, S., Iovino, D., et al. (2022). CMIP6 simulations with the CMCC Earth System Model (CMCC-ESM2). *Journal of Advances in Modeling Earth Systems*. https://doi.org/10.1029/2021ms002814.

Lüning, K. (1979). Growth Strategies of Three *Laminaria* Species (Phaeophyceae) Inhabiting Different Depth Zones in the Sublittoral Region of Helgoland (North Sea). *Marine Ecology Progress Series, 1*, 195–207. https://www.int-res.com/articles/meps/1/m001p195.pdf%0Ahttp://link.springer.com/10.1007/s12072-010-9169-3.

Lüning, K., Fortes, M.D. (1980). Growth rates of North Sea macroalgae in relation to temperature, irradiance and photoperiod. *Helgolander Meeresunters, 29*, 15–29. https://doi.org/10.1007/BF01983538.

Marbà, N., Duarte, C.M., Cebrian, J., Gallegos, M.E., Olesen, B., Sand-Jensen, K. (1996). Growth and population dynamics of *Posidonia oceanica* on the Spanish Mediterranean Coast: Elucidating seagrass decline. *Marine Ecology Progress Series, 137 (1-3)*, 203–13. https://doi.org/10.3354/meps137203.

Mascaró, O., Valdemarsen, Holmer, T.M., Pérez, M., Romero, J. (2009). Experimental manipulation of sediment organic content and water column aeration reduces *Zostera marina* (eelgrass) growth and survival. *Journal of Experimental Marine Biology and Ecology, 373 (1)*, 26–34. https://doi.org/10.1016/j.jembe.2009.03.001.

Masson-Delmotte, Valérie, et al. Global warming of 1.5 C. An IPCC Special Report on the impacts of global warming of 1.5 (2018): 43-50.

Mauritsen, T., Bader, J., Becker, T., Behrens, J., Bittner, M., et al. (2019). Developments in the MPI-M Earth System Model version 1.2 (MPI-ESM1.2) and Its Response to Increasing CO_2. *Journal of Advances in Modeling Earth Systems, 11(4)*, 998–1038. https://doi.org/10.1029/2018MS001400.

Meinshausen, M., Nicholls, Z.R.J., Lewis, J., Gidden, M.J., Vogel, E., et al. (2020). The shared socio-economic pathway (SSP) greenhouse gas concentrations and their extensions to 2500. *Geoscientific Model Development, 13(8)*, 3571–3605. https://doi.org/10.5194/gmd-13-3571-2020.

Millar, R.V., Houghton, J.D.R., Elsäbetaer, B., Mensink, P.J., Kregting, L. (2020). Influence of waves and currents on the growth rate of the kelp *Laminaria digitata* (Phaeophyceae). *Journal of Phycology, 56 (1)*, 198–207. https://doi.org/10.1111/jpy.12943.

Moore, K.A., Wetzel, R.L. (2000). Seasonal variations in eelgrass (*Zostera marina* L.) responses to nutrient enrichment and reduced light availability in experimental ecosystems. *Journal of Experimental Marine Biology and Ecology, 244 (1)*, 1–28. https://doi.org/10.1016/S0022-0981(99)00135-5.

Moreno-Marín, F., Brun, F.G., Pedersen, M.F. (2018). Additive response to multiple environmental stressors in the seagrass *Zostera marina* L. *Limnology and Oceanography, 63 (4)*, 1528–44. https://doi.org/10.1002/lno.10789.

Müller, W.A., Jungclaus, J.H., Mauritsen, T., Baehr, J., Bittner, M., et al. (2018). A Higher-resolution Version of the Max Planck Institute Earth System Model (MPI-ESM1.2-HR). *Journal of Advances in Modeling Earth Systems, 10(7)*, 1383–1413. https://doi.org/10.1029/2017MS001217.

Nepper-Davidsen, J., Andersen, D.T., Pedersen, M.F. (2019). Effects of simulated heat wave scenarios on sugar kelp *Saccharina latissima*: exposure to high but sub-lethal temperatures causes long-term and partly irreversible reductions in performance. *Marine Ecology Progress Series, 630*, 25–39. https://doi.org/10.3354/meps13133.

Nejrup, L.B., Pedersen, M. (2008). Effects of salinity and water temperature on the ecological performance of *Zostera marina*. *Aquatic Botany, 88 (3)*, 239–46. https://doi.org/10.1016/j.aquabot.2007.10.006.

Niedzwiedz, S., Diehl, N., Fischer, P., Bischof, K. (2022). Seasonal and inter-annual variability in the heatwave tolerance of the kelp *Saccharina latissima* (Laminariales, Phaeophyceae). *Phycological Research, 70(4)*, 212-222. https://doi.org/10.1111/pre.12501.

Nitschke, U., Dixneuf, S., Ruth, A.A., Schmid, M., Stengel, D.B. (2013). Molecular iodine (I2) emission from two *Laminaria* species (Phaeophyceae) and impact of irradiance and temperature on I_2 emission into air and iodide release into seawater from *Laminaria digitata*. *Marine Environmental Research, 92*, 102–9. https://doi.org/10.1016/j.marenvres.2013.09.006.

O'Neill, B.C., Kriegler, E., Riahi, K., Ebi, K.L., Hallegatte, S., et al. (2014). A new scenario framework for climate change research: the concept of shared socioeconomic pathways. *Climatic Change, 122,* 387-400. https://doi.org/10.1007/s10584-013-0905-2.

Olesen, B., Enríquez, S., Duarte, C.M., Sand-Jensen, K. (2002). Depth-acclimation of photosynthesis, morphology and demography of *Posidonia oceanica* and *Cymodocea nodosa* in the Spanish Mediterranean Sea. *Marine Ecology Progress Series, 236*, 89–97. https://doi.org/10.3354/meps236089.

Olesen, B., Krause-Jensen, D., Marbà, N., Christensen, P.B. (2015). Eelgrass *Zostera marina* in subarctic Greenland: Dense meadows with slow biomass turnover in cold waters. *Marine Ecology Progress Series, 518*, 107–21. https://doi.org/10.3354/meps11087.

Olesen, B., Sand-Jensen, K. (1994). Demography of Shallow Eelgrass (*Zostera Marina*) Populations–Shoot Dynamics and Biomass Development. *The Journal of Ecology, 82 (2)*, 379. https://doi.org/10.2307/2261305.

Olesen, B., Sand-Jensen, K. (1993). Seasonal acclimatization of eelgrass *Zostera marina* growth to light. *Marine Ecology Progress Series, 94 (1),* 91–99. https://doi.org/10.3354/meps094091.

Olsen, Y.S., Sánchez-Camacho, M., Marbà, N., Duarte, C.M. (2012). Mediterranean Seagrass Growth and Demography Responses to Experimental Warming. *Estuaries and Coasts, 35 (5)*, 1205–13. https://doi.org/10.1007/s12237-012-9521-z.

Olischläger, M., Iñiguez, C., Koch, K., Wiencke, C., López Gordillo, F.J. (2017). Increased pCO_2 and temperature reveal ecotypic differences in growth and photosynthetic performance of temperate and Arctic populations of *Saccharina latissima*. *Planta, 245 (1)*, 119–36. https://doi.org/10.1007/s00425-016-2594-3.

Ospina-Alvarez, A., de Juan, S., Alos, J., Basterretxea, G., Alonso-Fernandez, A., Follana-Berna, G., Palmer, M., Catalan, I., (2020). MPA network design based on graph theory and emergent properties of larval dispersal. *Marine Ecology Progress Series, 650*, 309–326. https://doi.org/10.3354/meps13399.

Pagès, J.F., Gera, A., Romero, J., Alcoverro, T. (2014). Matrix composition and patch edges influence plant-herbivore interactions in marine landscapes. *Functional Ecology, 28 (6)*, 1440–48. https://doi.org/10.1111/1365-2435.12286.

Pagès, R., Baklouti, M., Barrier, N., Ayache, M., Sevault, F., Somot, S., Moutin, T. (2020). Projected Effects of Climate-Induced Changes in Hydrodynamics on the Biogeochemistry of the Mediterranean Sea Under the RCP 8.5 Regional Climate Scenario. *Frontiers in Marine Science*, *7(November)*, 1–17. https://doi.org/10.3389/fmars.2020.563615.

Palacios, S.L., Zimmerman, R.C. (2007). Response of eelgrass *Zostera marina* to CO_2 enrichment: Possible impacts of climate change and potential for remediation of coastal habitats. *Marine Ecology Progress Series, 344,* 1–13. https://doi.org/10.3354/meps07084.

Payne, M.R., Barange, M., Cheung, W.W., MacKenzie, B.R., Batchelder, H.P., et al. (2016). Uncertainties in projecting climate-change impacts in marine ecosystems. *ICES Journal of Marine Science, 73(5)*, 1272-1282. https://doi.org/10.1093/icesjms/fsv231.

Pessarrodona, A., Assis, J., Filbee-Dexter, K., Burrows, M.T., Gattuso, J.P., Duarte, C.M., et al. (2022). Global seaweed productivity. *Science Advances, 8(37)*, eabn2465. https://doi.org/10.1126/sciadv.abn2465.

Pastor, A., Ospina-Alvarez, A., Larsen, J., Hansen, F.T., Krause-Jensen, D., Maar, M. (2022) A network analysis of connected biophysical pathways to guide eelgrass (*Zostera marina*) restoration. *Marine Environmental Research, 179*, 105690. https://doi.org/10.1016/j.marenvres.2022.105690.

Paul, M., de los Santos, C.B. (2019). Variation in flexural, morphological, and biochemical leaf properties of eelgrass (*Zostera marina*) along the European Atlantic climate regions. *Marine Biology, 166 (10)*, 1–12. https://doi.org/10.1007/s00227-019-3577-2.

Pazzaglia, J., Santillán-Sarmiento, A., Helber, S.B., Ruocco, M., Terlizzi, A., Marín-Guirao, L., Procaccini, G. (2020). Does Warming Enhance the Effects of Eutrophication in the Seagrass *Posidonia oceanica*? *Frontiers in Marine Science, 7 (December)*. https://doi.org/10.3389/fmars.2020.564805.

Pedersen, M.F., Borum, J. (1993). An annual nitrogen budget for a seagrass *Zostera marina* population. *Marine Ecology Progress Series, 101*, 455–59.

Pedersen, M.F. (1995). Nitrogen limitation of photosynthesis and growth: Comparison across aquatic plant communities in a Danish estuary (Roskilde Fjord). *Ophelia, 41 (1)*, 261–72. https://doi.org/10.1080/00785236.1995.10422047.

Petrell, R.J., Alie, S.Y. (1996). Integrated cultivation of salmonids and seaweeds in open systems. *Hydrobiologia, 326-327,* 67–73. https://doi.org/10.1007/BF00047788.

Ploton, P., Mortier, F., Réjou-Méchain, M., Barbier, N., Picard, N., et al. (2020). Spatial validation reveals poor predictive performance of large-scale ecological mapping models. *Nature Communications*, *Sep 11;11(1)*, 1-1. https://doi.org/10.1038/s41467-020-18321-y.

Qi, H., Rorrer, G.L. (1995). Photolithotrophic cultivation of *Laminaria saccharina* gametophyte cells in a stirred-tank bioreactor. *Biotechnology and Bioengineering, 45(3)*, 251-260. https://doi.org/10.1016/0141-0229(95)00111-5.

Queirós, A.M., Stephens, N., Widdicombe, S., Tait, K., McCoy, S.J., et al. (2019). Connected macroalgal-sediment systems: blue carbon and food webs in the deep coastal ocean. *Ecological Monographs, 89(3),* e01366. https://doi.org/10.1002/ecm.1366.

Rasmussen, J.R., Olesen, B., Krause-Jensen, D. (2012). Effects of filamentous macroalgae mats on growth and survival of eelgrass, *Zostera marina*, seedlings. *Aquatic Botany, 99,* 41–48. https://doi.org/10.1016/j.aquabot.2012.01.005.

Ricart, A. M., Krause-Jensen, D., Hancke, K., Price, N.N., Masqué, P., Duarte, C.M. (2022). Sinking seaweed in the deep ocean for carbon neutrality is ahead of science and beyond the ethics. *Environmental Research Letters, 17(8)*, 081003. https://doi.org/10.1088/1748-9326/ac82ff.

Rigollet, V., Laugier, T., De Casabianca, M.L., Sfriso, A., Marcomini, A. (1998). Seasonal biomass and nutrient dynamics of *Zostera marina* L. in two Mediterranean lagoons: Thau (France) and Venice (Italy). *Botanica Marina 41 (2)*, 167–79. https://doi.org/10.1515/botm.1998.41.1-6.167.

Roberts, M.J., Baker, A., Blockley, E W., Calvert, D., Coward, A., et al. (2019). Description of the resolution hierarchy of the global coupled HadGEM3-GC3.1 model as used in

CMIP6 HighResMIP experiments. *Geoscientific Model Development, 12(12)*, 4999–5028. https://doi.org/10.5194/gmd-12-4999-2019.

Röhr, M.E., Holmer, M., Baum, J.K., Björk, M., Chin, D., et al. (2018). Blue Carbon Storage Capacity of Temperate Eelgrass (*Zostera marina*) Meadows. *Global Biogeochemical Cycles, 32 (10)*, 1457–75. https://doi.org/10.1029/2018GB005941.

Rorrer, G.L., Modrell, J., Zhi, C., Yoo, H.D., Nagle, D.N., Gerwick, W.H. (1995). Bioreactor seaweed cell culture for production of bioactive oxylipins. *Journal of Applied Phycology, 7 (2)*, 187–98. https://doi.org/10.1007/BF00693067.

Ruesink, J.L., Yang, S., Trimble, A.C. (2015). Variability in Carbon Availability and Eelgrass (*Zostera marina*) Biometrics Along an Estuarine Gradient in Willapa Bay, WA, USA. *Estuaries and Coasts, 38 (6)*, 1908–17. https://doi.org/10.1007/s12237-014-9933-z.

Ruíz, J.M., Pérez, M., Romero, J., Tomas, F. (2009). The importance of herbivory in the decline of a seagrass (*Posidonia oceanica*) meadow near a fish farm: An experimental approach. *Botanica Marina, 52 (5)*, 449–58. https://doi.org/10.1515/BOT.2009.053.

Ruocco, M., De Luca, P., Marín-Guirao, L., Procaccini, G. (2019). Differential Leaf Age-Dependent Thermal Plasticity in the Keystone Seagrass *Posidonia oceanica*. *Frontiers in Plant Science, 10 (December)*. https://doi.org/10.3389/fpls.2019.01556.

Sandoval-Gil, J.M., Ruiz, J.M., Marín-Guirao, L., Bernardeau-Esteller, J., Sánchez-Lizaso, J.L. (2014). Ecophysiological plasticity of shallow and deep populations of the Mediterranean seagrasses *Posidonia oceanica* and *Cymodocea nodosa* in response to hypersaline stress. *Marine Environmental Research, 95*, 39–61. https://doi.org/10.1016/j.marenvres.2013.12.011.

Savva, I., Bennett, S., Roca, G., Jordà, G., Marbà, N. (2018). Thermal tolerance of Mediterranean marine macrophytes: Vulnerability to global warming. *Ecology and Evolution, 8 (23)*, 12032–43. https://doi.org/10.1002/ece3.4663.

Scafetta, N. (2022). Advanced Testing of Low, Medium, and High ECS CMIP6 GCM Simulations Versus ERA5-T2m. *Geophysical Research Letters*, *49*(6), 1–13. https://doi.org/10.1029/2022GL097716.

Schaffelke, B.A. (1995). Storage carbohydrates and abscisic acid contents in *Laminaria hyperborea* are entrained by experimental daylengths. *European Journal of Phycology, 30 (4)*, 313–17. https://doi.org/10.1080/09670269500651101.

Scheschonk, L., Bischof, K., Kopp, M.E.L., Jueterbock, A. (2023). Differences by origin in methylome suggest eco-phenotypes in the kelp *Saccharina latissima*. *Evolutionary Applications, 16(2),* 262-278. https://doi.org/10.1111/eva.13382.

Seland, Ø., Bentsen, M., Olivié, D., Toniazzo, T., Gjermundsen, A., et al. (2020). Overview of the Norwegian Earth System Model (NorESM2) and key climate response of CMIP6 DECK, historical, and scenario simulations. *Geoscientific Model Development, 13(12)*. https://doi.org/10.5194/gmd-13-6165-2020.

Sellar, A.A., Jones, C.G., Mulcahy, J.P., Tang, Y., Yool, A., et al. (2019). UKESM1: Description and Evaluation of the U.K. Earth System Model. *Journal of Advances in Modeling Earth Systems, 11(12)*, 4513–4558. https://doi.org/10.1029/2019MS001739.

Silber, G. K., Lettrich, M. D., Thomas, P. O., Baker, J. D., Baumgartner, M., et al. (2017). Projecting marine mammal distribution in a changing climate. *Frontiers in Marine Science, 413*. https://doi.org/10.3389/fmars.2017.00413.

Simonson, E. J., Scheibling, R.E., Metaxas, A. (2015). Kelp in hot water: I.Warming seawater temperature induces weakening and loss of kelp tissue. *Marine Ecology Progress Series, 537 (October)*, 89–104. https://doi.org/10.3354/meps11438.

Sjótun, K., Fredriksen, S., Rueness, J. (1996). Seasonal growth and carbon and nitrogen content in canopy and first-year plants of *Laminaria hyperborea* (Laminariales, Phaeophyceae). *Phycologia, 35 (1)*, 1–8. https://doi.org/10.2216/i0031-8884-35-1-1.1.

Smale, D.A. (2020). Impacts of ocean warming on kelp forest ecosystems. *New Phytologist, 225.4*, 1447-1454. https://doi.org/10.1111/nph.16107.

Spillias, S., Kelly, R., Cottrell, R. S., O'Brien, K. R., Im, R. Y., et al. (2023). The empirical evidence for the social-ecological impacts of seaweed farming. *PLOS Sustainability and Transformation, 2(2)*, e0000042. https://doi.org/10.1371/journal.pstr.0000042.

Staehr, P.A., Borum, J. (2011). Seasonal acclimation in metabolism reduces light requirements of eelgrass (*Zostera marina*). *Journal of Experimental Marine Biology and Ecology, 407 (2),* 139–46. https://doi.org/10.1016/j.jembe.2011.05.031.

Staehr, P.A., Göke, C., Holbach, A.M., Krause-Jensen, D., Timmermann, K., et al. (2019). Habitat model of eelgrass in Danish coastal waters: development, validation and management perspectives. *Frontiers in Marine Science, 6*, 1–18. https://doi.org/10.3389/fmars.2019.00175.

Swart, N.C., Cole, J.N.S., Kharin, V.V., Lazare, M., Scinocca, J. F., et al. (2019). The Canadian Earth System Model version 5 (CanESM5.0.3). *Geoscientific Model Development, 12(11)*, 4823–4873. https://doi.org/10.5194/gmd-12-4823-2019.

Tatebe, H., Ogura, T., Nitta, T., Komuro, Y., Ogochi, K., et al. (2019). Description and basic evaluation of simulated mean state, internal variability, and climate sensitivity in MIROC6. *Geoscientific Model Development, 12(7)*, 2727-2765. https://doi.org/10.5194/gmd-12-2727-2019.

Treml, E.A., Halpin, P.N., Urban, D.L., Pratson, L.F. (2008). Modeling population connectivity by ocean currents, a graph-theoretic approach for marine conservation. Landscape Ecology, 23, 19–36. https://doi.org/10.1007/s10980-007-9138-y.

Vähätalo, A., Søndergaard, M., Schlüter, L., Markager, S. (1998). Impact of solar radiation on the decomposition of detrital leaves of eelgrass *Zostera marina*. *Marine Ecology Progress, Series 170 (September)*, 107–17. https://doi.org/10.3354/meps170107.

Wernberg, T., Krumhansl, K., Filbee-Dexter, K., Pedersen, M.F. (2019). Status and trends for the world's kelp forests. In World seas: An environmental evaluation (pp. 57-78). *Academic Press.*

Wilson, K.L., Kay, L.M., Schmidt, A.L., Lotze, H.K. (2015). Effects of increasing water temperatures on survival and growth of ecologically and economically important seaweeds in Atlantic Canada: implications for climate change. *Marine Biology, 162 (12)*, 2431–44. https://doi.org/10.1007/s00227-015-2769-7.

Wilson, R.J., Speirs, D.C., Sabatino, A., Heath, M.R. (2018). A synthetic map of the north-west European Shelf sedimentary environment for applications in marine science. *Earth System Science Data, 10(1)*, 109–130. https://doi.org/10.5194/essd-10-109-2018

Wilson, R.J., Heath, M.R. (2019). Increasing turbidity in the North Sea during the 20th century due to changing wave climate. *Ocean Science, 15(6)*, 1615-1625. https://doi.org/10.5194/os-15-1615-2019.

Wittmann, K.J., Ott, J.A. (1982). Effects of Cropping on Growth in the Mediterranean Seagrass *Posidonia oceanica* (L.) Delile. *Marine Ecology, 3 (2)*, 151–59. https://doi.org/10.1111/j.1439-0485.1982.tb00380.x.

Wu, T., Lu, Y., Fang, Y., Xin, X., Li, L., et al. (2019). The Beijing Climate Center Climate System Model (BCC-CSM): The main progress from CMIP5 to CMIP6. *Geoscientific Model Development, 12(4)*, 1573–1600. https://doi.org/10.5194/gmd-12-1573-2019.

Yang, Y.M., Wang, B., Cao, J., Ma, L., Li, J. (2020). Improved historical simulation by enhancing moist physical parameterizations in the climate system model NESM3.0. *Climate Dynamics, 54(7–8)*, 3819–3840. https://doi.org/10.1007/s00382-020-05209-2.

Yukimoto, S., Kawai, H., Koshiro, T., Oshima, N., Yoshida, K., et al. (2019). The meteorological research institute Earth system model version 2.0, MRI-ESM2.0: Description and basic evaluation of the physical component. *Journal of the Meteorological Society of Japan, 97(5)*, 931–965. https://doi.org/10.2151/jmsj.2019-051.

Young, C.S., Peterson, B.J., Gobler, C.J. (2018). The Bloom-Forming Macroalgae, Ulva, Outcompetes the Seagrass, *Zostera marina*, Under High CO2 Conditions. *Estuaries and Coasts, 41 (8)*, 2340–55. https://doi.org/10.1007/s12237-018-0437-0.

Zharova, N., Sfriso, A., Voinov, A., Pavoni, B. 2001. A simulation model for the annual fluctuation of *Zostera marina* biomass in the Venice lagoon. *Aquatic Botany 70 (2)*, 135–50. https://doi.org/10.1016/S0304-3770(01)00151-6.

Zhi, C., Rorrer, G.L. (1996). Photolithotrophic cultivation of *Laminaria saccharina* gametophyte cells in a bubble-column bioreactor. *Enzyme and Microbial Technology, 18 (4),* 291–99. https://doi.org/10.1016/0141-0229(95)00111-5.

Ziehn, T., Chamberlain, M.A., Law, R.M., Lenton, A., Bodman, R. W., et al. (2020). The Australian Earth System Model: ACCESS-ESM1.5. *Journal of Southern Hemisphere Earth Systems Science, 70(1)*, 193–214. https://doi.org/10.1071/ES19035.

Zimmerman, R.C., Smith, R.D., Alberte, R.S. (1989). Thermal acclimation and whole-plant carbon balance in *Zostera marina* L. (eelgrass). *Journal of Experimental Marine Biology and Ecology, 130 (2),* 93–109. https://doi.org/10.1016/0022-0981(89)90197-4.

Zimmerman, R.C., Reguzzoni, J.L., Alberte, R.S. 1995. Eelgrass (*Zostera marina* L.) transplants in San Francisco Bay: Role of light availability on metabolism, growth and survival. *Aquatic Botany, 51 (1-2)*, 67–86. https://doi.org/10.1016/0304-3770(95)00472-C.

Zimmerman, R.C., Kohrs, R.G., Alberte, R.S. (1996). Top-Down impact through a bottom-Up mechanism: The effect of limpet grazing on growth, productivity and carbon allocation

of *Zostera marina* L. (eelgrass). *Oecologia, 107 (4),* 560–67. https://doi.org/10.1007/BF00333949.

Zimmerman, R.C., Steller, D.L., Kohrs, D.G., Alberte, R.S. (2001). Top-down impact through a bottom-up mechanism. In situ effects of limpet grazing on growth, light requirements and survival of the eelgrass *Zostera marina*. *Marine Ecology Progress Series, 218,* 127–40. https://doi.org/10.3354/meps218127.

Zimmerman, R.C., Hill, V.J., Jinuntuya, M., Celebi, B., Ruble, D., Smith, M., Cedeno, T., Mark Swingle, W. (2017). Experimental impacts of climate warming and ocean carbonation on eelgrass *Zostera marina*. *Marine Ecology Progress Series, 566*, 1–15. https://doi.org/10.3354/meps12051.